TUDelft

Delft University of Technology

Chemical Sensors based on Si Nanowires

Surface modifications for the detection of ions, explosives and chemical vapors

Cao, Anping

DOI

Publication date
2018

Document Version
Final published version

Citation (APA)

Important note
To cite this publication, please use the final published version (if applicable).
Please check the document version above.

Chemical Sensors based on Si Nanowires
Surface modifications for the detection of ions, explosives and chemical vapors

Anping Cao

Chemical Sensors based on Si Nanowires
Surface modifications for the detection of ions, explosives and chemical vapors

Proefschrift

ter verkrijging van de graad van doctor

aan de Technische Universiteit Delft,

op gezag van de Rector Magnificus prof. dr. ir. T. H. J. J. van der Hagen;

voorzitter van het College voor Promoties,

in het openbaar te verdedigen op

dinsdag 9 januari 2018 om 12.30 uur

door

Anping CAO

Master of Science in Analytical Chemistry,

Xiangtan University

geboren te Hunan, China

This dissertation has been approved by the:

promotor: Prof. dr. E. J. R. Sudhölter

copromotor: Dr. ir. L. C. P. M. de Smet

Contents

Chapter 1

Introduction

1.1 Chemical sensors

Chemical sensors, according to the IUPAC definition, are devices that transform chemical information, ranging from the concentration of a specific sample component to overall composition analysis, into analytically useful signals.[1] Smoke alarms and CO detectors are just examples of sensors used in our daily life. Rapid ongoing industrial developments and the desire to further improve the quality of life stimulate the demand on chemical sensor research and development. The ideal chemical sensor is -an inexpensive, portable, foolproof device that responds with a perfect and instantaneous selectivity to a particular target chemical substance (analyte) present in any complex medium in order to produce a measurable (and wireless) signal output at any required analyte concentration-.[2] Such ideal chemical sensors, however, are still far from reality in spite of the enormous advances made over the past decades. Main challenges to the existing chemical sensors are related to the following aspects (4Ss):

- Selectivity,
- Sensitivity,
- Speed of response,
- Stability.

Selectivity means the recognition of the target's molecular structure or associated reactivity, from millions and billions of known molecular substances. Sensitivity or limit of detection (LOD) relates to the minimum quantity of the analyte that still give a measurable response, and chemical (bio)sensors are commonly required to detect the level of 10^{-9} molar or even less. In addition, direct and instant reading of the sensing results as well as and the stability of the sensor in terms of months or years are also demanded for the ideal device. It's common that the requirement of sensor sensitivity often conflicts with the reversibility. Because a high sensitivity (low LOD) often relates to a high association constant of target's binding, thus a poor dissociation kinetics, *i.e.* less reversible. However in an ideal case, the reversibility is still demanded for a long lifetime of the sensor device, so that it can be re-used/recycled in repeated measurements.

1.2 Electrochemical sensors

At the current state of the art, electrochemical sensing is one of the most suitable technologies for sensors development, as electrical signals can be efficiently acquired, processed, stored, transmitted and applied by final users.[3] A generalized scheme of electrochemical sensing process is presented in figure 1.1. Analytes

interact with the affinity element changing some of its physical properties (*e.g.*, mass, ΔM; conductivity, $\Delta\sigma$; or work function, $\Delta\Phi$). The transducer is an electrical platform that converts one of the above-mentioned physical quantities into a variation of its electric parameters (*e.g.*, capacitance, ΔC; inductance, ΔL; and resistance, ΔR). An efficient affinity element contributes to a high selectivity, sensitivity and fast response of the sensing process, and can be of different types, ranging from nanoparticles to molecular materials and polymers. At the same time, due to the low-cost and high sensitivity of various nanomaterials and nanostructures, the research of miniaturized transducer platform has been gradually growing.[4-6]
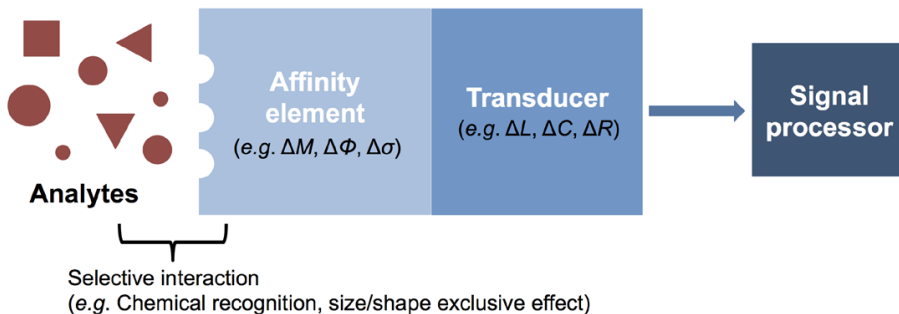
Figure 1.1 Schematic representation of an electrochemical sensor.

1.3 SiNW-based devices

Among all nanomaterials and nanostructures, silicon nanowires (SiNWs) are very good candidates as the sensing platform (transducer) due to several advantages they present. For example, electrical devices based on SiNWs allow one to analyze responses not only by the voltage between the electrodes, but also by a gate voltage, thanks to the semiconductor nature of silicon.[7] Also, the semiconducting properties of SiNW can be effectively controlled during the fabrication process, *e.g.* the doping type and level directly affect the charge carrier (electron or hole) density, and thermal annealing can improve the carrier mobility of SiNW.[8, 9] Moreover, the nanowire structure represents the minimum dimensionality for the electrical conduction. Compared with other nanostructures (*e.g.* nanoparticles), it provides a better model for investigating the dependence of electronic transport on size confinement and dimensionality.[10] Compared to devices prepared from carbon nanotubes and organic materials like wires made from conducting polymers, SiNW-based devices are more compatible with very-large-scale integration (VLSI) processes and complementary metal–oxide–semiconductor (CMOS) technologies.[11] In addition, in terms of the fundamental sensor mechanism, chemical sensors based on SiNWs are better

understood than devices based on metal-oxide nanowires and polymer nanowires.[12] Finally, the ability to chemically modify the surface of SiNWs enables not only the chemical immobilization of the affinity element, but also affects the device performance.[13]

There are different ways of classifying devices associated with SiNWs. The first one is related to the fabrication process of the nanowires. Nanowires can be grown from precursors, individual atoms and molecules to build the desired nanostructures, in some cases through smart use of self-assembly.[14] These are referred to as bottom-up fabrication methods and typically require the transfer and deposition of the nanowires onto a substrate, followed by the fabrication of contact pads. Alternatively, one can make use of top-down methods starting with patterns made on a large scale and then reducing the lateral dimensions to the nanoscale.[15] The first paper on SiNW-based sensor devices made use of bottom-up approaches,[16] but an increasing number of studies deal with top-down methods, mainly because they have the advantage of reproducibility and reliability, improved contact properties and the (high density) integration possibilities related to CMOS processes.[17, 18]

1.4 Working principle of SiNW-based device

Another way to categorize SiNW-based sensors is based on how the electrical characterization or read-out is performed. In cases where changes in the nanowire resistance (*i.e.*, current) are measured without the use of a so-called front-gate or back-gate electrode, one typically refers to resistor-based sensors. On the other hand, devices that make use of an applied gate are referred to as Field Effect Transistors (FETs). It is noted that there is no intrinsic relationship between the type of electrical read-out (resistor *vs.* FET) and the way of preparing the SiNWs (grown or top-down made). At the same time it is noticed that these days most NW-based FETs are prepared via top-down approaches.

Figure 1.2a depicts the schematics of the resistor-based configuration. Here, the SiNWs bridges the positive and negative electrodes to allow a current flow. The adsorption of the analyte onto the SiNW surface alters the surface state. By monitoring the resulting change of electrical resistance or conductance using a simple direct current (DC) circuit the analyte can be detected.[19] In the case of the FET-based configuration, the SiNW functions as a conductive channel. The terminal ends are now connected by so-called source and drain contacts, typically metallic or highly-doped semiconductor materials. The number of charge carriers and thus the conductance through the SiNW can be changed by a third gate electrode, either via

a back gate (as depicted in Figure 1.2b) or a front gate. For example, by applying a back-gate potential (V_{bg}) the nanowire can be brought into the depletion-mode, enabling one to measure in the subthreshold regime where the transducer is most sensitive.[7] Any (bio)chemical or recognition event that occurs near the nanowire surface influences the local electrical voltage experienced by the nanowire and may change the extent of depletion. The number of majority charge carriers varies, which is registered as a change in drain current (I_d) if a fixed source-drain voltage (V_{ds}) is applied. Another way of registering the recognition event is by adaption of the back-gate voltage ΔV_{bg} in such a way that at fixed V_{ds}, I_d is kept constant. In that case ΔV_{bg} reflects the change in boundary potential at the interface of the nanowire and its environment. Due to the large surface-to-volume ratio of nanowires and the gate effect of the amplifier configuration, nanowire-based devices have high potential for the development of single-molecule detection.[20]
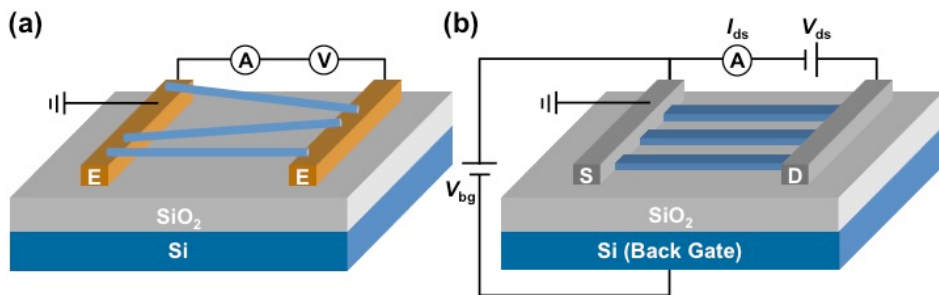
Figure 1.2 Simplified schematics of the SiNW-based **(a)** resistor and **(b)** SiNW-based FET to illustrate the differences in the electrical configuration and the way the nanowires are orientated with respect to the electrodes (E) and the source (S) and drain (D).

1.5 Thesis outline

The multiplexing of this thesis is to investigate SiNW (top-down prepared) as the sensor platform (transducer), with special emphasis on its surface modification with different affinity elements (*e.g.* ionophores, metal organic polyhedra, porous organic frameworks and nanoparticles), for the selective and sensitive electrochemical sensing in both liquid and gas phase.

An overview of the scientific work performed during this PhD thesis research is presented in terms of Chapters. The different parts of the research resulted in a number of publications. Chapter 2 is largely based on a literature review, and Chapters 3-5 present experimental work. The final Chapter covers a general discussion and the overall conclusions. In more detail:

Chapter 1 introduces the concept of chemical sensors and electrochemical sensors, and gives a general review of the development of SiNW-based sensors, including its categories and working principles. Section 1.3 and 1.4 are based on the contents in Section 1 and 2 of the review paper.[21]

Chapter 2 describes the state of the art of using SiNWs as gas/vapor sensors. Special attention is given to surface modification strategies and the sensing principles involved. An earlier version of this Chapter has been published in **Sensors** as *Silicon Nanowire-based Devices for Gas-Phase Sensing, 2014*, and was updated by adding the most recent developments in the field.[21]

Chapter 3 presents the experimental work on the surface modification of SiNWs with ionophores for multiple ions sensing. In this study, siloprene-based, ion-selective membranes (ISMs) were drop-casted onto a FET device that consisted of a single-chip array of SiNWs. Within one array, two sets of SiNWs were covered with ISMs, each containing two different ionophores, allowing the simultaneous, selective and sensitive detection of K^+ and Na^+ using a flow cell. The ISMs were also analyzed in a conventional ion-selective electrode (ISE) configuration, allowing a direct comparison. The work has been published in **Anal. Chem.** as *Ionophore-Containing Siloprene Membranes: Direct Comparison between Conventional Ion-Selective Electrodes and Silicon Nanowire-based Field-Effect Transistors, 2015*.[22]

Chapter 4 presents a novel nanoFET device for the sensitive and selective detection of explosives based on affinity layers of metal–organic polyhedra (MOPs). The judicious selection of the geometric and electronic characteristics of the assembly units (organic ligands and unsaturated metal site) embedded within the MOP cage allowed for the formation of multiple charge-transfer (CT) interactions to facilitate the selective explosive inclusion. Meanwhile, the host-stabilized CT complex inside the cage acts as an effective molecular gating element to strongly modulate the electrical conductance of the silicon nanowires. The work has been published in **Nano Lett.** as *Metal–Organic Polyhedra-Coated Si Nanowires for the Sensitive Detection of Trace Explosives, 2017*.[23]

Chapter 5 reports for the first time the covalent attachment of Polymer Organic Frameworks (POFs) onto SiNW surfaces and the effect on the electrical sensing properties of SiNW-based devices. The surface modification by POFs was easily performed by polycondensation on linker-modified SiNWs. Platinum nanoparticles were formed in these POFs by first impregnation with a metal precursor and

followed by *in-situ* reduction. The final system showed highly enhanced sensitivity for methanol vapor detection.

Chapter 6 discusses all the conclusions from the preceding Chapters and gives recommendations for future work.

References

1. Hulanicki, A.; Glab, S.; Ingman, F. *Pure Appl. Chem.* **1991,** 63, 1247-1250.
2. Council, N. R., *Expanding the Vision of Sensor Materials*. The National Academies Press: Washington, DC, 1995; p 146.
3. Paolesse, R.; Nardis, S.; Monti, D.; Stefanelli, M.; Di Natale, C. *Chem. Rev.* **2017,** 117, 2517-2583.
4. De, M.; Ghosh, P. S.; Rotello, V. M. *Adv. Mater.* **2008,** 20, 4225-4241.
5. Bae, C.; Yoo, H.; Kim, S.; Lee, K.; Kim, J.; Sung, M. A.; Shin, H. *Chem. Mater.* **2008,** 20, 756-767.
6. Liu, A. H. *Biosens. Bioelectron.* **2008,** 24, 167-177.
7. Gao, X. P. A.; Zheng, G. F.; Lieber, C. M. *Nano Lett.* **2010,** 10, 547-552.
8. Cui, Y.; Zhong, Z. H.; Wang, D. L.; Wang, W. U.; Lieber, C. M. *Nano Lett.* **2003,** 3, 149-152.
9. Cui, Y.; Duan, X. F.; Hu, J. T.; Lieber, C. M. *J. Phys. Chem. B* **2000,** 104, 5213-5216.
10. Xia, Y. N.; Yang, P. D. *Adv. Mater.* **2003,** 15, 351-352.
11. Stern, E. et al. *Nature* **2007,** 445, 519-522.
12. Penner, R. M. *Ann. Rev. Anal. Chem.* **2012,** 5, 461-485.
13. Bunimovich, Y. L.; Shin, Y. S.; Yeo, W. S.; Amori, M.; Kwong, G.; Heath, J. R. *J. Am. Chem. Soc.* **2006,** 128, 16323-16331.
14. Li, Y.; Qian, F.; Xiang, J.; Lieber, C. M. *Mater. Today* **2006,** 9, 18-27.
15. Stern, E.; Vacic, A.; Reed, M. A. *IEEE Trans. Electron. Devices* **2008,** 55, 3119-3130.
16. Cui, Y.; Lieber, C. M. *Science* **2001,** 291, 851-853.
17. Gunawan, O. et al. *Nano Lett.* **2008,** 8, 1566-1571.
18. Mescher, M.; de Smet, L.; Sudhölter, E. J. R.; Klootwijk, J. H. *J. Nanosci. Nanotechnol.* **2013,** 13, 5649-5653.
19. Chen, X. P.; Wong, C. K. Y.; Yuan, C. A.; Zhang, G. Q. *Sens. Actuators B: Chem.* **2013,** 177, 178-195.
20. Patolsky, F.; Lieber, C. M. *Mater. Today* **2005,** 8, 20-28.
21. Cao, A.; Sudhölter, E. J. R.; de Smet, L. C. P. M. *Sensors* **2014,** 14, 245-271.
22. Cao, A.; Mescher, M.; Bosma, D.; Klootwijk, J. H.; Sudhölter, E. J. R.; Smet, L. C. P. M. d. *Anal. Chem.* **2015,** 87, 1173-1179.
23. Cao, A.; Zhu, W.; Shang, J.; Klootwijk, J. H.; Sudhölter, E. J. R.; Huskens, J.; de Smet, L. C. P. M. *Nano Lett.* **2017,** 17, 1-7.

Chapter 2

Silicon Nanowire-based Devices for Gas Phase Sensing

Abstract: Since their introduction in 2001, Si NW-based sensor devices have gained considerable interest as a general platform for ultra-sensitive, electrical detection of biological and chemical species. Among these, most studies focus on detecting, sensing and monitoring analytes in aqueous solution. Furthermore, the number of studies on sensing gases and vapors using Si NW-based devices is increasing. This Chapter gives an overview of all research papers related to the application of electrical Si NW-based devices in the gas phase. Special attention is given to surface modification strategies and the sensing principles involved. In addition, future steps and technological challenges in this field are addressed at the end of the Chapter.

2.1 Introduction

Rapid ongoing industrial developments and further improvements of the quality of life put a large demand on the sensitive and selective detection of molecules in the gas phase for the environmental monitoring, process control and safety, and medical diagnostics.[1] Gas sensors were first mainly used in coal mines where online and precise monitoring of hazardous gases has to be carried out continually, in order to assure safety in the work place.[2] Soon after many gas/vapor sensors were also beginning to appear in the chemical industry, environmental pollution monitoring and the human health field, for instance, the detection of explosive gases in hydrogen production industry and methane distribution networks, the air-quality monitoring in urban areas, the breath analysis for traffic safety and non-invasive medical diagnostics.[3]

A search using the keywords "silicon nanowire" and "sensor" within the Web of Science yields more than 1200 papers over the past 16 years. Most of these studies are on the detection of analytes (target compounds) in the aqueous environment, mainly within the context of biosensing. However, only about several dozens of studies address sensing in the gas phase. Hence, in order to obtain a deep understanding of the gas-sensing mechanism in (modified) Si NW devices and to show and discuss the diverse approaches in device fabrication, this work aims to give an overview of all research papers related to the sensing in gas phase using electrical devices that consist of both in-plane orientated and vertical-standing Si NWs. For reviews on fabrication methods of Si NWs, we recommend these contributions, with a clear focus on the chemical-vapor-deposition fabricated NWs by the Lieber group[4-6] or top-down fabricated Si NW-based sensors from the Reed group.[7] For an extensive and very recent overview of different nanomaterials that have been explored to prepare NW-based gas sensor and volatile organic compounds (VOCs) sensor, we refer to the review by Chen *et al*.[8] and the recent reviews by Haick's group.[9, 10] Finally, in 2012 Penner wrote an review on chemical sensing with nanowires, that includes relevant sections on Si NW-based devices and also on examples of gas sensing, mostly associated with polymer and metal oxides.[11]

In the present review, a summary of the device specifications, including the modification methods applied, target compounds involved and the sensing performance of different Si NWs-based devices is presented in Table 2.1. The reviewed work has been divided in three different categories: gas sensors, vapor sensors, volatile organic compounds sensors. Selected contributions from these three

categories are reviewed and discussed in more detail. In all cases, we briefly start with the relevance of measuring the target compounds. Focus is given to the different surface modification strategies that are applied onto mostly surface oxidized Si NWs, and various signal enhancement methods by detecting the change of electrical properties. In the end we conclude the review and present an outlook.

2.2 Gas phase sensing

Table 2.1 gives an overview of all electrical sensor devices associated with Si NWs that have been studied in the gas environment. It is noted that a gas is a substance that has a single defined thermodynamic state at the temperature of investigation, while a vapor is a substance in the gas phase at a temperature lower than its critical point. So, according to this definition, VOCs are vapors as well, but most literature on sensing in a gas phase makes use of a sub-qualification: inorganic (gases and vapors) and organic (explosives, nerve agents and VOCs) compounds. Within one category the studies are listed in order of their appearance. Most, but certainly not all, examples cover devices with in-plane orientated Si NWs. With top down and bottom up (*i.e.* nanowire growth) we refer to the approach of Si NW fabrication, although in some cases top-down prepared Si NWs are transferred to another surface. It is noted that here we are interested in the electrical properties of the nanowires and hence the length is defined by the spacing between the two electrodes in those cases where Si NW have been placed onto electrodes (while the actual length of these nanowires could be longer). Nanowires have not been functionalized referred to as 'bare', *i.e.* a thin oxide layer. As all studies aimed to study the detection limits, the sensitivity (s) and measured concentration (mc) range studied are presented in one column.

Table 2.1 Overview of Si NW-based sensors for the detection of inorganic gases and vapors and organic explosives, nerve agents and VOCs.

		Year	Approach[a]	Si NW size[b]	Func.[c]	Princ.[d]	Target	Sensitivity[e]	Ref
Inorganic Compounds	Gases	2007	TD (p)	18 nm (w) 5 μm (l)	Bare	FET	NO_2	20 ppb (s)	14
		2007	BU (n)*	80 - 200 nm (d) ~2.5 μm (l)	Pd NPs	FET	H_2	5 % (mc)	32
		2009	TD (p)	75/130 nm (w) 20 μm (l)	Bare	R	NO_2, NH_3	250 ppm (mc) 250 ppm (mc)	15
		2009	TD (n)	No data	Bare	R	NO	500 ppb (mc)	29
		2010	TD (p)	22/75 nm (w) 2 μm (l)	Bare	R	NO_2	250 ppm (mc)	16
		2010	BU (p)	30 nm (d) 2 μm (g)	Bare	FET	H_2	3 ppm - 5 % (mc)	33
		2011	TD (n)	20 μm (h) 30 - 40 nm (d)	Pd coated	R	H_2	~5 ppm (s)	34
		2011	TD (p)	22 - 100 nm (w) 2 μm (l)	Bare	R	NO_2	250 ppm (mc)	17
		2012	BU (p)&	150 - 200 nm (d) 5 - 8 μm (l)	Amino groups modified	R	NO_2	10 ppb (mc)	18
		2012	TD (p)	40 nm (d) 100 μm (l)	Bare	R	O_2	100% (mc)	44
		2013	TD (p)	100 nm (w) 3 μm (l)	Pd NPs	R	H_2	0.5 % (mc)	35

		Year	Approach[a]	Si NW size[b]	Func.[c]	Princ.[d]	Target	Sensitivity[e]	Ref
Inorganic Compounds	Gases	2013	TD (p)	20 - 300 nm (d) ~29 μm (l)	Bare	R	H_2	20 - 1000 ppm (mc)	36
		2014	TD (p)	No data	Bare	R	H_2	~100% (mc)	38
		2014	TD (p)	100 nm (w) 1 μm (l)	Pd NPs	FET	H_2	0.1 - 1% (mc)	39
		2015	TD (n)	70 nm (w) 10 μm (l)	Pd NPs	FET	H_2	0.01 - 0.1% (mc)	40
		2015	TD (p)	20 - 100 nm (d) 13 μm (l)	Ag/Au/ Pd/Pt NPs	R	H_2	15 - 174 ppm (mc)	41
		2015	TD (n)	100 nm (w) 1 μm (l)	Pd NPs	FET	H_2	0.1 - 0.5% (mc)	42
		2015	TD (p)	30 nm (w)	SnO_2 film	FET	NO, O_2, NH_3	1 ppm (s, O_2/NO), 10 - 100 ppm (mc, NH_3)	30
		2015	TD (p)	10 - 100 nm (d) 1.35 μm (l)	Au/Pt NPs	R	CO_2	0.5 - 2 mbar (mc)	46
		2016	TD (p)	42 μm (l)	Bare	R	H_2	50 - 10000 ppm (mc)	37
		2016	TD (n)	No data	Bare	R	NO_2	1 - 5 ppm (mc)	20
		2016	TD (n/p)	~50 - 200 nm (d) ~30 μm (l)	Bare	R	NO_2	3 ppb (s)	24

		Year	Approach[a]	Si NW size[b]	Func.[c]	Princ.[d]	Target	Sensitivity[e]	Ref
Inorganic Compounds	Gases	2016	TD (p)	100 nm (d) 11 - 25 µm (l)	Bare	R	NO₂	0.05 - 4 ppm (mc)	21
		2016	TD	No data	Bare	R	NO₂	50 ppb (mc)	22
		2016	TD (p)	400 - 500 nm (d) 2 - 2.2 µm (l)	WO₃	R	NO₂	0.25 - 5 ppm (mc)	25
		2016	TD (n)	No data	ZnO	R	NO₂	5 - 50 ppm (mc)	23
		2017	TD (p)	7 µm (l)	GQDs[1]	R	NO₂	50 - 500 ppm (mc)	26
	Vapors	2003	BU (n)[&]	~20 nm (d) 5 mm (g)	HF-etched	R	NH₃, H₂O	1000 ppm (mc), 60 % humidity (mc)	48
		2006	TD (p)	76±5 nm (d) 4 µm (g)	Bare	FET	NH₃	No data	50
		2006	BU (p)	~200 nm (d) 7 µm (l)	Bare	R	NH₃, HCl	Sat. con. (mc)[10]	49
		2008	TD (p)	16 nm (w) 5 µm (l)	Peptides	R	NH₃, AcOH	100 ppm (mc) 100 ppm (mc)	53
		2011	TD (p)	25 nm (w) 300 nm (l)	EBTAM/ OTS[2] modified	FET	H₂O	Ambient (mc)	58
		2011	BU (p)[&]	90 nm (d) 1.6 µm (l)	Au modified	R	H₂O	30 - 95 % (mc)	57

		Year	Approach[a]	Si NW size[b]	Func.[c]	Princ.[d]	Target	Sensitivity[e]	Ref
Inorganic Compounds	Vapors	2011	TD (p)	~200 nm (d) 4-6 µm (l)	PTE[3] modified	R	NH_3, NO_2	1 ppb 10 ppb	54
		2012	BU (n)	100 nm (d) 20 µm (l)	Bare	R	NH_3, smoke	No data	51
			TD (n)	100 nm (d) 10 µm (l)					
		2013	BU (p)[&]	50 nm (d)	Te	R	NH_3	10 - 400 ppm (mc)	55
		2014	BU (n)	No data	Bare	R	NH_3	2 - 700 ppm (mc)	52
Organic Compounds	Explosives	2010	TD (p)	0.2/1/4 µm (w) 4/2 µm (l)	DPCP[4] receptor	FET	DPCP	500 - 800 ppb (mc)	63
		2010	BU (p)	2µm (g)	APTES[5]	FET	TNT[8]	10^{-2} ppt (s)	59
		2012	TD (p)	100/200/400 nm (w) 100 µm (l)	H_2/O_2 plasma treated	R	TNT	Sat. con. (mc)	61
	Nerve Agents	2010	BU (p)	50 nm (w) 3 µm (l)	Bare	R	DMMP[9]	No data	62
		2011	TD (p)	25 nm (w) 300 nm (l)	TABINO[6]	FET	DPCP	500 - 800 ppb (mc)	65
		2011	TD (p)	0.2/1/4 µm (w) 4/2 µm (l)	DPCP receptor	FET	DPCP	500 ppb (mc)	64

16

		Year	Approach[a]	Si NW size[b]	Func.[c]	Princ.[d]	Target	Sensitivity[e]	Ref
Organic Compounds	VOCs	2011	BU	30-70 nm (d) ≥400 nm (l)	Bare	FET	VOCs	No data	67
			TD[#]	50 nm (d)					
		2011	BU (p)	60 nm (d) 2 μm (g)	alkyl trichloro-silane	FET	(non) polar VOCs	ppm level (mc)	71
		2012	BU (p)	50±5 nm (d) 2 μm (g)	alkyl trichloro-silane	FET	Non polar VOCs	ppm level (mc)	72
		2012	BU (p)	50±5 nm (d) 2 μm (g)	alkyl trichloro-silanes	FET	(non) polar VOCs	ppm level (mc)	73
		2013	BU (p)	40±8 nm (d) 8.5±1.5 μm (l)	APTES + 4 different carbonyl chlorides	FET	(non) polar VOCs	0.01 - 0.08 p_a/p_o (mc)[11]	74
		2013	BU (p)	40±8 nm (d) 8.5±1.5 μm (l)	APTES + acyl chlorides[7]	FET	(non) polar VOCs	0.01 - 0.08 p_a/p_o (mc)	75

		Year	Approach[a]	Si NW size[b]	Func.[c]	Princ.[d]	Target	Sensitivity[e]	Ref
Organic Compounds	VOCs	2014	BU (p)	40 ± 8 nm (d) 8.5 ± 1.5 μm (l)	APTES+ R(CH$_2$)$_4$COCl	FET	(non) polar VOCs	0.01 - 0.08 p$_a$/p$_o$ (mc)	77
		2015	BU (p)	40 ± 8 nm (d) 8.5 ± 1.5 μm (l)	C$_3$H$_n$MgCl (n = 3, 5, 7)	FET	(non) polar VOCs	0.01 - 0.08 p$_a$/p$_o$ (mc)	76
		2015	TD (n)	~500 nm (w)	Bare	FET	Ethanol	10 - 2000 ppm (mc)	68
		2015	TD (n)	16 - 46 nm (w)	Bare	FET	Ethanol	100 ppm (s)	69
		2015	BU (p)	40 ± 8 nm (d) 8.5 ± 1.5 μm (l)	Silane/ Silane-chloride	FET	Gastric cancer VOCs	5 - 150 ppb (mc)	78
		2016	TD (p)	45 nm (w) 10 μm (l)	Bare	FET	Ethanol hexane	0.1 - 0.8 p/p$_o$ (mc)	70

a) TD: top down, BU: bottom up, p: positive type doping, n: negative type doping; b) w: width, l: length, d: diameter, g: gap between two electrode contacts; c) Func.: functionalization; d) Princ.: principle; e) s: sensitivity, mc: measurement concentration; *) no doping, but show n-type behavior; &) type of doping not reported, but deduced from the sensor response data; #) non-doped; 1) GQDs: graphene quantum dots; 2) EBTAM: 3-(4-ethynylbenzyl)-1, 5, 7-trimethyl-3-azabicyclo[3.3.1] nonane-7-methanol; OTS: octadecyltrichlorosilane; 3) PTE: porous top electrode; 4) DPCP: diphenyl chlorophosphate; 5) APTES: 3-aminopropyltriethoxy silane; 6) TABINOL: 3-(4-ethynylbenzyl)-1, 5, 7-trimethyl-3-azabicyclo [3.3.1] nonane-7-methanol; 7) APTES-modified SiNW were reacted with acyl chlorides to form amides; 8) TNT: 2,4,6-trinitrotoluene; 9) DMMP: dimethylmethylphosphonate; 10) Sat. con.: saturated concentration; 11) p_a: VOC's partial pressure, p_o: vapor pressure.

2.2.1 Inorganic gases

2.2.1.1 Nitrogen Dioxide (NO_2)

The ability to accurately monitor the concentrations of NO_2 in the air is very important, because it is a potentially toxic gas that can lead to respiratory symptoms in humans and detrimentally influence the growth of plants.[12] In addition NO_2 (~0.01 ppm) can lead to the formation of ground-level smog and acid rain. The atmospheric concentration of NO_2 is typically around 0.01 ppm, while values above 0.65 ppm are reported to be very unhealthy by the U.S. Environmental Protection Agency.[13] In 2007, Heath and co-workers reported a study on a NO_2 sensor based on Si NWs, made by transferring hundreds of pre-aligned, top-down prepared silicon nanowires from a silicon-on-oxide (SOI) wafer onto plastic.[14] Layers of deposited Ti and SiO_2 were used to fabricate source/drain contacts and a gate, respectively. Fig. 2.1a presents a schematic illustration of the active area of thin-film transistors (TFTs) made by this so-called superlattice nanowire pattern transfer (SNAP) approach, while Fig. 2.1b gives a Scanning Electron Microscope image of the sensor platform and a photograph of the flexible sensor chip. The changes in the nanowire resistance were measured and further analyzed when sensor chips were exposed to NO_2 and also a series of VOCs in nitrogen. Fig. 2.1c shows the normalized response of a Si NW sensing element to different NO_2 concentrations, clearly showing that NO_2 concentrations down to at least 20 ppb can be detected. It was concluded that due to the strong electron-withdrawing capabilities of NO_2, the withdrawing of electrons from the p-type Si causes hole accumulation and thus an increase in its conductance, when it is exposed to NO_2 in nitrogen. In these experiments the nanowires had a 25 nm thick SiO_2 layer as a gate dielectric.
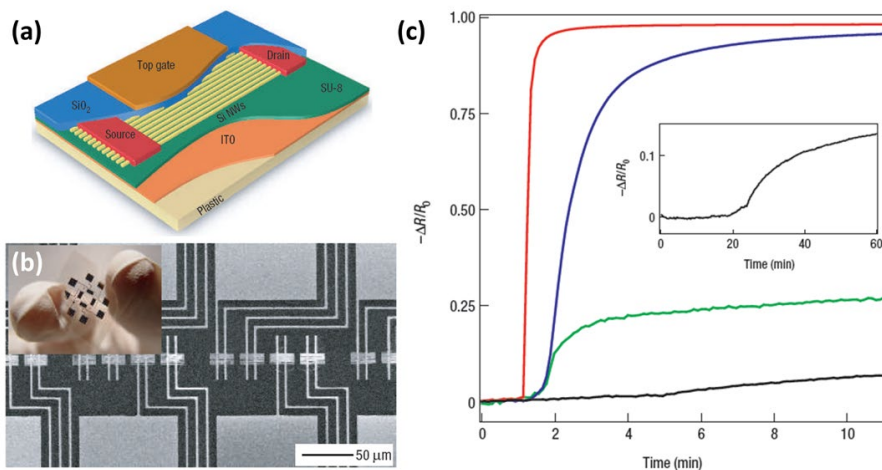
Figure 2.1 Electrical characterization of nanowire thin-film transistors on plastic. **(a)** Schematic illustration of the active area of a transistor, with the electrodes and various layers labeled. **(b)** Scanning Electron Microscope image of the sensor platform. Each device (horizontal strip) is contacted by two Ti electrodes (oriented vertically) that extend to larger pads (top and bottom image edges). Inset: Digital photograph of the flexible sensor chip. **(c)** Electrical response of a nanowire sensor to 20 ppm (red curve), 2 ppm (blue curve), 200 ppb (green curve) and 20 ppb (black curve) NO_2 diluted in N_2. The gas is introduced to the sensing chamber after 1 min of flowing N_2. Inset: An extended response of the sensor to 20 ppb NO_2; the gas is introduced after 20 min of flowing N_2. This figure is composed of figures taken from reference 14, reprinted with permission from the Nature Publishing Group ©.

The SiO_2 surface was also modified using silanization to obtain aldehyde-, alkane- and amino-terminated layers. By this way a 'nano-electronic nose' library was built, and the devices were found to be capable to distinguish low concentrations of acetone and hexane vapors via an analytical mapping of the array response patterns. The authors report that the mechanism of these responses may result simply from vapor-wire dipole-dipole effects, but could also involve dehydration of the surface, displacement of adsorbed oxygen and/or changes in surface-charge screening. To conclude, this interesting combination of highly sensitive Si NWs and flexible plastic support could open up opportunities in portable, wearable or even implantable sensors.

Soon after, a series of three studies from the Fudan University and the Rutherford Appleton Laboratory was published on different fabrication strategies p-type Si NW-based sensors for the detection of NO_2. All studies are based on a bilayer (SU8/PMMA) or trilayer (SU8/SiO_2/PMMA) nanoimprint lithography, which was combined with different processes steps, including reactive ion etching (RIE)

process,[15] or wet etching,[16] and angle deposition.[17] In the case of the wet-etching approach the cross-section of the Si NWs was trapezoidal, while in the other cases rectangular cross section were obtained. In all cases the silicon nanowires are covered with SiO_2 and a photolithography step was taken to define the Al contact pads. The resulting devices have been analyzed as a resistor (so no gate). In more detail, changes in the current have been recorded upon changing the environment of only N_2 to 250 ppm NO_2 in N_2. It is noted that only this concentration was used and that –in contrast to McAlpine *et al.*– the system was not tested for lower NO_2 concentrations. The detection mechanism was explained along the lines of the study of the Heath group: the exposure to NO_2 lead to an increase in the hole concentration, in the region near the surface of the p-type Si NW due to its electron withdrawing properties. In all three studies, two different Si NW widths were compared and in all cases a higher sensitivity was observed for the smaller width.

In 2012 Cuscunà *et al.* reported an alternative on-chip fabrication method for devices with Si NWs, and tested the detection of NO_2.[18] While most bottom-up approaches for the Si NW-based sensors usually need the processes of removing and transferring the Si NWs from the growth substrate to another support, they exploited Si NWs directly grown onto a selected area, over and between pre-patterned, interdigitated Cr/Al electrodes defined on oxidized silicon wafers (Fig. 2.2). Subsequently, the Si NWs were modified with amino groups by plasma polymerization after removal of native oxide by etching. It was shown that the introduction of amino functionalities highly enhanced the capability to detect NO_2, and even more in a humid environment (50% RH). This was rationalized by the authors as follows. Amines have a basic nitrogen with a lone pair capable to bind to strong electron withdrawing molecules like NO_2. An electron transfer from the modified surface to NO_2 is established, causing changes in the electrical conductivity. The authors believe that NO_2 can react with water, giving nitric acid (HNO_3), which provokes the strong interaction with the amino-terminated Si NW. What is not considered in this paper, however, is that the removal of the native oxide may also affect the device sensitivity as shown by Bunimovich *et al.*.[19] Furthermore it is stressed that this example makes use of a Si NWs network, rather than single Si NWs. The fabricated device had a close connection between the Si NWs and electrodes and a large number of NW-NW self-welded junctions (Fig. 2.2c, inset), which provided very high conductance and then made the sensor capable to achieve a detection limit down to a few ppb level. Based on these results, the authors concluded

that the extension to other gases is possible by exploiting the existing knowledge on chemical modifications of the Si surface.
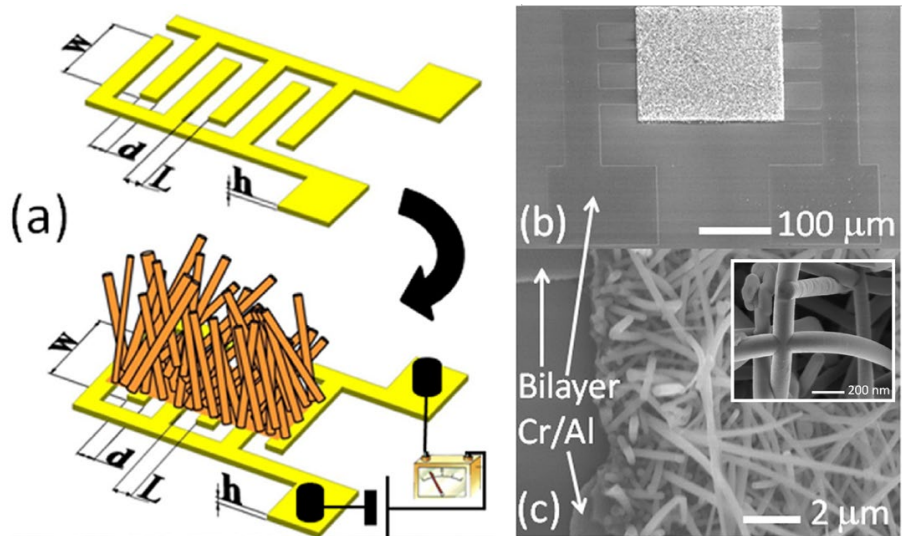

Figure 2.2 (a) A schematic representation of the interdigitated structure used as a substrate to grown Si NWs. W=200 μm, L=3-21 μm, h =100 nm, SEM images of **(b)** the final chemoresistive sensor and **(c)** Si NW network detail onto the interdigitated structure. **(c)** The inset shows SEM image of self-welding NW-NW junctions present in the Si NW network. This figure is composed of figures taken from reference 18, reprinted with permission from the American Institute of Physics ©.

In 2016, several studies have been reported on NO₂ sensing using top-down prepared SiNWs.[20-25] For instance, Liao *et al.* combined ZnO nanorods with porous SiNWs, and these heterostructures showed an enhanced sensing performance toward NO₂ in N₂ in the concentration range of 5 – 50 ppm, compared to the ZnO nanorods and porous SiNWs, individually.[23] Qin and co-authors reported the fabrication of WO₃ nanowire functionalized SiNWs.[25] This nanocomposite, prepared by metal-assisted chemical etching (MACE), showed an enhanced sensing response toward NO₂ compared to the bare SiNWs. This effect was attributed to the change in width of the space charge region between the SiNWs and WO₃ nanowires. Later on, they reported that porous SiNWs prepared by MACE were extremely sensitive to the presence of NO₂ as low as 50 ppb at room temperature.[21] Wang *et al.* investigated the impact of etching time of the MACE method on the specific surface area of the SiNWs and the performance of SiNW sensors toward NO₂ sensing.[20] Durand *et al.* reported the fabrication of so-called "3D SiNW networks" using conventional microelectronics tools, and the resulting device with a oxide surface was validated

for the detection of NO_2 down to ppb levels, in the presence of moisture or interfering gases CO and C_3H_8.[22] Selective NO_2 sensing was partially achieved in this case, as well as in the studies mentioned above, *i.e.* ZnO-SiNW, WO_3-SiNW and MACE-prepared SiNWs, while all the interfering gases were non-oxidizing. However, the response toward other electron-withdrawing gases are still missing from these studies. To protect the MACE-fabricated SiNWs against from oxidation and to promote the interaction between the SiNWs and NO_2, Li *et al.* studied core-shell structures of graphene quantum dots (GQDs)/SiNW array.[26] The resulting sensor exhibited high sensitivity for NO_2 detection and immensely reduced the recovery time (~ 60 sec for the (GQDs)/SiNW array *vs.* ~100 min for the silicon wafer).

Recently, Wu's group demonstrated that vertical SiNW arrays can be joined with each other at the tip ends by a Joule-heating treatment.[24] The tip-tip contacted (TTC) SiNWs not only resolved the problem of electrode contact encountered in conventional NW sensors, but also elongated the NW length, increasing the void space for fast gas diffusion. In their work, three types of TTC structures including p-p contact, n-n contact, p-n contact were constructed, and the sensitivity toward NO_2 was measured to be 150 ppb, 3 ppb and 18 ppb, respectively. Figure 2.3 summarized the mechanism of the gas sensing behavior on different types of TTC structures as proposed by the authors. Briefly, the electron withdrawal properties of NO_2 are believed to result in more holes in the valence band of p-p contact SiNWs (Fig. 2.3a), and less electrons in the conduction band of n-n contact SiNWs (Fig. 2.3b). Furthermore, for the p-n contact SiNWs, the interfacial junction plays an important role on the gas sensing; when the bias voltage is set to a forward direction (Fig. 2.3c), the barrier energy at the interface was reduced. Once the forward bias voltage exceeds the turn-on voltage, the resistance of the junction can be ignored. After being exposed to NO_2, opposite responses on p and n tips result in the offset of the resistance. In contrast, when a reverse bias voltage is applied on the p-n contact SiNWs, the resistance of junction becomes significant, the reverse current mainly relies on the electrons flowing through the depletion region at the tip interface (Fig. 2.3d). These electrons can be trapped by absorbed NO_2, leading to a big change in the reverse current.
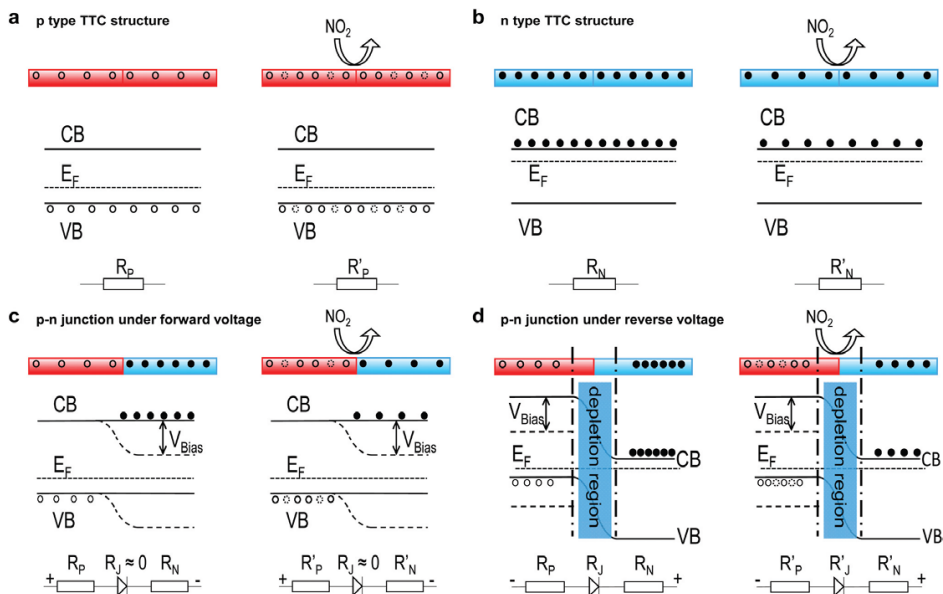
Figure 2.3 Schematics and energy band diagrams of different contact structures before and after being exposed to NO$_2$. **(a)** p-Type SiNW contact structure, **(b)** n-type SiNW contact structure, p–n homojunction under forward voltage **(c)** and reverse voltage **(d)**. (●, electron; ○, hole). This figure is composed of figures taken from reference 24, reprinted with permission from The Royal Society of Chemistry ©.

2.2.1.2 Nitrogen Oxide (NO)

The detection of NO in patients is important, because changes in NO levels can be indicative of certain illnesses such as Alzheimer's or asthma.[27] Currently, chemiluminescence is commonly used for the detection of NO gas in a patient's breath.[28] While this technique is extraordinarily sensitive, with a detection limit of 300 ppt, the required instrumentation is large, expensive, and needs various supporting accessories, such as vacuum pumps and an ozone generator. There is a need to develop new NO gas sensor with sturdier, scalable production and cost effectiveness. Lee's group reported a NO sensor based on porous n-type Si NWs prepared by metal-assisted chemical etching method.[29] NO was detected in dry, synthetic air. In this report, the reaction of NO oxidization into NO$_2$ with O$_2$ is very low yield at low NO concentration, then NO could be adsorbed by high-density vertically aligned porous Si NWs, and charge transferred from NO to Si NWs assembly because of the strong electron-donating power of NO molecules, as a result, increasing electron carriers and conductance of Si NW assembly. The sensor made from porous Si NWs shows fast response and excellent reversibility to sub-ppm NO concentrations. The interference of other gases has also been investigated and the as-

prepared devices showed a small resistance for NH_3 (at 3000 ppm) and little resistance changes upon the exposure to benzene, methanol, ethanol and other (non-specified) organic vapors of which structures and data are presented in the paper. While the mechanism is not discussed NO seems to be the smallest molecules tested, so possibly a size-exclusion effect in the porous structure can explain the selectivity. Recently, Han and co-authors reported a novel chemically gated FET based on SiNWs modified with SnO_2.[30] The potential change induced by the molecular adsorption and desorption (e.g., NO, O_2, NH_3) allows the electrically floating SnO_2 layer to gate the silicon channel. A limited selectivity was achieved, as the device was designed to be normally off, it only responded to one type of gas (reducing or oxidizing gas). P-type SiNWs could only be turned on by the reducing gases, since a negative potential was induced upon the presence of the gas while the SnO_2 sensing layer accepted electrons from the reducing gases. Most importantly, the normally off-state of the device makes it useful for the low-power applications.

2.2.1.3 Hydrogen (H_2)

Hydrogen is used in many industrial processes such as hydrogenation, petroleum transformation, cryogenic cooling, and chemical production. As H_2 is odorless, colorless, and flammable at concentrations over 4%, it poses safety concerns and creates a need for effective H_2 leakage sensors with a lower limit of detection (LOD) to identify small leaks. A review on electrochemical H_2 sensors by Korotcenkov *et al*.[31] also suggest the need for cost effective, low power, and compact sensors with a long-term stability, minimal cross-sensitivity and fast response.

Many H_2 sensors reported to date are based on the selective absorption of H_2 by palladium, which results in the reversible formation of palladium hydride (PdH_x), changing the electrical and optical properties of Pd. Bare Si NWs do not show appreciable sensitivity to H_2, so efforts have been made to find suitable functionalization schemes to decorate Si NWs with H_2-sensitive materials. The Lee group built a Pd-functionalized Si NWs based sensor for H_2 detection.[32] Si NWs were grown and their oxide layer was removed by immersion in hydrofluoric acid, then dipping into a saturated palladium chloride ($PdCl_2$) solution to form a coating of Pd nanoparticles. The most applied method to reduce Pd^{2+} ions is by the addition of a reducing agent, e.g. ascorbic acid. Here the authors conclude that surface groups (*i.e.* Si-H) act as a reductor. The modified Si NWs were subsequently dispersed onto a silicon wafer with a 300 nm oxide layers. Gold electrodes were deposited and *I-V* measurements were carried out with a two-probe analysis system. Upon exposure to

5% hydrogen, the current signal of the sensor increased about 20 times. The response time was three seconds only, which is much faster than that of the macroscopic Pd wire sensor. The sensing mechanism was explained by the Fermi level modulation upon chemical absorption of H_2 in Pd nanoparticles that leads to the band diagram change at the metal-semiconductor interfaces.

To combine the benefits of Si NW sensors with the high performance reported for Schottky-based bulk sensors, Skucha *et al*. worked on the design, fabrication, and characterization of a H_2 sensor based on a Pd/Si NW Schottky barrier field-effect transistor (SBNWFET).[33] To form an array, grown Si NWs were contact printed on top of a SiO_2/Si substrate and subsequently Pd contacts were prepared via an evaporation method (Fig. 2.4a). This elegant architecture allows bi-directional sensing and, moreover, makes use of the contact pads as an affinity layer. Under ambient conditions an Ohmic contact forms between Pd and Si (Fig. 2.4b). Hydrogen adsorbs dissociatively on Pd to from hydrogens atoms (rather than H^+ ions as the authors erroneously report), which thereafter diffuse into the Pd contacts and are believed to settle at the Pd/NW interface. These interface charges induce a dipole layers and cause the work function of the metal to effectively decrease (Fig. 2.4c). Eventually this leads to the formation of a Schottky barrier, which impedes holes from crossing over from the metal to the NW at the reverse biased source contact, which –in turn– limits the current flow. This sensor achieved significantly higher sensitivity than (nano)sensors based on other sensing principles and enabled reliable detection of H_2 concentrations down to 5 ppm due to its low drift. The authors speculate that the printing process can be extended to other types of nanowire sensors either by functionalizing printed Si NWs with receptors (as in the case for DNA or protein sensing) or by heterogeneously printing different types of nanowires that are naturally selective to other gaseous or chemical agents.
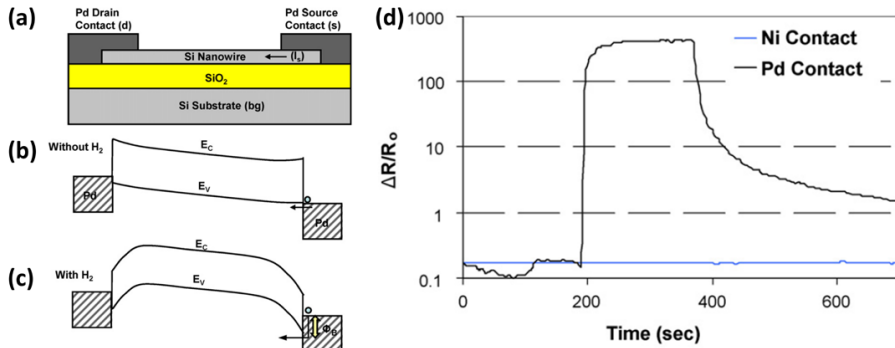
Figure 2.4 (a) Schematic of the SBNWFET, consisting of p-type doped nanowires; **(b)** Energy band diagram before H_2 is introduced, where E_C and E_V stand for the energy levels of the conduction and valence band, respectively. The holes do not experience a barrier and the contact is Ohmic. The native SiO_2 layer is omitted in this diagram because it is too thin to affect transport; **(c)** Energy band diagram after hydrogen is introduced, showing a formation of a Schottky barrier; **(d)** Comparison of the responses of Ni and Pd contacted NWFETs to 1% H_2. This figure is composed of figures taken from reference 33, reprinted with permission from the Elsevier B.V. ©

An overwhelming majority of the Si NWs-based electrical devices consist of in-plane orientated Si NWs. Also, typically contact pads are prepared on each terminal side of the NW. However, Lee and co-workers reported a non-classical sensor that is made with Pd-coated, vertical-standing, rough Si NWs, which showed an excellent performance in sensing H_2 in air.[34] Using a top-down, electroless Si etching method, they achieved vertical-standing Si with a controllable density. The NWs were reported to be rough, but the roughness was not quantified. Pd was then sputter-deposited only on the upper part of the Si NWs in the semi-dense configuration to avoid electrical short cuts between the two on-top electrodes, which were made using a silver paste (Fig. 2.5c1). The Pd-coated Si NWs showed good reversibility and excellent H_2-sensing performance in terms of detection limit (~5 ppm) and response time (<3 s). Figure 2.5a shows the real-time electrical responses of the sensor to varying H_2 concentrations in air at room temperature, and top-down plot is the sensitivity vs. H_2 concentration, which reveals an interesting variation between the low and high H_2 concentration ranges. The authors propose a model for this unusual finding: in the high H_2 concentration range (regime II), the current flows through the Pd film deposited on the top region of the nanowires, as the nearest nanowires are connected by a rather large volume expansion of the Pd film after H_2 absorption. In the low H_2 concentration range (regime I), it is hard to make a contact between

neighboring Si NWs with relatively large distance between them. This is due to the smaller volume expansion of the Pd film, resulting in a smaller conductance increase. It is proposed that the current paths are now activated by the bridging effect of some slanted Si NWs. Thus, according to this proposed model, the slope in regime I is higher than in regime II based on the rationale that the current conduction is limited by gaps between Si NWs, and the slanted Si NWs acted as conduction bridges.
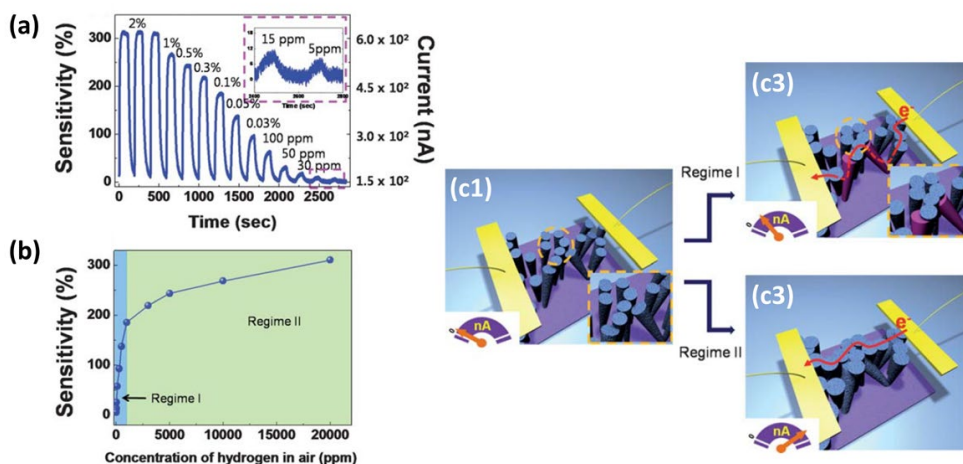

Figure 2.5 (a) Real-time electrical response curve of a device with vertical-standing Si NWs coated with a 7 nm thick Pd film to varying H_2 concentrations in air at room temperature. The inset shows clear response behaviors even at very low H_2 concentrations down to 5 ppm. **(b)** A plot of sensitivity vs. H_2 concentrations revealing two regimes with different rates of sensitivity change. **(c)** A proposed model of the hydrogen-sensing mechanism. Panel **(c1)** represents the initial devices with Pd-coated Si NWs with two on-top electrodes as indicated by the yellow lanes. The inset of the left panel shows a magnified distribution of Si NWs inside a cluster, indicating that the wires do not touch each other. Panel **(c2)** illustrates nanowire contacts inside clusters with gaps between neighboring clusters. In this case, the current flows through slanted nanowires between clusters. The inset is a magnified picture of contacted distribution of Si NWs inside a cluster. Panel **(c3)** illustrates the formation of current paths between neighboring clusters by large volume expansion of the Pd film caused by absorption of high concentrations of H_2. This figure is composed of figures taken from reference 34, reprinted with permission from The Royal Society of Chemistry ©.

Another study on Si NW gas sensing application reports on the selective surface modification of the Si NWs that are part of an array.[35] The topic of selective Si NW modification was already addressed by Bunimovich *et al*. who made use of hydrosilylation chemistry to modify the surface of Si NW on a device, leaving the SiO_2 areas in between the wires untreated.[19] Yun *et al*. introduced a novel method for the selective surface modification of Si NWs based on nanoscale localized Joule heating.[35] In the method, the Joule heating generated a localized heat along the Si

28

NW enabling endothermic reactions. Two different selective surface reactions were explored: hydrothermal synthesis of Pd nanoparticles and the thermal decomposition of polymer thin films to unmask one nanowire specifically before further modification (Fig. 2.6a, methods 1 and 2, respectively). Both types of devices were exposed to 0.5% H_2 mixed with air show the presence of Pd nanoparticles via measuring the nanowire resistance. Since this method does not require a tedious alignment process for selective and localized surface modification, the authors expect that an integrated and multiplexed nanowire sensors can be easily developed by using their method.
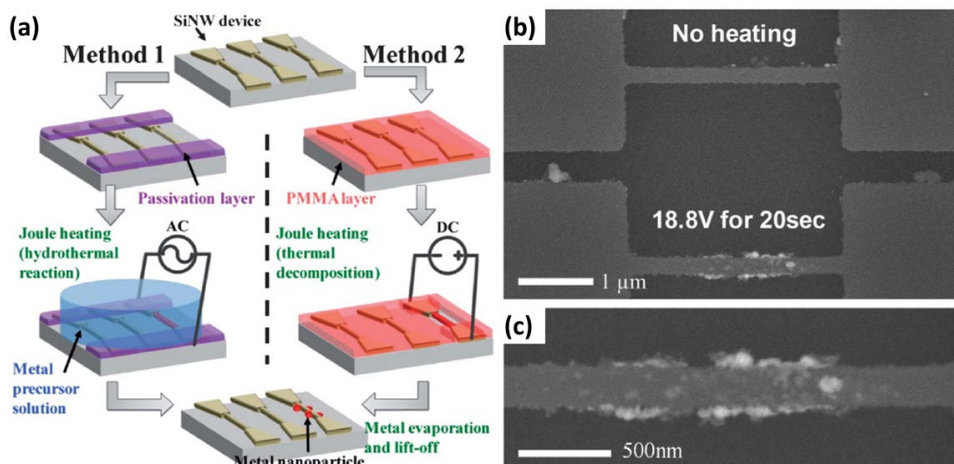

Figure 2.6 (a) Schematic description of surface modification by self-heating of a nanowire: in method 1, nanoparticles were formed by hydrothermal reaction via Joule heating of a Si NW. In method 2, a metal thin film was locally deposited on a Si NW through PMMA decomposition, metal evaporation and lift-off. SEM images of the nanoparticle decorated Si NW via Joule heating in a liquid metal precursor environment: **(b)** Pd nanoparticles selectively coated on the heated Si NW and **(c)** high magnification SEM image of Pd nanoparticles on the heated Si NW. This figure is composed of figures taken from reference 35, reprinted with permission from The Royal Society of Chemistry ©.

In 2013, Huang *et al*. reported rice-straw-like SiNW arrays for H_2 sensing. The novel structure was formed using a repeated etching technique after the fabrication of SiNWs using the MACE method. The resulting sensor showed a better response (~2.5 times higher) than the straight-aligned SiNW arrays, thanks to the increased NW surface area with additional binding sites for the gas molecules.[36] Three years later, the Qin group reported arrays with rough SiNWs for H_2 sensing. In their study, KOH etching was utilized as the post-treatment, instead of repeated MACE on the

smooth SiNWs as made by a one-step MACE. While the range of detection concentration was very similar for these two types of etched sensors, rice-straw-like SiNWs showed low responses to the interfering gases N_2, O_2, and CO_2. However, a selectivity test among the same type of reducing gases was not included in this study. For the SiNWs roughened by a KOH method, the selectivity was proved to be good after the exposure to other five reducing vapors (acetone, methanol, methane, ethanol, and isopropanol).[37] In order to deposit a uniform electrode on the tips of vertically aligned SiNW arrays, the Choi group employed graphene as a barrier layer to form an electrical junction between the SiNW arrays top and graphene. The graphene/SiNW heterostructures combined the advantages of both materials and yielded Schottky-diode behaviour that acted well as a molecular sensor under H_2 or O_2 exposure.[38]

In 2014, Park and co-workers fabricated a H_2 sensor based on Pd NPs-modified SiNWs, exceptionally with two side-gates.[39] The hydrogen sensitivity was achieved due to Pd NPs functionalized on the SiNW surface and two local side-gates. These two gates allowed individual addressing of the sensor and adjusting the working region to the subthreshold regime. Catalytic layers such as Pd NPs are important for the H_2 sensing, but the detailed effect of Pd NPs on the electrostatic properties of SiNW-based FET was hardly investigated. Therefore, Park, Choi and co-workers conducted an in-depth analysis of the electrostatics of Pd NP decorated-SiNW-based FETs.[40] By comparing the experimental results with numerical simulations, the authors concluded that the improvement of the electrostatic properties (e.g., the subthreshold swing and on-current) of the sensor is due to the coupling effect between the electrostatic potentials in the Pd NPs and those of the bottom gate. This study is important in predicting the electrostatics of SiNW-based FET for the detection of various gases when alternative metal NPs are used as the affinity layer.

Furthermore, Ahmed *et al*. proved that resistor-based NWs modified with NPs of various noble metals, such as Pt, Pd, Ag and Au, showed different performances in H_2 sensing, which can be rationalized by the metal-dependent catalytic activity toward hydrogen and metal-dependent work function.[41] The modification of the various metal NPs on the SiNWs was easily realized using a so-called electroless metal deposition (EMD) method in aqueous HF solution containing a metal salt (e.g. $AgNO_3$, $PdCl_3$, $AuCl_3$, PtO_2). The sensing results demonstrate that the modification improves considerably the response of the sensor, in particular with Pt NPs, while Ag NP and Pd NP-modified devices gave a slower response and lower recovery for H_2 sensing. To enhance the response and recovery performances of the Pd NP-

modified SiNWs, Park and co-workers fabricated a self-heated device.[42] The self-heated sensor also reduced the influence of interfering gases such as water vapor and CO_2. A short-pulsed heating step during recovery was found to be effective for the additional reduction of operation power, which is important for ultralow-power applications such as needed in telecommunication devices and wireless sensing nodes.

2.2.1.4 Other gases

Development of gas sensor technology has led to significant progress in pollution control and environmental protection. An excellent example is the control of automobile exhaust emissions, made possible by the use of oxygen gas sensors.[43] Since the early 1970's there have been sustained studies on oxygen sensors. In 2012, the very first O_2 sensor based on SiNWs was reported by the Lee group. The researchers constructed an air-bridged Ohmic contact on vertically aligned SiNWs.[44] A thin suspended polymer layer was formed on the uppermost part of the vertically aligned SiNWs, by performing partial impregnation on SiNWs using polystyrene (PS) at its glass transition temperature. Then an oxygen plasma step was performed to etch away the top layer of PS and expose the tips of the SiNW. Finally, a sputter deposition of Au on the PS barrier was conducted to get the air-bridged top metal contact. Although information on the concentration range of O_2 detection and the LOD of the molecular sensor is missing in the report, the resistance of the p-SiNW array-based sensor promptly decreased and increased in the presence and absence of O_2 molecules, respectively.

One of the most important gases for environmental monitoring and in medical applications is CO_2. Currently CO_2 sensors are used to monitor the indoor air quality and in capnography - that is the measurement of CO_2 in respiration during medical treatment. For these applications, the current main technology is infrared spectroscopy, but its application is limited by its high power consumption and large instrumental size.[45] Therefore, more simple CO_2 sensors with a low power consumption are of great importance. Very recently, Naama *et al*. showed that noble metal NPs (Au NPs and Pt NPs)-modified SiNWs can be used for CO_2 sensing.[46] The modification of the SiNWs with metal NPs was the same as in the report of Ahmed, using the EMD method of fabrication. Similarly, the sensor response depends strongly on the type of metal. While the Pt-modified structure behaved as an Ohmic contact, the Au modified device exhibited rectification properties, which means a Schottky structure was obtained. These results showed that the Schottky structure was more sensitive to CO_2 gas than the Ohmic structure. The high

sensitivity was attributed to the fact that the forward current in the Schottky structure was strongly influenced by the change in barrier height at low bias potential; exposure to CO_2 gas reduced the Au NPs work function as well as the barrier height.

2.2.2 Inorganic vapors

2.2.2.1 Ammonia (NH_3)

Ammonia (NH_3) is primarily a concern in areas of high agricultural activity, because it is a natural waste product of livestock. Industrial sources include the manufacturing of basic chemicals, metals, textiles, and paper products as well as automotive emissions. High levels of NH_3 can result in irritation of the eyes and respiratory tracts of humans and can negatively impact wildlife, livestock, and agricultural health.[47]

In 2003, Lee and co-workers demonstrated the potential of Si NW-based gas sensors when they reported on the electrical response of Si NWs bundles to NH_3 and water vapors in N_2.[48] This work is the first example of applying Si NWs in an electrical sensor device for gas sensing purposes. It has to be noted though that in this study no single wires, but bundles of Si NWs have been used. Bundles of etched and non-etched Si NWs were made by pressing wires (~0.4 mg) onto a surface of glass. Two electrodes were made by applying Ag glue at the two ends of the bundle. The spacing of the two electrodes was as large as 5 mm. The non-etched Si NWs hardly show any changes in electrical resistance after the adsorption of NH_3 and H_2O molecules, because of the amorphous silicon oxide shell on the surface of Si NWs formed during the nanowire preparation. The etched Si NWs were exposed to air, allowing the formation of native oxide. As compared to the oxide layer formed at high temperature during the Si NW growth, native oxide is less uniform and much thinner, explaining the large sensitivity difference in resistance between the etched and non-etched Si NWs.

Subsequently, several research groups have focused on improving the response to NH_3 of sensors composed of Si NWs without any chemical functionalization. For example, Kamins and *et al.* fabricated metal-catalyzed, p-doped Si NWs bridging two Si electrodes and exposed them to vapors containing NH_3 or HCl at reduced pressure.[49] The current was measured in the dark at an applied voltage of 0.1 V. Exposure to NH_3 resulted in a reduction of the conductance due to the adsorption of positively charged species (NH_4^+) on the nanowires, which decreases the density of positive mobile carriers, *i.e.* holes in the case of p-type devices). In the case of HCl the conductance increased, which was attributed to the adsorption of Cl^- ions. The

32

researchers also used additional nanowire structures as reference devices that are protected from the analyte. From the work it is not clear how this exactly was realized, but at least it is one of the few papers on SiNWs and gas sensing that is addressing the issue of reference sensors. It is believed that one reference may serve a group of sensors, which would limit the area needed for these reference devices. Furthermore, Talin *et al*. reported a Si NW array transistor, made by a top-down technique based on nanoimprint lithography (NIL).[50] When exposed to ammonia gas or cyclohexane solutions containing nitrobenzene or phenol, the threshold voltage of the field-effect transistor shifted. This shift was found to be proportional to the Hammett parameter (*i.e.* a parameter related to the electron donating or electron withdrawing character of the substituents on the benzene ring) and the concentration of the nitrobenzene and phenol analytes. In addition, Pichon's group developed two bare Si NWs based-resistors for ammonia and smoke detection, and the two types of non-intentionally doped Si NWs are fabricated by the vapor-liquid-solid (VLS) growth technique (which is a bottom-up approach) and the sidewall spacer realization (which is a top-down approach), respectively.[51] Later on, they investigated the effect of n-type doping on VLS-made SiNWs for NH_3 sensing.[52] The results showed that the relative sensitivity decreased, whereas the absolute sensitivity increased upon increasing doping levels. This was attributed to a decrease of ammonia adsorption with higher doping levels. They concluded that the doping level of the SiNWs should be optimized for the detection of ammonia in a given concentration range.

Since the biosensors can exploit well-established "lock-and-key" interactions to achieve high selectivity, Heath's group developed novel Si NWs-based sensors modified by peptides for the selective detection of ammonia and acetic acid vapors.[53] First, the Si NWs were fabricated by superlattice nanowire pattern transfer (SNAP), and treated with O_2 plasma, then immersed in the surface modifying reagent 3-aminopropyltrimethoxysilane (APTES) solution to realize amine-terminated Si NW surfaces (Fig 2.7a, left). Next, oligopeptides with the desired recognition sequences (NH_3 and CH_3COOH) were synthesized, and coupled to the APTES-modified Si NWs (Fig. 2.7a, right). Upon exposure to NH_3 and acetic acid vapors, the hybrid materials demonstrated the ability of discriminating the target molecules at low concentrations from, what the authors call "chemically camouflaged" mixtures. The electrical responses are given in Figs. 2.7b and 2.7c. It was concluded that the results serve as a model platform for what can be achieved in terms of selective and sensitive "electronic noses".
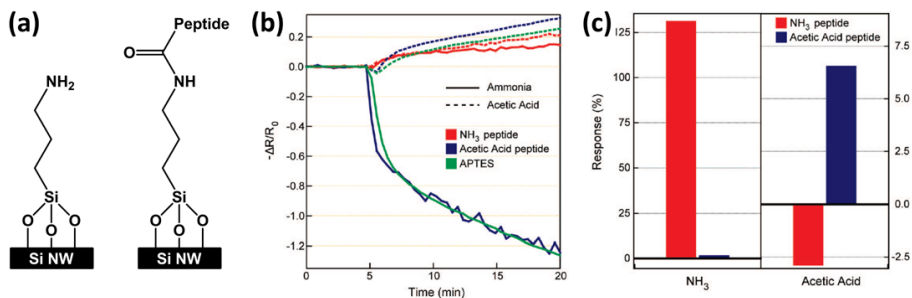
Figure 2.7 (a) Schematic representation of the (left) APTES- and (right) peptide-modified Si NW surface. Note that two different peptides have been used, *i.e.* an ammonia recognition peptide and an acetic acid recognition peptide. **(b)** Electrical responses of the three different devices (APTES, NH_3 peptide and acetic acid peptide) to ammonia and acetic acid vapors (100 ppm in N_2) introduced to the sensing chamber after 5 min of flowing N_2. **(c)** Conductance responses of the peptide-nanowire hybrid sensors, averaged over a 5 min time window of target vapor exposure (starting 10 min after the analyte gas exposure), and normalized to the amine-terminated sensor. The abscissa is labeled with the analyte vapors. Figures **(b)** and **(c)** are taken from reference 53, reprinted with permission from American Chemical Society ©.

To realize high sensitivity of gas sensing, In *et al*. reported a novel method to fabricate ordered arrays of vertically aligned Si NWs provided with a periodically porous top electrode.[54] Two separate nanosphere lithography steps were used to fabricate large, well-ordered arrays of vertical nanowires and then fabricate a periodically porous top electrode (PTE) that makes consistent electrical connections to every nanowire in the array (Fig. 2.8a). And PTE is an electrode layer lying on top of the nanowire array that is packed with uniform holes of controllable size and distribution. Fast and highly sensitive detection of NH_3 and NO_2 in humidified air using the PTE nanowire array sensor configuration is demonstrated (Fig. 2.8b). NO_2 detection down to 10 ppb is demonstrated and an order-of-magnitude improvement in sensor response time is shown in the detection of NH_3. The authors attributed the high sensitivity to the novel vertical array configuration, which helps to greatly increase the sensitivity of the sensor while the pores in the top electrode layer significantly improve sensing response times by allowing analyte gases to pass through freely.
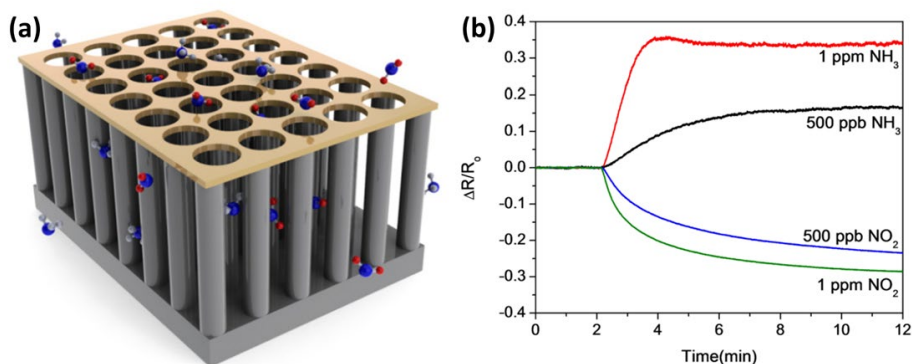
Figure 2.8 (a) Schematic illustration of the periodically porous top electrode (PTE) nanowire array sensor concept. **(b)** Sensor response to various concentrations of NO_2 and NH_3 following 2 min of clean air: 1 ppm of NH_3 (red), 500 ppb of NH_3 (black), 1 ppm of NO_2 (green) and 500 ppb of NO_2 (blue) at ~30% RH. This figure is composed of figures taken from reference 54, reprinted with permission from IOP Publishing Ltd ©.

Tellurium, an intrinsic p-type semiconductor with a band gap of 0.35 eV, has been used in various sensing applications for different gases,[55] such as NH_3, Cl_2, NO_2, NO and CO_2. To combine the advantages of tellurium (Te) with those of SiNWs, Shao and co-workers recently constructed TeNP-modified SiNWs for the detection of NH_3 and propylamine. The TeNPs, decorated on SiNWs made by a BU approach, were found to be 5 nm in diameter. The surface modification was realized by immersing the HF-etched SiNWs into a Na_2TeO_3 aqueous solution. The resulting device was sensitive for NH_3 and propylamine in the range of 10-400 ppm and 5-25 ppm, respectively.

2.2.2.2 Humidity (H_2O)

Humidity sensing is an important field for chemical sensors which have been used extensively in our daily life, since the humidity sensors can monitor the environmental moisture for human comfort and can also be used in automotive, medical, construction, semiconductor, meteorological, and food processing industries.[56] As a semiconductor material, Si can be used for humidity sensing, since free carriers (holes) in porous Si are highly depleted after the adsorption of water vapor. Hsueh *et al*. reported Si NWs based humidity sensors, and the Si NWs grow directly on the glass substrate by low temperature VLS process.[57] The Au layer on the top of NWs made the intentional non-doping Si NWs behavior p-typed, then the measured current decreased monotonically as they increased the relative humidity from 30% to 95%. These results suggest that Si NWs prepared on glass substrate are potential useful as a cost-effective alternative for humidity sensing. Meanwhile,

Passi *et al*. fabricated single crystalline Si NWs using top-down approach, and studied the transfer characteristics and sensing properties of the Si NWs with and without surface functionalization under ambient conditions.[58] And to reduce the adsorption of H_2O molecules onto the surface of Si NWs, surface modification is done by grafting either 3-(4-ethynylbenzyl)-1, 5, 7-trimethyl-3-azabicyclo (3.3.1) nonane-7-methanol (EBTAM) on H-terminated Si surfaces, or octadecyltrichlorosilane (OTS) onto native oxide formed on the Si NWs surface. Then the reduction of hysteresis is observed, which indicates the importance of functionalization in order to avoid any environment effect on the transport properties of the Si NWs.

2.2.3 Organic compounds

2.2.3.1 Explosives

With the increased threat of terrorist activity, there is an unfortunate need for the detection of chemical vapors indicative of malicious intent. One of the most commonly used high explosives in the past years is 2,4,6-trinitrotoluene (TNT). TNT does not only poses a security threat, but it is also of great environmental concern because of soil and water contamination. However, the low volatility of most explosives makes it challenging to develop and integrate methods to detection traces of explosives. One of the lowest detection limits for TNT (as low as 10^{-2} ppt in air) was realized by the Patolsky group using large-scale arrays of Si NW-FET devices. The devices were chemically modified with 3-aminopropyltriethoxy silane (APTES) to obtain an amine-terminated layer.[59] The thickness of the APTES layer was found to be ~6.5 to 12 Å, *i.e.* between a monolayer and a bilayer. The authors note that the structure and thickness of APTES films indeed are governed by the deposition time and the composition of the silane solution.[60] No attempts to prepare a true APTES monolayer were reported here. The authors continue their work by describing two kinds of strong (reversibly) interactions may occur between the electron-deficient aromatic ring of TNT and the electron-rich amino group of APTES (Fig. 2.9a, inset). First, the charge transfer from amino groups to aromatic rings leads to the formation of so-called Meisenheimer complexes. Second, a TNT molecule is a Brønsted-Lowry acid, which can be deprotonated at the methyl group by a basic amine. In both cases charges are formed near the sensing surface, thus leading to abrupt changes in the conductance of the device. The cross-reactivity of the devices was studied using structurally related compounds (Fig. 2.9b). The results clearly show a strong preference for binding TNT over other similar compounds (Fig. 2.9a). It should be noted that all these experiments were performed using 0.1% DMSO/H_2O

36

solution of the compounds. In a final experiment it is shown that TNT can also be detected directly in air at low concentrations of TNT (between ppb and ppt concentrations), with unprecedented sensitivities down to at least 10^{-2} ppt in air.

In 2012, Wang and co-workers reported a chemiresistive device based on arrays of hydrogen and oxygen plasma-treated Si NWs for the detecting the vapors of common nitro explosives and their degradation by-products.[61] The following compounds were tested: DNT (2,4-dinitrotoluene), TNT (2,4,6-trinitrotoluene), RDX (cyclotrimethylenetrinitramine), PETN (penta erythritol tetranitrate), picric acid (2,4,6-trinitrophenol) and an explosive degradation by-product, 2-nitrotoluene. In their work, the width of nanowires was varied (100, 200 and 400 nm). The sensitivity –defined as the relative resistance change due to the presence of chemicals– was found to increase when the cross-section of the nanowires decreases. Both plasma treatments can significantly improve the sensitivity and response times. This was explained by its cleaning effect providing more adsorption/binding sites for the target molecules. It was further rationalized by the authors that in the surface Si-OH group that are formed upon the oxygen plasma treatment might form charge transfer complexes with the nitro groups of nitro explosives too strengthen the chemiresistive. Surface studies such as X-ray photoelectron spectroscopy (XPS) and Hall measurements at room temperature were performed on reference Si samples to confirm that oxygen plasma treatment changes the type of majority carriers from p to n and inverts the sign of the resistance change.
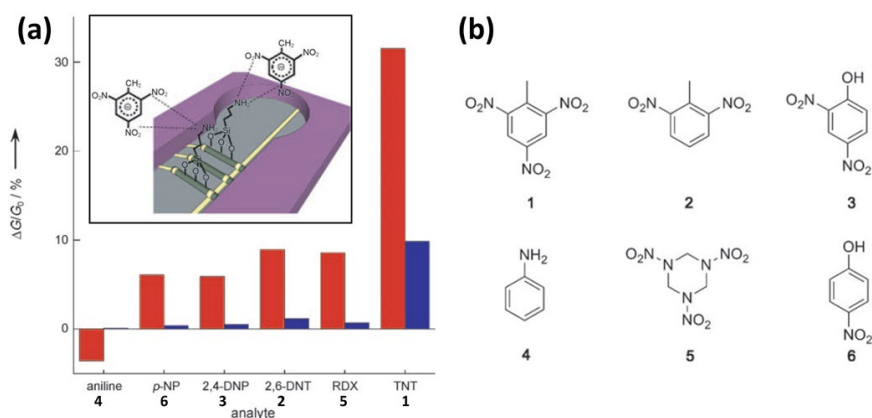

Figure 2.9 (a) The response of an APTES-functionalized SiNW device toward towards (red) 5 μM solutions and (blue) 5 nM solutions. The inset shows the two different kind of interactions between TNT and the NH₂-terminated SiNWs, **(b)** Molecular structures of six different N-containing compounds: TNT (1), 2,6-dinitrotoluene (2), 2,4-dinitrophenol (3),

aniline (4), 1,3,5-trinitroperhydro-1,3,5-triazine (5) and p-nitrophenol (6). Figure based on graphs taken from reference 59 and used with permission from Wiley-VCH©.

2.2.3.2 Nerve Agents

The ability to detect minute traces of chemical warfare agents (CWAs) is mandatory both for military forces and homeland security, since CWAs can be fatal even at low concentration levels. Towards the development of sensors for CWAs, specifically nerve agents, simulants are often used, such as dimethyl methylphosphonate (DMMP) and diphenylchlorophosphate (DPCP). Several groups have made efforts towards developing Si NWs-based sensors for nerve agents. In a very brief proceedings without any sensing data, Lee's group reports on the electrical detection of the vapor of DMMP in N_2 using a device with bare Si NWs in a resistor mode.[62] More interestingly, Simonato and Raskin and co-workers reported highly sensitive detection of DPCP (Fig. 2.10a, top) using chemically functionalized silicon nanoribbon FETs[63] and silicon nanowire FETs,[64, 65] respectively. In their work, the silicon nanostructures were fabricated and then functionalized by covalent grafting through thermal hydrosilylation of compound 1 onto the HF pre-treated substrates. This type of chemistry results in an organic monolayer that is linked via an stable Si-C bond. Compound 1 is known to react cleanly with DPCP to produce the so-called aza adamantane quaternary ammonium salt, compound 2 (Fig. 2.10b). Figure 2.10c shows the change in I_{DS} when a modified device is exposed to 500-800 ppb of DPCP in air. With the exception diClDPCP, the use of more than about 20 other VOCs, including DMMP, showed hardly any change in the drain current (see Fig. 2.10a for the structures of diClDPCP and DMMP). The absence of response in the case of DMMP was explained by the low chemical reactivity of DMMP with compound 1 due to the electron donating properties of the methoxy group.[64] In our opinion, another explanation may be related to a reaction between the P-Cl functionality and the primary alcohol of compound 1 to form an intermediate. This would also explain the absence of response for DMMP as a methoxy group is less reaction than Cl. Also, it would explain the sensor response of diClDPCP as it contains a P-Cl functionality just like DPCP.
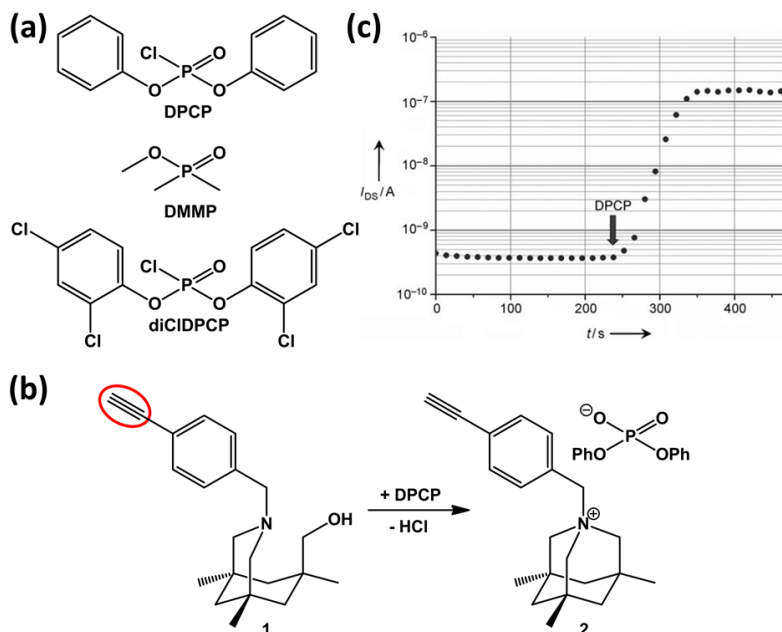
Figure 2.10 (a) Molecular structure of DPCP and two structurally related phosphates. **(b)** Sensitive receptor towards DPCP. Compound **1** converts into compound **2** upon exposure nerve agent simulant DPCP. The red oval indicates an alkyne group, which can react with H-terminated Si to form a stable Si-C bond. **(c)** Change in drain current of a SiNW FET device that has been modified with compound **1** upon the exposure to DPCP, which was introduced at t = 240 s. Figure **(c)** is taken with permission Wiley-VCH© (from reference 63).

The authors realize that apart from the positively charged nitrogen present in compound **2** also the negatively charged counterion is present, making the monolayer likely to remain neutral. It was further rationalized that the drain current change upon DPCP exposure could not be explained by changes in the density of the Si surface states. This made them conclude that the drain current changes could be explained by a charge transfer between Si and the molecules, which in turn leads to interface dipoles and a change in the Si surface potential. 3D technology-computer-aided-design (TCAD) simulations before and after gas detection have been performed to gain insight into the physical mechanisms involved in the gas detection and to investigate the impact of the surface-to-volume ratio on sensor sensitivity.[65] It was found that by reducing the nanowire with from 1 μm to 25 nm, the sensitivity was only slightly improved, but that the V_{BG} window, in which the high sensitivity is reached, was significantly enlarged.

2.2.3.3 Volatile Organic Compounds (VOCs)

Volatile organic compounds (VOCs) are carbon-based chemicals that have a relatively high vapor pressure at room temperature, which is the results from their low boiling points. Most odors consists of VOCs. Other examples include biogenic VOCs produced by plants, which are involved in plant growth, development, reproduction and defense. However, some VOCs are dangerous to human health or cause harm to the environment. Moreover, particular VOCs exist in the exhaled breath of humans could be used for the detection of some diseases, including lung cancer.[66] Thus, the ability to monitor VOCs is important for environmental safety and medical reasons.

In 2011, Niskanen *et al*. reported Si NWs that can be used as versatile chemical vapor sensors without elaborate functionalization.[67] It is obvious that the functionalization of the SiNW surface could help the recognition task greatly. However, their research is a proof-of-principle demonstration that even non-functionalized nanowires can distinguish between various VOCs in –what they call– completely uncontrolled ambient conditions with the help of elementary machine learning. The results show that they are able to distinguish between acetone, ethanol and water with 100% accuracy while methanol, ethanol and 2-propanol were classified with 96% accuracy in ambient conditions. The mechanism is not discussed in great detail, although they conclude it is clear that the sensing is based on the field effect and that the dielectric coupling effect is likely to be dominant owing to large dielectric constants of the studied compounds (ranging from 18-80). In fact, the authors emphasize that the strength of their classification technique means that knowledge of the exact nature of the sensing mechanism is not required. The set of responses was found to be unpredictable, making them conclude that in this approach would be unsuitable for traditional sensing based on deterministic methods. On the other hand, the identification and extrapolation of sensing patterns via supervised machine learning seems achievable.

To determine the LOD of a NW-based chemical sensor, Henning and co-workers reported a scanning gate microscopy (SGM) method based on atomic force microscopy (AFM), where the AFM tip was used as a local gate to control the conductance of the NW.[68] The presented method was validated with an electrostatically formed nanowire (EFN) of which the active area and shape were tunable by biasing a multiple gate FET, as shown in Figure 2.11. The tip-induced charge is quantified with an analytical electrostatic model and it was shown that the SiNW was sensitive to about one elementary charge. Furthermore, the NWs with

diameters of 30 and 80 nm were characterized for ethanol vapor sensing in a concentration range of 10 - 2000 ppm. In another report, Henning and coworkers tuned the diameter of NWs in the range of 16 and 46 nm.[69] A high sensitivity of 100 ppm for ethanol detection was obtained for the NW (16 nm) covered with bare SiO_2. The authors conclude that combining surface modification with this novel structure would further increase the device sensitivity and selectivity.

Recently, Reed and co-workers reported a multi-mode electronic nose (e-nose) for the detection of VOCs by integrating a gravimetric-sensitive device, *i.e.*, film bulk acoustic resonator (FBAR), and a SiNW-based FET.[70] The FBAR is able to detect both polar and apolar VOCs, while the SiNW is insensitive for apolar VOCs and only can detect polar VOCs. Thus this multi-mode e-nose can easily discriminate between polar and apolar VOCs. In addition, the FBAR gives direct information on the amount of adsorbed VOC. Although this report was limited to the detection of two gases simultaneously, such complementary sensors can become useful for the analysis of more complex vapor/gas mixtures.
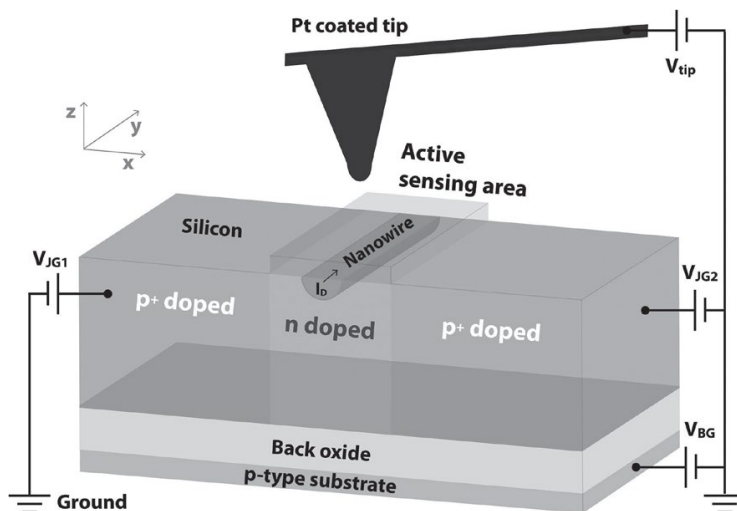

Figure 2.11 An illustration of the scanning gate microscopy configuration with a multiple gate sensing device. By applying voltages to the two junction gates (V_{JG1} and V_{JG2}) and the back gate (V_{BG}), a nanowire-like channel (dark blue) is formed inside the n-doped silicon region along the y-axis of the device. The silicon layer, with a thickness of 150 nm, is on top of the back oxide. The active sensing area is covered with a 6 nm thick thermally grown SiO_2 layer. Picture is taken with permission Wiley-VCH© (from reference 68).

Over the past few years the research group of Haick published a number of interesting and systematic studies on the fundamentals and applications of

functionalized SiNW-based FETs for VOC detection.[71-75] Both polar (water, ethanol, 1-butanol, 1-hexanol, 1-octanol and 1-decanol) and nonpolar (n-hexane, n-octane and n-decane) VOCs have been studied in oil-free air having 15% relative humidity. It was shown that the formation of a silane monolayer having a low fraction of Si-O-Si bonds between the adjacent molecules (*i.e.* no cross linking) greatly enhanced the sensitivity toward nonpolar VOCs.[71] In more detail, a monolayer of hexyltrichlorosilane (HTC) was prepared using a two-step amine-promoted reaction procedure (Figs. 2.12a-f). The improved sensitivity was attributed to the adsorption of nonpolar VOCs between or on top of the alkyl chains and/or in the pinholes of the monolayer, inducing conformational changes in the organic monolayer. This will affect the dielectric constant, the effective dipole moment of the organic monolayer, and/or the charged surface state density of the SiO_2/monolayer interface. These effects, in turn, change the conductivity of the Si NW.

In a second study the detection of nonpolar species with HTC-modified devices is further studied experimentally, while also the detection process has been modeled based on changes in the carrier mobility, voltage threshold, off-current, off-voltage, and subthreshold swing of the devices.[72] The detection of the nonpolar species to was attributed to molecular gating and based on two indirect effects: (i) a change in the dielectric medium close to the Si NW surface and (ii) a change in the charged surface states at the functionality of the Si NW surface. Subsequently, they modified the devices with alkyl trichlorosilanes with different alkyl length to study the interactive effect of hysteresis and surface chemistry.[73] The density of the exposed or non-passivated Si−OH groups (trap states) on the Si NW surface was found to play by far a crucial effect on the hysteresis characteristics of the gated silicon nanowire sensors, relative to the effect of hydrophobicity or molecular density of the organic monolayer. In a more recent work, the Haick group provided further insight into the sensing mechanism of the molecularly modified SiNW to polar and nonpolar VOCs.[74]
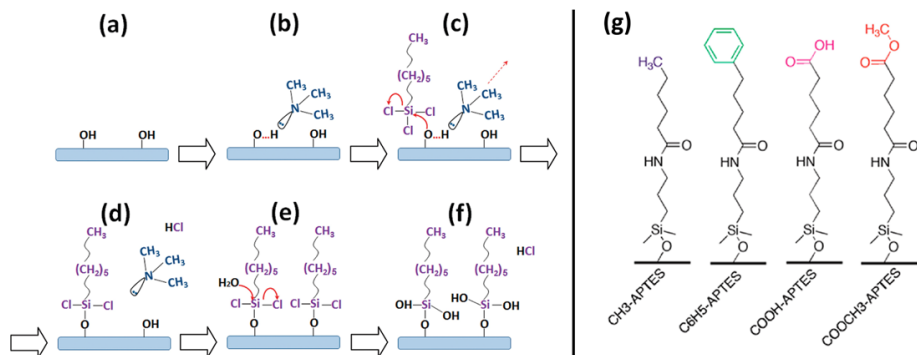
Figure 2.12 Simplified scheme for the attachment of hexyltrichlorosilane (HTS to the SiO_2 surface: **(a)** Preparation of surface hydroxyl (Si−OH) groups. **(b)** Exposure to trimethylamine (TMA) to form a hydrogen bond with the Si−OH group to make the oxygen atom more nucleophilic. **(c)** Exposure to 1.5 mM HTS in chloroform. At this stage, the oxygen atom of the Si−OH group attacks the silicon atom of HTS and to form a Si−O−Si bond as given in **(d)**. **(e)** The presence of water residues assists the replacement of chlorine atoms by OH groups to form the final product given in **(f)**. **(g)** Schematic illustration of molecular layer with different functional groups on the SiNW surface. Figures **(a)-(f)** and **(g)** and taken from references 73 and 75, respectively, reprinted with permission from American Chemical Society ©.

In this case APTES-modified devices were further functionalized with acyl chloride (with different chain length) to form amide bonds. The resulting devices showed a negative response in the threshold voltage changes and the relative hole mobility changes upon exposure to polar and to nonpolar VOCs. In reference experiments, the bare SiNW FET showed no clear response in the threshold voltage to VOCs. For each VOC, the change in threshold voltage increased with the chain length of the molecular modification, while the changes in hole mobility were found to be constant. Data analysis with an electrostatic-based model suggests that the sensor response in terms of the change in threshold voltage depends on the concentration and the vapor pressure of the VOC as well as on the VOC−molecular layer binding energy, and VOC adsorption-induced dipole moment changes of the molecular layer. Also 4 different acyl chlorides were used in the formation of amides, resulting in layers with different terminal functionalities (Fig. 2.12g).[75] It was concluded that the electron-donating/withdrawing properties of the functional groups in these layers likely control the dipole moment orientation of the adsorbed VOCs and, consequently, determine the direction of the change in threshold voltage. Additionally, it was found that the diffusion of VOCs into the molecular layer likely determined by the type of functional groups, is the main reason for change in the hole mobility.

Recently, the Haick group investigated the effect of replacing the oxide insulator by three different organic moieties, *i.e.* a propyl (Si-CH_2-CH_2-CH_3), a propenyl (Si-CH=CH-CH_3) and a propynyl (Si-C≡C-CH_3) group.[76] The sensing results showed that propenyl- and propynyl-modified sensors provided higher accuracy and sensitivity for specific analyte detection, whereas the propyl-modified sensor consistently performed with the lowest specificity because of the high noise level, variability and drift. It was explained that the double bond could transfer electrons to the adjacent C-C bond, and increase the electron density of the FET, therefore increasing the sensitivity. In the triple bond case, electrons were donated to the SiNWs, resulting an increase of "virtual electrons" in the p-SiNWs. Therefore, the minimal sensitivity response and more reliable and stable performance was obtained on propynyl-modified sensor. It was concluded that the best accuracy would be achieved by combining features from different sensors, a concept that is more widely explored by Haick. (*vide infra*) In another report the Haick group applied an artificial neural network (ANN) analysis on SiNW-based devices and studied the sensor responses in a very detailed way by looking at a variety of device parameters (threshold voltage, hole mobility, and subthreshold swing), to obtain highly accurate and selective detection of VOCs.[77] Two series of silane monolayers were coated on the surface of SiNWs. One series contained silanes with a similar backbone, but different functional (head) groups, *e.g.* electron-donating and electron-withdrawing groups. The silanes of the other had the same functional group with varying chain lengths. Each modified-SiNW was characterized for the detection of a wide variety of VOCs. Then the multiple sensing responses by each SiNW formed a fingerprint for each VOC, which can be used for VOC discrimination. This study proved that cross-reactive sensor arrays can bring selectivity and accuracy to the multiple detection through sophisticated pattern recognition algorithms. As addressed in peptide-modified SiNW work, another way to achieve a high selectivity is based on the lock-and-key recognition. Very recently, the Haick group reported on the combination of both approaches for the diagnosis of (gastric) cancer from exhaled volatolome.[78] SiNWs modified with trichloro(phenethyl)silane (TPS) were found to be highly sensitive and selective to the VOCs that are linked with gastric cancer conditions in exhaled breath. On the other hand, SiNWs coated with other molecules, e.g. propyl-gallate and heptanoyl chloride, served as cross-reactive devices. The highly selective performance of the sensors was validated in a real clinical study, using breath samples collected from patients with gastric cancer and from volunteers that have no cancer. Blind analysis validated the ability to use the sensors for simultaneous detection and distinction between gastric cancer and control conditions.

44

This study paved the way of using SiNWs for simple, portable and non-invasive diagnosis of disease conditions.

2.3 Conclusions and outlook

Si NWs-based sensors have demonstrated sensitivity to a wide variety of gas-phase analytes that are important in industrial, environmental, and personal safety and in medical and even military scenarios, as summarized in Table 2.1. Close to two third of these studies are on top-down prepared nanowires. While top-down approaches are generally believed to be beneficial in terms of sensitivity and reproducibility due to better contacts and higher uniformity, the large variety of approaches as listed in Table 2.1 makes it difficult to say whether this is also the case for the studied nanowires reviewed here. Interestingly, in two studies devices prepared from the bottom-up and top-down approach have been used.[51, 67] However, differences in the oxide layer thickness or Si crystallinity and differences in the level of impurities prevent a clear, direct comparison, as recognized by the authors. In any case, top-down approaches are preferable in the preparation devices that consists of large arrays of Si NWs to keep the difference between the nanowires and their contacts (and hence their performance) as low as possible. Also, it should be realized that the bottom-up nanowires are typically wires indeed, while in the case of top-down nanowires the cross section of the wire is not spherical, but rectangular, trapezoidal or triangular. Nanosheets or nanoribbons would be a more appropriate name for 'nanowires' with a rectangular cross section that have a rather high width/height aspect ratio.

About half of the papers on gas phase sensors/detectors that consists of Si NWs makes use of the bare NW surface, *i.e.* oxide surface. The other papers show that surface modification can be advantageous in terms of selectivity, e.g. Pt for H_2 sensing as shown in different studies or the use of recognition peptide sequences for NH_3 and CH_3COOH.[53] Surface modification can also be useful for mechanistic studies as illustrated by the preparation of organic monolayers with different degree of cross linking[71] and chain length.[73, 74] The development of new and the implementation of existing functionalization strategies will enlarge the number of selective (gas phase) sensors. So far two approaches have been reported to modify individual nanowires present in an array, one based on the tuning of etching conditions[19, 58] and the other one on nanoscale localized Joule heating.[35] Wider implementation of these methods and the development of new strategies in this regard will further stimulate multiplexing sensor applications. As shown in the

studies, mostly from Haick's group, combination of lock-and-key recognition sensors and cross-reactive devices is extremely useful for fingerprint recognition of gases.[76, 77, 78] Also the identification of sensing (recognition) patterns via advanced analytical procedures based on data obtained with SiNW-based devices[53, 67] may have exciting applications in the analysis of complex biological and chemical gas mixtures.

To obtain higher sensitivities, multiple gates on SiNW-based FET devices can be in great promise. One example is that two side-gates can individually tune the SiNW to the most sensitive sub-threshold regime.[39] Moreover, by biasing the multiple-gates on the FET, SiNWs with various diameter (16 to 80 nm) could be electrostatically formed, and they were sensitive to about one elementary charge.[68, 69] Other ways to improve the sensitivity of the device include the formation of p-n junctions[24] by joining vertical SiNW arrays with the tip ends, and the formation of a Schottky barrier structure,[46] through the deposition of the proper metal NPs on the SiNWs. Adsorption of gases on these structures can lead to a change of the barrier energy/height, and thus will influence the current signal effectively.

Apart from sensitivity and selectivity, also the speed of response and stability are two important issues in the field of sensor development in general. Response times of the reviewed studies are typically at the s or min time scale. However, faster response times are needed for some applications, e.g. an automotive exhaust sensor that requires a response time of 10 ms in order to enable feedback control.[79] Furthermore, as the degradation of the selector layer will reduce sensor the performance, stability is a key issue to future applications that require operation under harsh temperature and environmental conditions. While response reversibility has been shown in most, if not all cases, stability studies over time have not been addressed extensively. This will be a huge challenge for organic selector layers in particular.

To conclude, as investigations of the influence of Si nanowire dimensions, surface roughness and doping level on sensor sensitivities are just beginning to be reported, more work in this direction is needed. Clearly, a lot can be learned of the more extensive work on the application of SiNW-based devices in the liquid environment. Improvements of the four S's –sensitivity, selectivity, speed and stability– are essential in any discussion of chemical sensor development,[79] but it must be realized that some relevant topics can be studied within the domain of gas phase sensors only. Obviously this holds for the development of suitable gas selector

layers, but also for a rather fundamental topic on the effect of having no possibility of using a (typical) liquid gate reference electrode on the sensor performance. In general, the results presented in this review confirm the applicability of sensors that consists of SiNWs for a wide range of gas sensing applications. It is anticipated that this scientific and technological work soon may result in spin-off commercial products that will a have substantial contribution to the quality of life.

References

1.   Tricoli, A.; Righettoni, M.; Teleki, A. *Angew. Chem. Int. Ed.* **2010,** 49, 7632-7659.
2.   Sharma, S.; Madou, M. *Phil. Trans. R. Soc. A* **2012,** 370, 2448-2473.
3.   Kauffman, D. R.; Star, A. *Angew. Chem. Int. Ed.* **2008,** 47, 6550-6570.
4.   Li, Y.; Qian, F.; Xiang, J.; Lieber, C. M. *Mater. Today* **2006,** 9, 18-27.
5.   Patolsky, F.; Zheng, G.; Lieber, C. M. *Anal. Chem.* **2006,** 78, 4260-4269.
6.   Carlen, E. T.; van den Berg, A. *Lab on a chip* **2007,** 7, 19-23.
7.   Stern, E.; Vacic, A.; Reed, M. A. *IEEE Trans. Electron. Devices* **2008,** 55, 3119-3130.
8.   Chen, X.; Wong, C. K. Y.; Yuan, C. A.; Zhang, G. *Sens. Actuators B: Chem.* **2013,** 177, 178-195.
9.   Konvalina, G.; Haick, H. *Acc. Chem. Res.* **2014**, 47, 66–76.
10. Broza, Y. Y.; Haick, H. *Nanomedicine* **2013,** 8, 785-806.
11. Penner, R. M. *Annu. Rev. Anal. Chem.* **2012,** 5, 461-485.
12. Okano, K.; Totsuka, T. *New Phytol.* **1986,** 102, 551-562.
13. Mintz, D. *Guidelines for the reporting of daily air quality* U.S. environmental protection agency office of air quality planning and standards: North Carolina, 2006.
14. McAlpine, M. C.; Ahmad, H.; Wang, D.; Heath, J. R. *Nat. Mater* **2007,** 6, 379-384.
15. Wan, J. *et al. Microelectron. Eng.* **2009,** 86, 1238-1242.
16. Gao, C. *et al. Microelectron. Eng.* **2010,** 87, 927-930.
17. Gao, C. *et al. Microelectron. Eng.* **2011,** 88, 2100-2104.
18. Cuscunà, M. *et al. Appl. Phys. Lett.* **2012,** 101, 103101.
19. Bunimovich, Y. L.; Shin, Y. S.; Yeo, W.; Amori, M.; Kwong, G.; Heath, J. R. *J. Am. Chem. Soc.* **2006,** 128, 16323-16331.
20. Wang, Y.; Hu, M.; Wang, Z.; Liu, X.; Yuan, L. *Mater. Sci. Semicond. Process.* **2016,** 56, 307-312.
21. Qin, Y.; Liu, Y.; Wang, Y. *ECS jornal of solid state science and technology* **2016**, 5, 380-383.
22. Durand, B.; Lecestre, A., Menini, P.; Guilhem Larrieu. G. *IEEE NMDC* **2016**.
23. Liao, J.; Li, Z.; Wang, G.; Chen, C.; Lv, S.; Li, M. *Phys. Chem. Chem. Phys.* **2016,** 18, 4835-41.
24. Lin, L.; Liu, D.; Chen, Q.; Zhou, H.; Wu, J. *Nanoscale* **2016,** 8, 17757-17764.
25. Zhang, W.; Hu, M.; Liu, X.; Wei, Y.; Li, N.; Qin, Y. *J. Alloys Compd.* **2016,** 679, 391-399.

26. Li, T. Y.; Duan, C. Y.; Zhu, Y. X.; Chen, Y. F.; Wang, Y. *J. Phys. D: Appl. Phys.* **2017,** 50, 114002.
27. Gill, M. *et al. Acad. Emerg. Med.* **2005,** 12, 579-586.
28. Robinson, J. K.; Bollinger, M. J.; Birks, J. W. *Anal. Chem.* **1999,** 71, 5131-5136.
29. Peng, K.; Wang, X.; Lee, S. *Appl. Phys. Lett.* **2009,** 95, 243112.
30. Han, J. W.; Rim, T.; Baek, C. K.; Meyyappan, M. *ACS Appl. Mater. Interfaces* **2015,** 7, 21263-21269.
31. Korotcenkov, G.; Han, S. D.; Stetter, J. R. *Chem. Rev.* **2009,** 109, 1402–1433.
32. Chen, Z. H.; Jie, J. S.; Luo, L. B.; Wang, H.; Lee, C. S.; Lee, S. T. *Nanotechnology* **2007,** 18, 345502.
33. Skucha, K.; Fan, Z.; Jeon, K.; Javey, A.; Boser, B. *Sens. Actuators B: Chem.* **2010,** 145, 232-238.
34. Noh, J.; Kim, H.; Kim, B.; Lee, E.; Cho, H.; Lee, W. *J. Mater. Chem.* **2011,** 21, 15935-15939.
35. Yun, J.; Jin, C. Y.; Ahn, J. H.; Jeon, S.; Park, I. *Nanoscale* **2013,** 5, 6851-6856.
36. Huang, B. R.; Yang, Y. K.; Cheng, H. L. *Nanotechnology* **2013,** 24, 475502.
37. Qin, Y.; Wang, Y.; Liu, Y.; Zhang, X. *Nanotechnology* **2016,** 27, 465502.
38. Kim, J.; Oh, S. D.; Kim, J. H.; Shin, D. H.; Kim, S.; Choi, S. H. *Sci Rep* **2014,** 4, 5384.
39. Ahn, J. H.; Yun, J.; Choi, Y. K.; Park, I. *Appl. Phys. Lett.* **2014,** 104, 013508.
40. Choi, B. *et al. Solid-State Electron.* **2015,** 114, 76-79.
41. Baba Ahmed, L.; Naama, S.; Keffous, A.; Hassein-Bey, A.; Hadjersi, T. *Prog. Nat. Sci.: Mater. Int.* **2015,** 25, 101-110.
42. Ahn, J. H.; Yun, J.; Moon, D. I.; Choi, Y. K.; Park, I. *Nanotechnology* **2015,** 26, 095501.
43. Ramamoorthy, R.; Dutta, P. K.; Akbar, S. A. *J. Mater. Sci.* **2013,** 135, 5328-5331.
44. Han, H.; Kim, J.; Shin, H. S.; Song, J. Y.; Lee, W. *Adv. Mater.* **2012,** 24, 2284-2288.
45. Star, A.; Han, T. R.; Joshi, V.; Gabriel, J. C. P.; Grüner, G. *Adv. Mater.* **2004,** 16, 2049-2052.
46. Naama, S.; Hadjersi, T.; Keffous, A.; Nezzal, G. *Mater. Sci. Semicond. Process.* **2015,** 38, 367-372.
47. van der Eerdena, L. J. M.; de Visserb, P. H. B.; van Dijk, C. J. *Environ. Pollut.* **1998,** 102, 49-53.
48. Zhou, X. T.; Hu, J. Q.; Li, C. P.; Ma, D. D. D.; Lee, C. S.; Lee, S. T. *Chem. Phys. Lett.* **2003,** 369, 220-224.
49. Kamins, T. I.; Sharma, S.; Yasseri, A. A.; Li, Z.; Straznicky, J. *Nanotechnology* **2006,** 17, S291-S297.
50. Talin, A. A.; Hunter, L. L.; Léonard, F.; Rokad, B. *Appl. Phys. Lett.* **2006,** 89, 153102.
51. Demami, F.; Ni, L.; Rogel, R.; Salaun, A. C.; Pichon, L. *Sens. Actuators B: Chem.* **2012,** 170, 158-162.
52. Pichon, L.; Rogel, R.; Jacques, E.; Salaun, A. C. *Phys. Status Solidi C* **2014,** 11, 344-348.
53. McAlpine, M. C. *et al. J. Am. Chem. Soc.* **2008,** 130, 9583-9589.
54. In, H. J.; Field, C. R.; Pehrsson, P. E. *Nanotechnology* **2011,** 22, 355501.
55. Yang, L.; Lin, H.; Zhang, Z.; Cheng, L.; Ye, S.; Shao, M. *Sens. Actuators B: Chem.* **2013,** 177, 260-264.

48

56. Vijayan, A.; Fuke, M.; Hawaldar, R.; Kulkarni, M.; Amalnerkar, D.; Aiyer, R. C. *Sens. Actuators B: Chem.* **2008,** 129, 106-112.

57. Hsueh, H. T. *et al. IEEE Sens. J.* **2011,** 11, 3036-3040.

58. Passi, V.; Dubois, E.; Celle, C.; Clavaguera, S.; Simonato, J. P.; Raskin, J. P. *ECS trans.* **2011,** 35, 313-318.

59. Engel, Y.; Elnathan, R.; Pevzner, A.; Davidi, G.; Flaxer, E.; Patolsky, F. *Angew. Chem. Int. Ed.* **2010,** 49, 6830-6835.

60. Howarter, J. A.; Youngblood, J. P. *Langmuir* **2006,** 22, 11142-11147.

61. Wang, D.; Sun, H.; Chen, A.; Jang, S. H.; Jen, A. K.; Szep, A. *Nanoscale* **2012,** 4, 2628-2632.

62. Kim, Y. L., Lee J.M.; Lee, S.H.; Lee, W. *Proceedings of the 3rd International Nanoelectronics Conference (INEC)*, Hongkong, China, January 3-8, 2010, Paul K. Chu (Ed), IEEE Press, Hong Kong, China, **2010**, 736-737.

63. Clavaguera, S. *et al. Angew. Chem. Int. Ed.* **2010,** 49, 4063-4066.

64. Clavaguera, S.; Raoul, N.; Carella, A.; Delalande, M.; Celle, C.; Simonato, J. P. *Talanta* **2011,** 85, 2542-2545.

65. Passi, V. *et al. IEEE Electron. Device Lett.* **2011,** 32, 976-978.

66. Whittle, C. L.; Fakharzadeh, S.; Eades, J.; Preti, G. *Ann. N. Y. Acad. Sci.* **2007,** 1098, 252-266.

67. Niskanen, A. O.; Colli, A.; White, R.; Li, H. W.; Spigone, E.; Kivioja, J. M. *Nanotechnology* **2011,** 22, 295502.

68. Henning, A. *et al. Small* **2015,** 11, 4931-4937.

69. Henning, A.; Swaminathan, N.; Godkin, A.; Shalev, G.; Amit, I.; Rosenwaks, Y. *Nano Research* **2015,** 8, 2206-2215.

70. Chang, Y.; Qu, H.; Duan, X.; Mu, L.; Reed, M. Sensors **2016** IEEE.

71. Paska, Y.; Stelzner, T.; Christiansen, S.; Haick, H. *ACS Nano* **2011,** 5, 5620-5626.

72. Paska, Y.; Stelzner, T.; Assad, O.; Tisch, U.; Christiansen, S.; Haick, H. *ACS Nano* **2012,** 6, 335-345.

73. Paska, Y.; Haick, H. *ACS Appl. Mater. Interfaces* **2012,** 4, 2604-2617.

74. Wang, B.; Haick, H. *ACS Appl. Mater. Interfaces* **2013,** 5, 5748-5756.

75. Wang, B.; Haick, H. *ACS Appl. Mater. Interfaces* **2013,** 5, 2289-2299.

76. Halpern, J. M.; Wang, B.; Haick, H. *ACS Appl. Mater. Interfaces* **2015,** 7, 11315-21.

77. Wang, B.; Cancilla, J. C.; Torrecilla, J. S.; Haick, H. *Nano Lett* **2014,** 14, 933-8.

78. Shehada, N.; Bronstrup, G.; Funka, K.; Christiansen, S.; Leja, M.; Haick, H. *Nano Lett* **2015,** 15, 1288-95.

79. Kim, I.; Rothschild, A.; Tuller, H. L. *Acta Materialia* **2013,** 61, 974-1000.

Chapter 3

Ionophore-Containing Siloprene Membranes: Direct Comparison between Conventional Ion-Selective Electrodes and Silicon Nanowire-based Field-Effect Transistors

Abstract: Siloprene-based, ion-selective membranes (ISMs) were drop casted onto a field-effect transistor (FET) device that consisted of a single-chip array of top-down prepared silicon nanowires (SiNWs). Within one array two sets of SiNWs were covered with ISMs, each containing two different ionophores, allowing the simultaneous sensing of K and Na ions using a flow cell. It is shown that both ions can be effectively detected in the same solution over a wide concentration range from 10^{-4} to 10^{-1} M without interferrence. The ISMs were also analyzed in a conventional ISE configuration, allowing a direct comparison. While the responses for K^+ were similar for both sensor configurations, remarkably the Na^+ response of the ISM-covered SiNW device was found to be higher than the one of the ISE configuration. The addition of a Na^+ buffering hydrogel layer between the SiO_2 of the SiNW and the ISM reduced the response, showing the importance of keeping the boundary potential at the SiO_2/ISM interface constant. The responses of the siloprene-covered SiNW devices were found to be stable over a period of at least 6 weeks, showing their potential as a multichannel sensor device.

3.1 Introduction

The selective and sensitive detection of ionic species in aqueous media is of importance for several applications, including environmental monitoring, medical diagnostics and food analysis.[1, 2] One conventional method for monitoring biologically relevant ions (*e.g.* Na^+, K^+, Ca^{2+} and Cl^-) relies on ionophore-based, ion-selective electrodes (ISEs).[3] The working principle is relatively simple, with the essential part being an ion-selective membrane (ISM) that is able to selectively exchange ions with the analyte solution establishing an interface potential. Essentially, the activity of a (specific) ion dissolved in a solution is converted into an electrical potential, which can be measured by a voltmeter.

In the 1970s, Bergveld pioneered the ion-selective field-effect transistor (ISFET).[4, 5] In a FET an electric field is used to control the shape—and hence the conductivity—of a semiconducting channel through which charges carriers flow. The conductivity of the channel is not only a function of the applied potential bias between source and drain, but interestingly it also depends on the surface potential of the channel, the so-called gate, or any layer present onto this channel. Just like in the case of ISEs, the surface potential depends on the ion activity, enabling the use of a FET for detecting ions. Depending on the ion-selective materials present on top of the channel the FET can be made ion-specific.

FETs have the advantages of being solid-state and micro-scale, allowing measurements with very short response time.[6] During the past decade, the ISFET concept has been applied to nanoscale devices such as carbon nanotubes,[7] graphene[8] or nanowires.[9] Due to their reliable and reproducible electrical properties, and the possibility of down-scaling and integration for the simultaneous detection of multiple parameters, silicon nanowire FETs (SiNW-FETs) particularly have gained a lot of interest over the last ~15 years. Examples include ion sensing,[10] label-free biosensing,[11-13] the detection of chemical molecules,[14] *e.g.* explosives[15] and disease-related volatile organic compounds.[16-18]

For the detection of distinct ions other than protons, a number of studies have been performed using SiNW-FETs with various types of surface modification. For instance, specific peptides have been utilised for the sensing of Ca^{2+},[19] Cu^{2+} [20] and also for the simultaneous detection of Pb^{2+} and Cu^{2+}.[21] In all these cases, the oxide-covered SiNWs were first modified with silanes to form a platform enabling the covalent binding of oligopeptides. Alternatively, a thiol-functionalized silane was used, resulting in devices that showed a high sensitivity to Hg^{2+} and Cd^{2+} compared

to other (hard Lewis acid) cations.[22] Also crown ethers have been used to prepare SiNW devices for the sensing of Na^+ and K^+. For example, Zhang *et al.* covalently bound a crown ether derivative onto a Si-C linked monolayer,[23] while Wipf *et al.* first covered the SiNWs with gold to immobilize a thiol-functionalized crown ether derivative.[24]

More recently, crown ethers with a high affinity to K^+ have also been employed to SiNW-based devices via plasticized polyvinyl chloride (PVC) membranes, analogue to the extensive work performed on ISFETs.[5, 25] First, Chang *et al.* reported an extensive study on the extracellular K^+ monitoring with a valinomycin-coated SiNW device.[26] To this end, a plasticized PVC membrane with a thickness of ~8 μm was prepared via drop-casting onto a chip containing eight devices. The sensitivity of the modified devices covers a broad range of concentrations from 10^{-6} to 10^{-2} M. Second, Schönenberger and coworkers[27] followed the same strategy of surface modification, albeit that they first covered the SiNWs with a layer of Al_2O_3 with a thickness of 20 nm. A response of 38 mV/decade was reported. These two PVC-based studies focus on the detection of K^+ only.

It must be noticed that, compared to covalent surface modification on the SiNW-FETs, a PVC-based membrane made by drop-casting is much easier to handle as less critical pretreatments are required.[28] On the other hand, the lifetime of FETs with a PVC membrane is limited due to the relatively low adherence of the PVC membranes to SiO_2 surfaces.[29, 30] Furthermore, the presence of a plasticizer in the PVC membranes limits the lifetime due to its slow release. Silopren™, a silicon-based polymer, was found to be an interesting alternative to PVC as it shows a good adhesion to the SiO_2 surface.[29] Moreover, due to its intrinsic elastomeric properties, siloprene does not require a plasticizer.

In the current study, we report SiNW-FETs modified with two different ionophores incorporated into siloprene for the sensing of alkali metal ions. Taking the advantage of SiNW arrays in a single chip, we separately modified SiNWs with two different ion-selective membranes (ISMs), in order to simultaneously detect K^+ and Na^+. These ISMs were tested in a conventional ISE configuration as well as on SiNW-FETs allowing a direct comparison. Results showed a high selectivity and sensitivity for both K^+ and Na^+, thus demonstrating that our device can be used as a multichannel ion sensor.

3.2 Experimental

3.2.1 Materials and chemicals

SiNW-FETs were produced as reported previously.[31, 32] Briefly, the SiNWs (p-doped at a concentration of 10^{16} cm^{-3}) are 3 μm in length, 300 nm in width and 40 nm in height, and covered with a silicon dioxide gate oxide with a thickness of 8 nm. The thickness of the buried oxide (BOX) layer is 300 nm. Figure 3.2a shows a Scanning Electron Microscope (SEM) image of a SiNW. The devices were wire bonded using conductive glue and gold wires (25 μm in diameter) with four functional devices per chip (Figure 3.2b).

Valinomycin (potassium ionophore I), sodium ionophore IV (DD-16-C-5), potassium tetrakis (4-chlorophenyl) borate (PTCB), CH_2Cl_2, siloprene K 1000 (a silanol-terminated polydimethylsiloxane), K-11 (cross-linking agent), KCl, NaCl, agar and sodium alginate were purchased from Sigma–Aldrich, and used as received.

The sensing experiments are conducted using solutions with a constant ionic strength of 0.1 M, prepared using KCl and/or NaCl. The potassium concentration was varied from 10^{-5} M to 10^{-1} M and NaCl was added to make the total ionic strength 10^{-1} M. While the concentration of sodium was varied, KCl was added to make the constant ionic strength of 10^{-1} M. We have applied the commonly used mixed-ion solution method, in which at fixed concentration of the interfering ion, the response is measured at different ion concentrations of the primary ion.[33, 34] Sensor responses were plotted as function of concentration of primary ion (ion for which the sensor is selective) and not as function of activity.

3.2.2 Preparation of ion-selective membranes

Table 3.1 Compostion specifications of the two drop-casting solutions prepared in this study.

Compounds	K-ISM	Na-ISM
Valinomycin	3.3 mg (3 μmol)	-
Na ionophore IV	-	3.3 mg (7.3 μmol)
PTCB	0.6 mg (1.2 μmol)	0.3 mg (0.6 μmol)
CH_2Cl_2	3 ml	1 ml
K-11	35 mg	10 mg
Siloprene K 1000	350 mg	100 mg

Two types of siloprene membranes were prepared: potassium ion-selective membranes (K-ISMs) and sodium ion-selective membranes (Na-ISMs). K-ISMs were prepared according to literature.[30] Briefly, approximately a 5:1 weight ratio of valinomycin and PTCB was dissolved in CH_2Cl_2. After this, siloprene K 1000 and K-11 in a 10:1 wt% ratio were added. Also the Na-ISMs were prepared according to literature:[35] a 10:1 weight ratio of sodium ionophore IV and PTCB, dissolved in CH_2Cl_2, were added to a mixture of siloprene K 1000 and K-11. The specific composition of both types of membranes is given in Table 3.1.

After stirring the membrane solutions for 10 min, a volume of 0.25 ml was pipetted into a well (11 mm in diameter and 2.5 mm in height) of a teflon mold for experiments using the ion-selective electrode (ISE) setup. After the solvent was evaporated overnight, the ISE membranes were gently taken from the mold and placed on a modified ISE tip filled with a 3 M KCl filling solution for the detection of K^+, and a 1 M NaCl filling solution in the case of Na^+ sensing (Figure 3.1).

Membranes for the nanowire-based experiments were prepared by drop-casting 5 µl of the membrane solution onto the devices. Then the fluidics were placed on the chips and sealed to prevent leakage of the aqueous solution as described earlier (Figure A-1.1). To study the thickness of the membranes on the SiNW-FETs, similar droplets were placed on SiO_2 substrates. After drying these membranes, height measurements were performed using a Dektak 8 Stylus Profilometer. The thicknesses of K-ISM and Na-ISM were found to be 62 ± 3 µm, and 50 ± 3 µm, respectively.
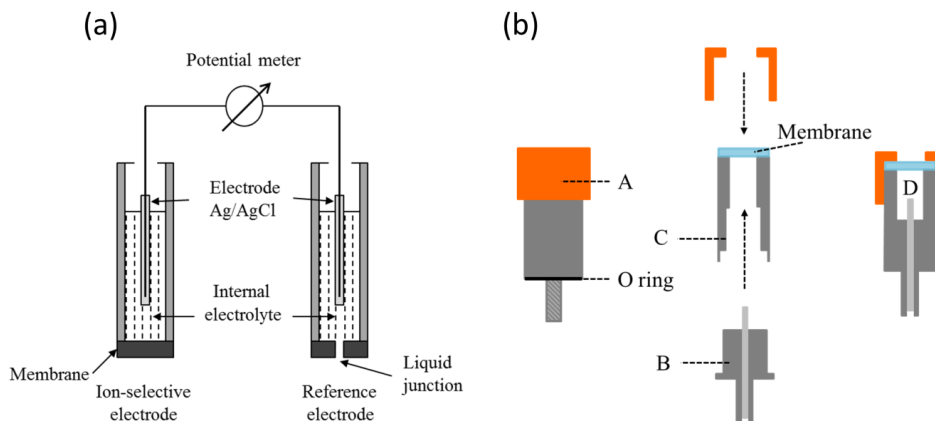

Figure 3.1 (a) Experimental set-up of an ion-selective electrode (ISE) measurement, **(b)** Schematic representation of the tip of ISE: (left) the configuration of the home-made ISE, (centre) assembly of all the tip-components: component B is clamped in component C, then

volume D is filled with a filling solution, after which the membrane is placed on component C. In the last step cap A is gently pushed over component C; (right) a cross section of the various tip components after assembly.

The following approach was used to prepare a drop-casting solution of a hydrogel. First 0.01 g of agar was added to 1 ml of Milli-Q water, followed by the addition of 0.0216 g of sodium alginate. The mixture was stirred and heated (80 °C) for 0.5 h, until a clear solution was obtained. A pipette was used to dropcast 5 µl of the resulting solution onto the SiNW device. After 3 hours an ISM was drop casted onto the hydrogel-covered device as described above by using 12 µl of the membrane solution. It was observed that the siloprene membrane containing ionophores (valinomycin or Na ionophore IV) were slightly cloudy after the curing step, most likely resulting from some crystallization of ionophores.[29]

3.2.3 Electrical measurements

The ISE tests were performed using a Metrohm 278 pH lab system with a Metrohm Ag/AgCl reference electrode and a custom-made working electrode (inner electrode is silver/silver chloride), as shown in Figure 3.1. The ion-selective electrode has a tip in which the membrane can be (re)placed. For SiNW-FETs measurements, a standard Keithley 4200 semiconductor characterization system equipped with three source measurement units was used for the electrical characterization of the SiNW device during exposure. The device was placed in a specially designed measurement box to ensure more stable source and drain contacts compared to the use of a probe station (Figure A-1.2). A 50 mV source-drain bias was applied. The drain current (I_{ds}) was measured while the gate potential was swept. The gate potential can be applied either via the back gate contact (V_{bg}) or an Ag/AgCl electrode in the solution, *i.e.* the front gate (V_{fg}). All experiments shown in this paper were performed using front gate sweep and keeping V_{bg} grounded. From the *I-V* plots we obtained the threshold voltage (V_t) at a constant conductance value of 1 nS. It is noted that other parameters can be obtained as well when characterizing SiNW-based devices, including the carrier mobility, the on/off ratio and the I_{sd} at a specific V_g.[36, 37] However, here we have chosen to detect changes in V_t only as this parameter is directly affected by changes of the boundary potential at the ion-selective membrane solution interface. Figure 3.2c gives a schematic representation of the measurement setup. The error bars in Figures 3.3, and 3.5-3.7 result from 3 subsequent measurements using the same device.

3.3 Results and discussion

3.3.1 ISE experiments

Before performing FET measurements, the ISMs were first tested using the conventional ISE-setup in order to check the ion-selective properties of the membranes. The ionic responses of the potassium ion-selective electrode (K-ISE) were measured towards different concentrations of KCl solutions (from 10^{-5} to 10^{-1} M) at a constant ionic strength (10^{-1} M). Upon increasing K^+ concentration a positive slope was observed of 55 mV/decade in the concentration between 10^{-4} to 10^{-1} M (Figure A-1.3a). This is close to the expected Nernstian slope of $2.3RT/nF = 59$ mV/decade, where R is the gas constant, T the absolute temperature, F the Faraday constant and n the charge of the primary ion.[38] In addition, the Na-ISE gave a linear response toward sodium with a slope of 48 mV/decade over the concentration range from 10^{-4} to 10^{-1} M (Figure A-1.3b), which is comparable to data reported in literature.[35] All the ISE results indicate that siloprene-based ISMs worked properly.
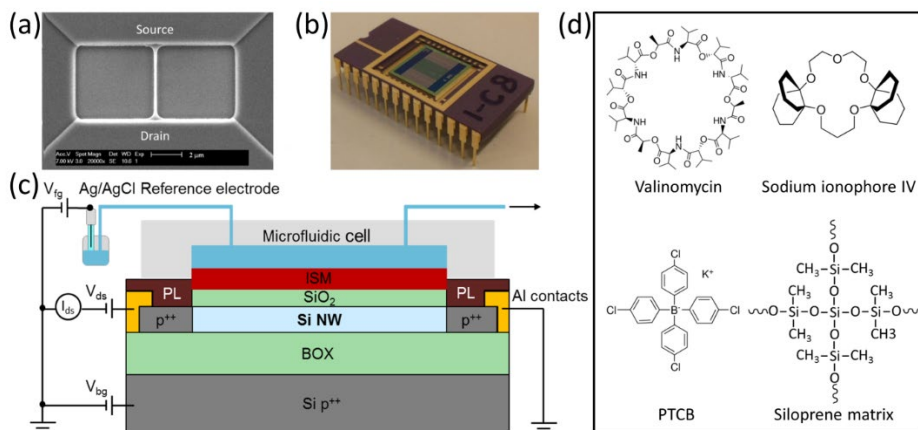

Figure 3.2 (a) Scanning Electron Microscope (SEM) image of a SiNW (thin vertical lines) with contact areas on the top (source) and bottom (drain). **(b)** Optical image of a SiNW chip after wire-bonding onto a chip holder. The size of the SiNW chip is 1 cm × 1 cm. **(c)** Schematic cross section of the device, including the electrical connections and flow microfluidic device (not to scale). PL is passivation layer. The liquid is delivered by suction to the microfluidic cell by a pump (indicated by the arrow, top right). The Ag/AgCl reference electrode is integrated in the beaker containing the solution to which the nanowire was exposed. The working point of the nanowire transistor is adjusted by two gates: a back-gate voltage V_{bg} (grounded) and a liquid gate voltage V_{fg} (applied to the reference electrode). **(d)** Structures and names of the chemicals used in the preparation of the ISMs.

3.3.2 SiNW-based FETs experiments

Next we measured the response of ISM-modified SiNW devices to different concentrations of K^+ and Na^+. Figure 3.3a shows the variation of drain current versus front-gate voltage (I_{ds}-V_{fg}) curves of a K-ISM modified SiNW-FET at different K^+ concentrations from 10^{-5} to 10^{-1} M and at constant ionic strength. Upon increasing the K^+ concentration the curves shift to more negative gate values. This shift is due to the buildup of a positive boundary potential at the ISM interface through the specific adsorption of potassium by valinomycin in the siloprene membrane. In order to keep the I_{ds} constant, this positive potential has to be compensated by a more negative front gate potential. It is also seen from this plot that the more negative front gate potential is applied, the more electrons are repelled, and the more holes (the majority charge carriers) are present, resulting in an increased I_{ds}. In order to evaluate the V_t shifts the data was replotted in Figure 3.3b as conductance (*i.e.* $G = I_{ds}/V_{fg}$) versus V_{fg} on a semilog plot. The V_t was read out the arbitrary values of $G = 1$ nS as indicated by the arrow in Figure 3.3b. Next, the normalized V_t was plotted as function of the K^+ concentration (inset Figure 3.3b.). The data clearly show a perfect linear behaviour from 10^{-4} to 10^{-1} M, with a slope of -57.8 mV per decade. It should be realised that this slope is related to ΔV_t, and the V_t shifts in such a manner to compensate for the change of the ISM boundary potential. Thus a negative slope from the V_t plot reflects a positive slope of the boundary potential. The slope is very close to the Nernstian response of ~59 mV/decade, and very much comparable to our result of the performed reference ISE experiment. The (absolute) slope found by us is more close to the Nernst slope than the one recently reported for a valinomycin-containing PVC membrane onto a gold-coated SiNW device (-38 mV/decade).[27] The only other study on valinomycin-modified SiNW devices reports on changes in conductance rather than V_t, making it not possible to compare the sensisities directly.[26]
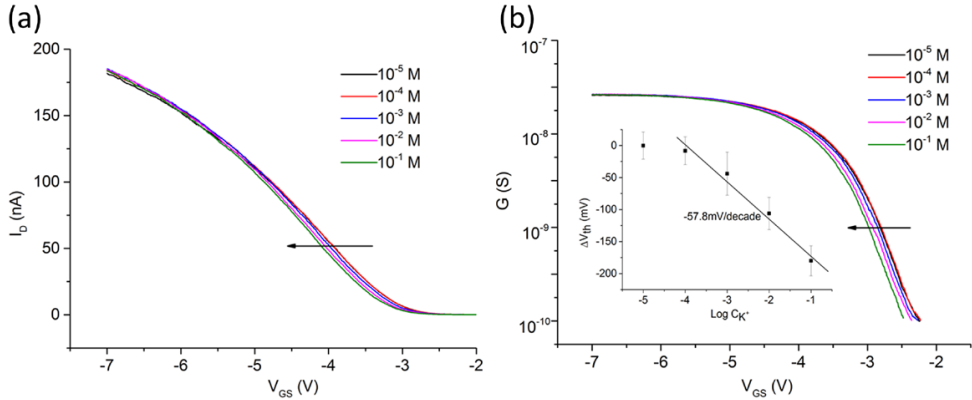
Figure 3.3 (a) Typical I_{ds}-V_{fg} characteristic of one SiNW modified with a K-ISM when exposed to solutions with different K^+ concentrations and at constant ionic strength. **(b)** Conductance G vs. V_{fg} on a semilog plot for the K-ISM modified SiNW-based FETs in different concentrations of K^+. Inset: ΔV_t at different concentration of K^+, is a linear function of K^+ concentration with the slope of -57.8 mV/decade

Next, we studied the hysteresis by comparing the V_t values obtained from the forward and backward electrical response (Figure 3.4). We found a hysteresis effect of ~30 mV at a sweep rate of 125 mV/s. A low hysteresis indicates a low density of trapped charges, and recently Haick and coworkers addressed this topic systematically by tuning the density charge of trapping at the SiO_2 surface.[39] Unfortunately, in most cases the back-gate mode of operation has been used,[11, 39, 40] making it difficult to compare hysteresis effects quantitatively. Extremely low hysteresis effects have been reported by Vu *et al.* for pH measurements using a liquid-gated, SiNW-based device, although the sweeping rate details are not mentioned.[41] The hysteresis we found is comparable to the one reported in a recent study on a front-gate operated organic polymer FET.[42]
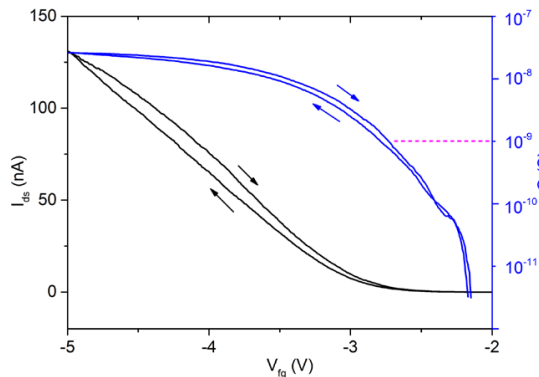

Figure 3.4 Forward and backward bias sweeps of a K-ISM modified SiNW device in a solution of 0.01 M KCl and 0.09 M NaCl at a sweep rate of 125 mV/s. The arrows indicate

60

the direction of the sweep. The dashed line corresponds to the value of the conductance at which V_t—and hence the hysteresis—has been determined.

It should be noted that the timing of the experiments is very important. Although the response of the system at higher concentrations is almost instantaneous (<1 min), the response at the lowest concentrations is much slower, *i.e.* up to ~10 min were needed for the system to stabilize. For that reason we waited 10 minutes after changing each concentration, before collecting the *I-V* plots to determine the V_t values. This type of membranes is known to have a detection limit of 10^{-5} M,[43, 44] below which the potassium ions leach out of the membrane. The slow response rate can be explained by the equilibration rate from the bulk of the solution through the stagnant layer to the membrane surface, *i.e.* for lower concentrations in the solution, a lower concentration gradient is present.

The trend in the V_t shifts observed with the Na-ISM modified SiNW-FETs is similar to the one of the K-ISM modified devices. In Figure 3.5a, the results show that a more negative gate potential has to be applied with increasing sodium ion concentration. We observe that the FET behavior of the devices used to obtain Figures 3.3 and 3.5 is different. It is noted that the back-gate mode *I-V* characteristics of the devices were already different before the deposition of ISMs. The data presented in Figure 3.5a was processed to make Figure 3.5b showing the conductance G versus the gate potential. The inset shows a linear response with an unexpectedly high slope value of -71.9 mV/decade. Before discussing the origin of this high slope we first present our work on testing the ability of the device to simultaneously detect different types of alkali ions.
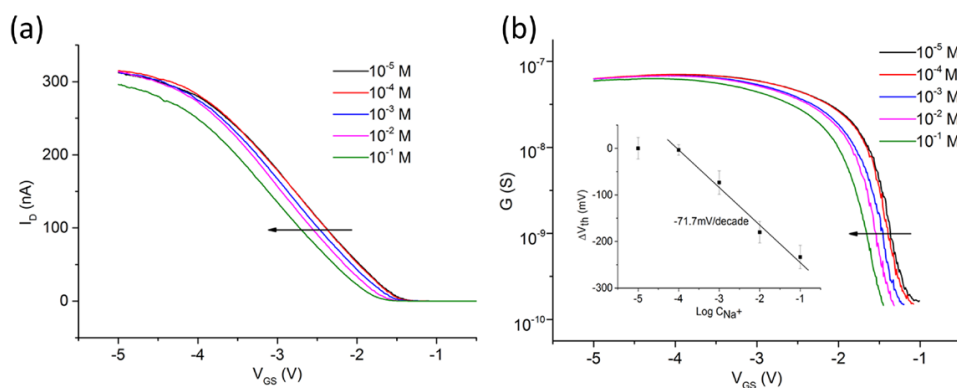

Figure 3.5 (a) Typical I_{ds}-V_{fg} characteristic of one SiNW modified with a Na-ISM when exposed to solution with a range of Na^+ concentrations at constant ionic strength **(b)** Conductance G vs. V_{fg} on a semilog plot for the Na-ISM modified SiNW based FETs in

different concentrations of Na$^+$. Inset: V_t at different concentration of Na$^+$, is a linear function of Na$^+$ concentration with a slope of -71.7 mV/decade.

To this end, we monitered the *I-V* characteristics of a chip containing two sets of nanowires that were covered with two different ISMs in the presence of aqueous solutions containing different concentrations of K$^+$ and Na$^+$. As shown in Figure 3.6a, upon increasing the K$^+$ concentration from 10^{-4} to 10^{-1} M, the V_t of the K-ISM modified SiNW shifts linearly towards more negative values (red curve). Simultanously, the response of the Na-ISM modified SiNW, present on the same chip, did hardly change, which can be understood by the fact that the Na$^+$ concentration was almost constant, *i.e.* between 0.09 and 0.09999 M (black curve). Finally, in 0.1 M KCl solution, without Na$^+$ ions being present, the V_t of the Na-ISM-modified SiNW shifts to a much less negative value. Similarly, a linear V_t shift of the Na-ISM modified SiNW was observed for Na$^+$ concentration between 10^{-4} to 10^{-1} M (Figure 3.6b, black curve). The response of the K-ISM modified SiNW is almost constant for Na$^+$ concentrations between 10^{-5} to 10^{-2} M, while a significant V_t shift towards a less negative value in 0.1 M NaCl solution due to the absence of K$^+$ (Figure 3.6b red curve). These results demonstrate that K$^+$ binds to the valinomycin-modified SiNW and Na$^+$ binds to sodium ionophore-modified SiNW, with a high specificity and without interference, which is in line with ISE studies.[45] This shows that ISM-covered SiNW FETs have a high potential as a multichannel ion sensor.
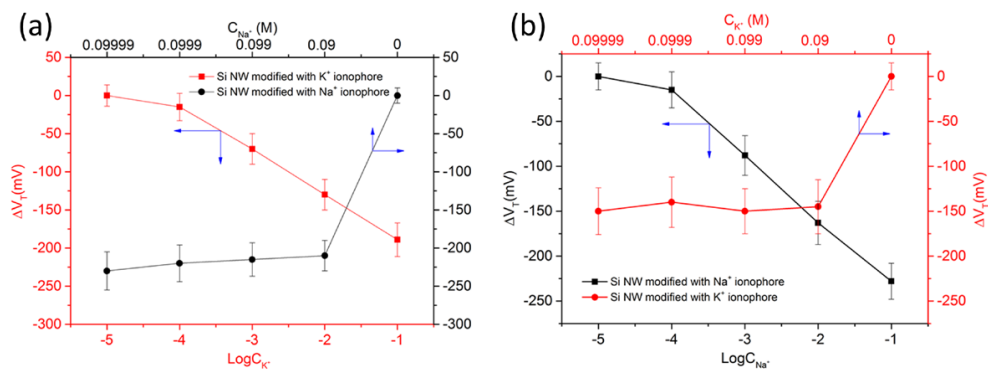

Figure 3.6 Simultaneously testing the concentrations of K$^+$ and Na$^+$ in the artificially mixed solutions (with a constant [Cl$^-$] and a constant ion strength) by K-ISM and Na-ISM modified SiNW FETs. Red curve: Threshold shift ΔV_t vs. K$^+$ concentration from K-ISM modified SiNW based FETs. Black curve: Threshold shift ΔV_t vs. Na$^+$ concentration from Na-ISM modified SiNW based FETs: **(a)** K$^+$ concentration varied from 10^{-5} to 10^{-1} M, NaCl was added to make the ionic strength to 10^{-1} M; **(b)** Na$^+$ concentration varied from 10^{-5} to 10^{-1} M, KCl

was added to make the ionic strength to 10^{-1} M. Note that the bottom x-axes are logarithmic and that the top x-axes are expanded for ion concentrations ≥ 0.09 M.

The results obtained so far show that the application of ISMs in a conventional ISE and SiNW configuration results in a similar response for K^+, while the results for Na^+ are quite different. The observed slope value of -71.8 mV/decade for the Na-ISM was unexpectedly high. In an attempt to rationalize it, we first discuss work of the Schönenberger's group, reporting that the sensitivity of a dual-gated SiNW-FETs can go beyond the Nernst limit.[46] In their research, V_{bg} was used to read out ΔG, which changed by pH shifts of bulk solution at a fixed V_{fg}. This resulted in a sensitivity beyond the Nernst limit, due to a larger BOX thickness compared to the front oxide FOX thickness. In our case, however, we varied the front gate potentials, while the back contact was grounded, making our response independent of the BOX thickness.

We note that the Nernst theory describes the thermodynamic behavior of a surface in contact with an electrolyte and that the sensitivity of a SiNW-FET using a liquid gate is fundamentally limited. However, as in our liquid gate Na^+/SiNW experiments V_t shifts more than theoretically expected and the performances of membranes has been proven by conventional ISE experiments, we conclude that the additional effect must be related to the presence of the SiNW-FETs. It is therefore reasoned that the high slope of -71.7 mV/decade is the result of the addition of two boundary potentials, *i.e.* the boundary at the Na-ISM solution interface and a boundary potential near the SiO_2 interface. The boundary potential expected at the Na-ISM interface is expected to be 48 mV/decade as observed for the conventional ISE.

Being aware that the underlying SiO_2 is sensitive to the pH variations, we first checked all the pH values of our testing solutions (Table A-1.1). After all, in case protons penetrate through the ISM, they may contribute to an additional boundary potential. It turned out, however, that there is no significant difference of pH values in our used solutions. So the effect of protons can be excluded.

The extra (positive) boundary potential may also arise from an equilibration process of sodium ions, which have passed the Na-ISM and entered to some extent the SiO_2, since it is known that Na^+ can be mobile in SiO_2 insulating layers.[47] To verify this possibility, measurements were done with bare SiNW FETs that were soaked in NaCl solutions with different concentration. In more detail, a device was first soaked in 0.1 M NaCl for 1 h to let the sodium ions equilibrate with the SiO_2 lattice. Then the I_{ds}-V_{fg} plot was determined. Next, the device was dried and

contacted with 0.01 M NaCl + 0.09 M KCl (to keep ionic strength constant) and the I_{ds}-V_{fg} plot was measured. From these plots it was deduced a -22 mV/decade shift of V_t upon increasing the NaCl concentration (Table A-1.2). This corresponds with a decreasing boundary potential of 22 mV/decade. A decrease is indeed expected upon lowering the cation concentration. A value of 22 mV/decade, much lower than expected for Nernstian behavior ($2.3RT/nF = 59$ mV/dec), might indicate that in the equilibration process between sodium ions at the SiO_2 interface ($[Na^+]_{interface}$) and the sodium concentration inside the SiO_2 lattice ($[Na^+]_{SiO2}$) is not constant. The Nernst equation for the boundary potential E_b is given by Equation 1:

$$E_b = E^0 + (2.3RT/nF)\log([Na^+]_{interface}/[Na^+]_{SiO2}) \quad (1)$$

If the $[Na^+]_{SiO2}$ slightly increases, *i.e.* is not constant, with increasing $[Na^+]_{interface}$ it is seen that by plotting E_b *versus* log $[Na^+]_{interface}$ the slope will be lower than $2.3RT/nF = 59$ mV/dec.

Several SiNW-FET studies have reported that various alkali metal cations (Na^+ and K^+) affect the conductance of bare devices covered with a SiO_2 layer. However, the results are inconsistent. For example, Clément *et al.* reported a linear Nernstian response to Na^+ using SiO_2-covered SiNW-FETs.[48] On the contrary, the response of SiO_2 coated SiNW-FETs to both Na^+ and K^+ reported by Park *et al.* was found to be non-linear.[49] It is noted that in these studies the electrical conductivity was not kept constant, which affects the response.[31] In our case, however, the electrical conductivity of the two solutions is nearly the same.

To obtain additional evidence that this specific interaction between sodium ions and the SiO_2 lattice leads to an additional positive boundary potential, we designed an experiment to keep the $[Na^+]_{interface}$ constant, by the application of a 0.1 M sodium alginate/agar in hydrogel layer between the SiO_2 interface of the SiNW and the siloprene Na-ISM. The sodium alginate concentration was chosen to prevent the uptake of sodium ions from the solution (no favorable concentration gradient); also leakage of the sodium ions into the solution is unlikely because of the large size of the alginate polyanion.

The I_{ds}-V_{fg} plots have been recorded for these devices as function of the sodium ion concentration at constant ionic strength (Figure 3.7). From these plots the V_t shift of -58.3 mV/dec upon increasing the sodium concentration. This corresponds with an increasing boundary potential of + 58.3 mV/dec at the Na-ISM solution interface. Clearly, it can be concluded that the sodium alginate/agar layer between the SiO_2 and Na-ISM keeps the sodium ion concentration $[Na^+]_{interface}$ constant, resulting in a

64

fixed boundary potential at the SiO_2 interface. Under these conditions the Na-ISM on the Si NW works perfectly.
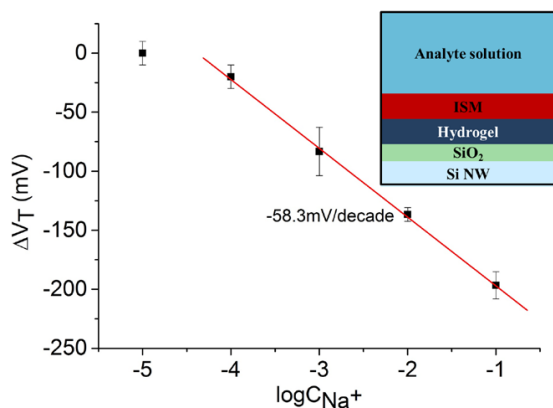

Figure 3.7 Response of the SiNW-based FETs modified with an agar hydrogel (containing 0.1M sodium alginate) and a Na-ISM. Inset: Schematic cross section of the device after the modification with a sodium alginate-containing agar hydrogel and an ISM (not to scale).

Finally the siloprene-modified SiNW devices have been investigated for their stability in time. During a period of 6 weeks the ISM-modified, SiNW-based FET devices were stored in 0.1 M NaCl + 0.1 M KCl. At time intervals of 1 week the devices were characterized by monitoring the I_{ds}-V_{fg} plot under conditions of 0.01 and 0.1 M of both NaCl and KCl, and the shift of V_t determined as described before (Figure A-1.4). During the whole period all our modified silicon nanowires kept their ion-sensitive properties, showing that the ISM was present. In addition, the device covered with agar hydrogel and Na-ISM also showed a consistent result within 5 weeks. As a reference experiment, PVC-based ISMs and siloprene-based ISMs were deposited on glass slides. After being soaked in aqueous solutions for 2 hours, PVC membranes were slightly detached from the glass surface, while siloprene membranes were still attached. We believe that the better stability benefits from the good adhesion between siloprene and the silanol-terminated surface, since the condensation reaction can take place between the silanol and the tetraethoxysilane present in the cross-linking agent.

3.4 Conclusions

We have demonstrated that SiNW-FETs modified with different siloprene-based ISMs form a promising platform for the sensitive, selective and simultaneous detection of alkali metal ions. Moreover, the following features endow this method

with excellent sensing performances and high stability: (1) the high affinity between the set of two different ionophores and corresponding ions, *i.e.* valinomycin and Na ionophore IV bind potassium and sodium ions, respectively, (2) good adhesion between siloprene-based membrane and the surface of SiNW-FETs, (3) individually addressable SiNWs on a single chip made by top-down approach. In addition, for the first time, we applied the siloprene-based ISMs on both conventional ISE configuration and SiNW-FETs, which gave us the possibility to directly compare the responses. While the responses to solutions of K^+ were very much comparable for both sensor systems, the Na^+ response of the ISM-covered SiNW device was found to be higher than the one of the ISE reference experiment and even higher than Nernstian behavior. We ascribed this to the presence of an additional positive boundary potential due to the interaction between Na^+ and SiO_2. We found that the addition of a Na^+ buffering hydrogel layer between the SiO_2 of the SiNW and the ISM kept the additional positive boundary potential constant. The response was found to be Nernstian as it only depends on the boundary potential of the ISM/electrolyte interface now. Finally, the proposed method provides high possibility for multichannel ion sensor applications.

References

1.   Amine, A.; Mohammadi, H.; Bourais, I.; Palleschi, G. *Biosens. Bioelectron.* **2006,** 21, 1405-1423.
2.   Du, J.; Hu, M.; Fan, J.; Peng, X. *Chem. Soc. Rev.* **2012,** 41, 4511-4535.
3.   Bakker, E.; Buhlmann, P.; Pretsch, E. *Chem. Rev.* **1997,** 97, 3083-3132.
4.   Bergveld, P. *IEEE Trans. Biomed. Eng.* **1970,** BM17, 70-71.
5.   Bergveld, P. *Sens. Actuators, B* **2003,** 88, 1-20.
6.   Lee, C. S.; Kim, S. K.; Kim, M. *Sensors* **2009,** 9, 7111-7131.
7.   Tans, S. J.; Verschueren, A. R. M.; Dekker, C. *Nature* **1998,** 393, 49-52.
8.   Ang, P. K.; Chen, W.; Wee, A. T. S.; Loh, K. P. *J. Am. Chem. Soc.* **2008,** 130, 14392-14393.
9.   Duan, X. F.; Huang, Y.; Cui, Y.; Wang, J. F.; Lieber, C. M. *Nature* **2001,** 409, 66-69.
10.   Cui, Y.; Wei, Q. Q.; Park, H. K.; Lieber, C. M. *Science* **2001,** 293, 1289-1292.
11.   Stern, E.et al. *Nature* **2007,** 445, 519-522.
12.   Huang, Y. W. et al. *Anal. Chem.* **2013,** 85, 7912-7918.
13.   Zhang, G. J.; Huang, M. J.; Ang, J. A. J.; Yao, Q.; Ning, Y. *Anal. Chem.* **2013,** 85, 4392-4397.
14.   Cao, A.; Sudhölter, E. J. R.; de Smet, L. C. P. M. *Sensors* **2014,** 14, 245-271.
15.   Engel, Y.; Elnathan, R.; Pevzner, A.; Davidi, G.; Flaxer, E.; Patolsky, F. *Angew. Chem., Int. Ed.* **2010,** 49, 6830-6835.

16.   Broza, Y. Y.; Haick, H. *Nanomedicine* **2013,** 8, 785-806.
17.   Wang, B.; Cancilla, J. C.; Torrecilla, J. S.; Haick, H. *Nano Lett.* **2014,** 14, 933-938.
18.   Konvalina, G.; Haick, H. *Acc. Chem. Res.* **2014,** 47, 66-76.
19.   Hitzbleck, M.; Xuan Thang, V.; Ingebrandt, S.; Offenhaeusser, A.; Mayer, D. *Phys. Status Solidi A* **2013,** 210, 1030-1037.
20.   Bi, X.; Wong, W. L.; Ji, W.; Agarwal, A.; Balasubramanian, N.; Yang, K. L. *Biosens. Bioelectron.* **2008,** 23, 1442-1448.
21.   Bi, X.; Agarwal, A.; Yang, K.L. *Biosens. Bioelectron.* **2009,** 24, 3248-3251.
22.   Luo, L.et al. *Appl. Phys. Lett.* **2009,** 94, 193101.
23.   Zhang, G. J.; Agarwal, A.; Buddharaju, K. D.; Singh, N.; Gao, Z. *Appl. Phys. Lett.* **2007,** 90, 233903.
24.   Wipf, M. et al. *ACS Nano* **2013,** 7, 5978-5983.
25.   Jimenez-Jorquera, C.; Orozco, J.; Baldi, A. *Sensors* **2010,** 10, 61-83.
26.   Chang, K. S.et al. *Biosens. Bioelectron.* **2012,** 31, 137-143.
27.   Leung, K.; Nielsen, I. M. B.; Criscenti, L. J. *J. Am. Chem. Soc.* **2009,** 131, 18358-18365.
28.   Wang, J.; Huang, H.; Wang, M.; Yao, L.; Qiao, W.; Long, D.; Ling, L. *Ind. Eng. Chem. Res.* **2015,** 54, 5319-5327.
29.   Vanderwal, P. D.; Skowronskaptasinska, M.; Vandenberg, A.; Bergveld, P.; Sudholter, E. J. R.; Reinhoudt, D. N. *Anal. Chim. Acta* **1990,** 231, 41-52.
30.   Vanderwal, P. D.; Sudholter, E. J. R.; Boukamp, B. A.; Bouwmeester, H. J. M.; Reinhoudt, D. N. *J. Electroanal. Chem.* **1991,** 317, 153-168.
31.   Mescher, M.; Brinkman, A. G. M.; Bosma, D.; Klootwijk, J. H.; Sudhölter, E. J. R.; de Smet, L. C. P. M. *Sensors* **2014,** 14, 2350-2361.
32.   Mescher, M.; de Smet, L. C. P. M.; Sudhölter, E. J. R.; Klootwijk, J. H. *J. Nanosci. Nanotechnol.* **2013,** 13, 5649-5653.
33.   Morf, W. E. *The Principles of Ion-Selective Electrodes and of Membrane Transport*; Elsevier: New York, 1981.
34.   Bakker, E.; Meruva, R. K.; Pretsch, E.; Meyerhoff, M. E. *Anal. Chem.* **1994,** 66, 3021-3030.
35.   Suzuki, K. et al. *Anal. Chem.* **1996,** 68, 208-215.
36.   Bayn, A.; Feng, X.; Muellen, K.; Haick, H. *ACS Appl. Mater. Interfaces* **2013,** 5, 3431-3440.
37.   Ermanok, R.; Assad, O.; Zigelboim, K.; Wang, B.; Haick, H. *ACS Appl. Mater. Interfaces* **2013,** 5, 11172-11183.
38.   Ruzicka, J. *J. Chem. Educ.* **1997,** 74, 167-170.
39.   Paska, Y.; Haick, H. *ACS Appl. Mater. Interfaces* **2012,** 4, 2604-2617.
40.   Jang, H.et al. *Appl. Phys. Lett.* **2011,** 99, 252103.
41.   Vu, X. T.; GhoshMoulick, R.; Eschermann, J. F.; Stockmann, R.; Offenhaeusser, A.; Ingebrandt, S. *Sens. Actuators, B* **2010,** 144, 354-360.
42.   Knopfmacher, O.et al. *Nat. Commun.* **2014,** 5, doi:10.1038/ncomms3954.
43.   Moss, S. D.; Janata, J.; Johnson, C. C. *Anal. Chem.* **1975,** 47, 2238-2243.
44.   Novell, M.; Parrilla, M.; Crespo, G. A.; Xavier Rius, F.; Andrade, F. J. *Anal. Chem.* **2012,** 84, 4695-4702.
45.   Qin, Y.; Mi, Y. M.; Bakker, E. *Anal. Chim. Acta* **2000,** 421, 207-220.
46.   Knopfmacher, O. et al. *Nano Lett.* **2010,** 10, 2268-2274.
47.   Snow, E. H.; Grove, A. S.; Deal, B. E.; Sah, C. T. *J. Appl. Phys.* **1965,** 36, 1664.

48.   Clement, N.; Nishiguchi, K.; Dufreche, J. F.; Guerin, D.; Fujiwara, A.; Vuillaume, D. *Appl. Phys. Lett.* **2011,** 98, 014104.

49.   Park, I.; Li, Z.; Pisano, A. P.; Williams, R. S. *Nanotechnology* **2010,** 21, 015501.

Chapter 4

Metal Organic Polyhedra Coated Si Nanowires for the Sensitive Detection of Trace Explosives

Abstract: Surface-modified silicon nanowire-based field-effect transistors (SiNW-FETs) have proven to be a promising platform for molecular recognition in miniature sensors. In this work, we present a novel nanoFET device for the sensitive and selective detection of explosives based on affinity layers of metal−organic polyhedra (MOPs). The judicious selection of the geometric and electronic characteristics of the assembly units (organic ligands and unsaturated metal site) embedded within the MOP cage allowed for the formation of multiple charge-transfer (CT) interactions to facilitate the selective explosive inclusion. Meanwhile, the host-stabilized CT complex inside the cage acted as an effective molecular gating element to strongly modulate the electrical conductance of the silicon nanowires. By grafting the MOP cages onto a SiNWFET device, the resulting sensor showed a good electrical sensing capability to various explosives, especially 2,4,6-trinitrotoluene (TNT), with a detection limit below the nanomolar level. Importantly, coupling MOPs-which have tunable structures and properties-to SiNW-based devices may open up new avenues for a wide range of sensing applications, addressing various target analytes.

4.1 Introduction

Silicon nanowires (SiNWs) configured as electronic devices, pioneered by Lieber's group about 15 years ago, have been one of the most promising platforms for ultra-sensitive direct electrical detection and discrimination of biological and chemical species.[1,2] This is due to several advantages that include label-free and real-time detection, and more importantly compatibility with very-large-scale integration (VLSI) processes and complementary metal–oxide–semiconductor (CMOS) technologies as well as the ability to chemically modify the surface of SiNWs with receptors for the selective quantification of targeted molecules.[3-7] Among all the hazardous chemical species, hidden explosives, have been a pressing concern for human society, which is due to their wide applications in war zones and counter-terrorism.[8-10]

Until now, a few studies have reported on SiNW-based devices for the detection of explosive molecules.[11-14] For instance, SiNWs cleaned by O_2 or H_2 plasma were observed to behave as chemically modulated resistors, responding sensitively to the vapors of common nitro explosives and their degradation by-products.[12] This was explained by the formation of charge transfer complexes between the nitro group of the explosive and the hydroxyl groups on the SiNW surface. However, the hydroxyl-terminated SiNWs are sensitive to many oxidizing and reducing targets, rendering them unselective. The Patolsky group prepared and studied amino-terminated SiNW devices, which resulted in one of the lowest detection limits for TNT in aqueous solutions containing 0.1% dimethyl sulfoxide (DMSO) with a limit of detection (LOD) below the femto-molar level.[11] Despite the excellent sensitivity obtained, the binding concept, based on the formation of so-called Meisenheimer complexes, is rather unspecific in nature, resulting in a limited selectivity. Later on, they extensively studied a SiNW array platform for the fingerprinting of broad-class explosives, based on the surface immobilization of multiple non-specific chemical receptors onto the SiNW arrays, using a single-step chemical modification.[13] The sensitive and discriminative detection of explosive species was achieved by pattern recognition. This development illustrates well the two main directions in sensing in general: (i) the design and use of recognition elements that will bind an analyte selectively,[15] and (ii) the use of arrays of multiple sensing elements that allow the handling of practical, complex mixtures of analytes.

A strategy that can potentially reduce array sizes in combinatorial sensing, therefore, is to use designable receptor motifs that attempt to make receptors more

selective and at the same time allow extension into arrays. Recent advances in the design and synthesis of molecular architectures have resulted in the availability of a large variety of porous materials that are interesting candidates for gas separation and sensing purposes.[16-22] For example, metal-organic polyhedra (MOPs), discrete molecular cages with well-defined cavities and high symmetries that are constructed through the coordination of organic linkers and metal ions, have attracted significant attention for molecular recognition.[19, 22] Careful selection of the bridging ligands and metal ions permits the rational control of a well-defined inner space, gated pores, and nanoscale windows, and consequently interesting architectures can be made.[18] More importantly, inside the cage, the geometric and electronic characteristics that are embedded within each individual assembling unit allow for the integration of multiple weak molecular interactions. These include charge-transfer and Brønsted acid-base interactions, in a controlled fashion and thus provide specific inner environments for the selective uptake and binding of guest molecules. Moreover, the designable exposure of exo-reactive sites around MOPs assemblies enable further coupling of functional substrates such as Au plasmonic substrates to expand their application window.[22] These distinctive features make MOPs an excellent receptor candidate for surface modification and sensing.

SiNW-based FETs operate by a change of current flowing through the SiNW channel, which is induced by a local change in charge density due to the binding of an ion or a molecule.[23] We envisioned monitoring the specific trapping of explosive molecules in the MOP cage on the surface of SiNWs could be a particularly promising approach to obtain effective, portable and integratable sensors for the detection of trace explosives. Herein, we demonstrate that the coordination of MOPs onto the surface of SiNWs provides a useful model system for trace 2,4,6-trinitrotoluene (TNT) sensing (Figure 4.1a), which shows a high degree of selectivity and sensitivity to TNT over other similar explosives. Band-bending theory was used to interpret the detection scheme on the sensor platform. We combine experimental results with theoretical modeling in an effort to understand the selectivity mechanism of our receptor to its target analyte.

4.2 Experiments and methods

4.2.1 Cu-MOPs synthesis

According to the previous literature,[22] the MOPs cage was synthesized by slow addition of methanol into a N, N-diethyl formamide (DEF) solution of $Cu_2(OAc)_4$

and ligand H_2(2-NH_2-5-i-Pr-3,3′-PBEDDB) (L-NH_2). After 5 days the MOPs cage [Cu_4(L-NH_2)$_4$(S)$_4$]•xS (Cu-MOPs) was obtained.

4.2.2 Surface functionalization

The silicon wafers and SiNW chips were cleaned by sonication in acetone for 2 min, followed by a rinsing step with ethanol and mili-Q water, and then dried by N_2-gas flow. Then the devices were cleaned with air plasma for 2 min, thus obtaining clean and oxidized-device surfaces for the effective chemical modification of 2-(4-pyridylethyl)triethoxysilane (PETES) (Aldrich, CAS: 98299-74-2) to provide pyridyl-groups at the surface. Subsequently, the devices were submerged in a 0.1vol% solution of PETES in anhydrous toluene at room temperature overnight. Upon completion of the reaction time, the devices were removed from the silane solution and were rinsed under flowing toluene and methanol, then baked at 150 C° for 5 mins.

The PETES-modified devices were immersed into Cu-MOPs containing DEF solution (2 mM) at room temperature overnight. Afterwards, the devices were rinsed with methanol, CH_2Cl_2 for several times and dried using N_2 gas flow. The devices were stored under N_2 atmosphere.

4.2.3 X-ray photoelectron spectroscopy

X-ray photoelectron spectroscopy was performed using a Quantera SXM (scanning XPS microprobe) using monochromatized Al $K_α$ radiation at 1486.6 eV. X-ray beam at the standard beam-input and detector input angle of 45 degree. Survey spectra were an average of three scans acquired at pass energy of 160 eV and resolution of 1 eV/step.

4.2.4 Ellipsometry

The measurements were carried out on a commercial imaging nulling-ellipsometer (EP3 Nanoscope, Accurion). The light source was a He-Ne laser with $λ$ of 658 nm. Measurements were performed for three to five different spots on each specimen. The following refractive indices were used: n_{air}=1, n_{PETES}=1.465.

4.2.5 Sensor device fabrication

The modified SiNW chips were wire-bonded using conductive glue and Al wires (25 μm in diameter) to the chip holder. Then the fluidics were placed on the SiNW chips and sealed to prevent leakage of the solution as described earlier.[23]

4.2.6 Sensor characterization

For SiNW FETs measurements, a standard Keithley 4200 semiconductor characterization system equipped with three source measurement units was used for the electrical characterization of the SiNW device during exposure. The device was placed in a specially designed measurement box to ensure more stable source and drain contacts compared to the use of a probe station.

4.2.7 Calculation of the grafting density

$$\sigma = \frac{h\rho N_A}{M_N}$$

Here, σ is grafting density, h is the MOPs thickness obtained by ellipsometry (2 nm), ρ is the density of MOPs (0.9167 g/cm^3), N_A is Avogadro's number (6.022*10^{23} mol^{-1}), and M_n is MOPs molecular weight (2040 g/mol). The result of calculation is 0.54 molecules/nm^2.

4.2.8 Calculation of the Debye length

$$\lambda_D = \sqrt{\frac{\varepsilon_s k_B T}{q^2 N}}$$

Here, ε_s is the dielectric permittivity of the material ($\varepsilon_s=\varepsilon_{0*}\varepsilon_r$=1.04*10^{-12} F/cm). k_B is Boltzmann's constant (1.38×10^{-23}J/K), T is the absolute temperature (293K), q is the elementary charge (1.6×10^{-19}C), N is the density of dopants (10^{16} cm^{-3}).

4.2.9 DFT computational study

All results were calculated using the Vienna *ab initio* Simulation Package (VASP) with the projector augmented waves (PAW) approach.[24, 25] The cut-off energy of the plane wave basis-set was 405 eV. A gamma point only k-point mesh was used for one unit cell of MOPs. Such a cut-off energy and k-point mesh were tested to ensure the total energy value convergence within 1 meV/atom. The atomic positions were optimized with the conjugate gradient method until the forces acting on atoms were below 0.015 eV/Å. To account for the Van der Waals interactions, we adopted the DFT-D2 method proposed by Grimme.[26]

In order to study the charge redistribution or transfer between host MOPs and guest explosives, we performed an analysis on (1) electron densities of explosive, MOPs, and explosive-MOPs complex using the DDEC (Density Derived Electrostatic Chemical net atomic charges) method,[27-29] and (2) the difference-

electron density, which is calculated as the difference between the electron density of the explosive-MOPs complex and the electron density of the MOPs augmented by that of an isolated explosive molecule.
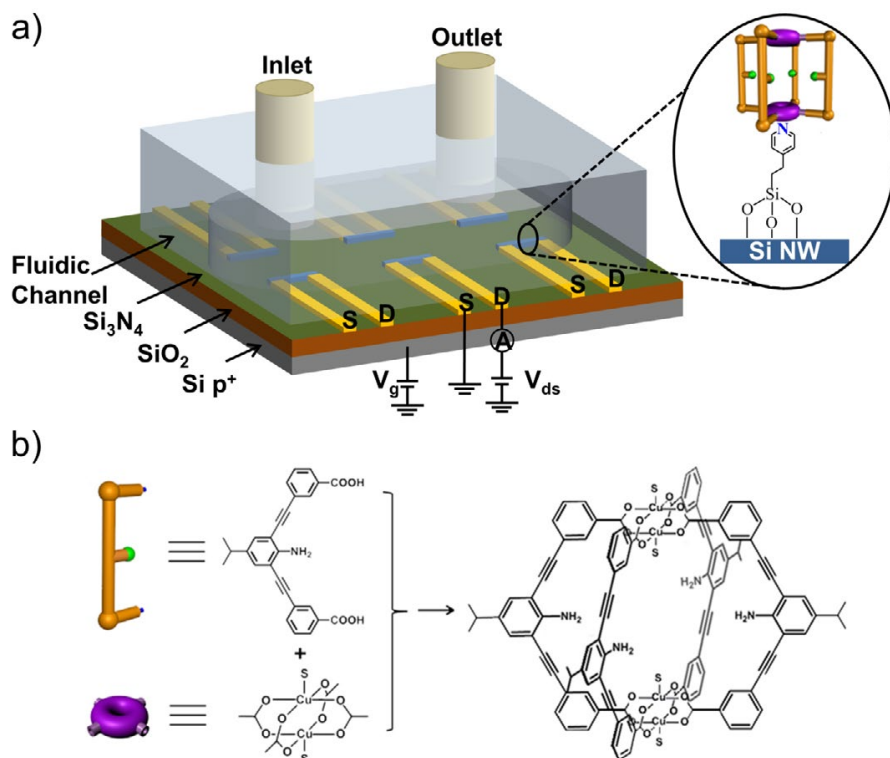
4.3 Results and discussion

Figure 4.1 (a) Schematic representation of the SiNW chip, including the electrical connections and microfluidic device, and zoom-in schematic illustration of the SiNW surface modified by a pyridyl-silane and subsequently a Cu-MOPs (not to scale, for matter of simplicity only 6 SiNWs are included here), **(b)** Schematic representation of the construction of the Cu-MOPs; S is the coordinated solvent molecule, which can be removed under vacuum at 60 °C to yield an empty molecular cage for subsequent trapping of an explosive.

Based on standard CMOS processing techniques, SiNW chips were fabricated by a top-down approach.[30] The chip surface was passivated by Si_3N_4 (100 nm) except for 28 SiNWs (p-doped at a concentration of 10^{16} cm^{-3}, $l = 3$ μm × $w = 400$ nm × $h = 100$ nm) areas covered by SiO_2 (8 nm). Silica-terminated surfaces have a well-established chemistry that allows the chemical modification of SiNWs without strongly affecting the properties of the semiconducting core.[11] A three-step procedure was employed to construct the MOPs-modified SiNW chip. First, the MOPs material was synthesized by adding methanol into a solution of $Cu_2(OAc)_4$ and the ligand H_2(2-NH$_2$-5-i-Pr-3,3'PBEDDB) (L-NH$_2$) in N,N-diethylformamide (DEF) solution.[22] After several days, the MOPs cages [Cu$_4$(L-NH$_2$)$_4$(S)$_4$]•xS (Cu-MOPs), where S is the solvent (DEF), were harvested. Next, the SiNW surfaces were activated by O_2 plasma and subsequently chemically modified with a monolayer of 2-(4-pyridylethyl)-triethoxysilane (PETES). Finally, by inserting the PETES-modified nanowire chip into a Cu-MOPs solution for 12 h, followed by washing with ethanol and activating in vacuum overnight, the Cu-MOPs-decorated SiNW chip was finally obtained suited for analyte sensing.

The structure of Cu-MOPs has already been determined by single-crystal X-ray analysis, MALDI-TOF, and scanning tunneling microscopy (STM) in our previous work.[22] As shown in Figure 4.1b, the cage possesses a M$_4$L$_4$ lantern-type cage structure with four bridging ligands surrounding two paddle wheel di-copper motifs, with a height of 19 Å and diameter of 26 Å, as well as an internal volume of 10.9×10.7×9.1 Å^3. Inside the cage, the four electron-donating -NH$_2$ sites and two unsaturated Cu^{2+} metal sites occupy the inner surface in a controlled fashion, and thus enhance guest binding events to achieve a good affinity by multiple weak interactions. Outside the cage, the exo-reactive site of copper allows the further decoration onto the PETES-modified SiNW by coordination interactions.

The surface modification of the PETES monolayer followed by the further immobilization of the Cu-MOPs cage onto the SiNWs was followed by spectroscopic ellipsometry and X-ray photoelectron spectroscopy (XPS). After the optimization of the concentration and deposition time, ellipsometry results showed that the thickness of the PETES layer was ca. 0.7 nm, indicating the modification with one molecular layer. In the corresponding XPS spectrum (Figure A-2.1), the C1s peak contains two components: the C-C/C-H/C=C peak at 284.6 eV, and the sp^2 C=N peak at 285.2 eV, further confirming the existence of PETES on the silicon surface. After the grafting of Cu-MOPs, the characteristic signal of Cu 2p was clearly detected at 933.4 eV. All these results corroborate the successful grafting of the Cu-

76

MOPs cages on the SiNW surface. Following the data processing method in the literature,[31] the surface density of Cu-MOPs was calculated to be 0.54 molecules/nm^2, indicating a dense coverage on the silicon surface. The short distance close to the Si surface and the dense grafting of the sensing element offers a good opportunity to achieve higher sensor sensitivity.

Figure 4.2a shows the scanning electron microscope (SEM) image of one SiNW. Before connecting the chip to the semiconductor characterization system, the modified chips were wire-bonded using conductive glue and Al wires (25 μm in diameter) to the chip holder (Figure 4.2b). To assess the sensing efficacy of our Cu-MOPs modified nano-device, explosive-containing solutions with different concentrations ranging from the ppb to ppm level were delivered to the sensor chip through a home-made fluid delivery system.[32] To avoid the hydrolysis or desorption of Cu-MOPs by water, absolute ethanol was chosen as a solvent. The dependence of the drain-source current (I_{ds}) on gate voltage (V_g) at fixed drain-source voltage (V_{ds}) for bare, PETES-, and Cu-MOPs-modified SiNW devices in the absolute ethanol environment is shown in Figure 4.2c. For all SiNWs, the current increased as a function of the applied negative V_g, which is typical for p-type devices. Clearly, surface functionalization of SiNW with pyridyl-silane and the further coordination of MOPs did not have a detrimental effect on the electrical properties of the devices, proven by the occurrence of similar threshold voltages (V_{th}). Meanwhile, we observed hysteresis, *i.e.* a lag in the response obtained in the forward and backward electrical scans of I_{ds} vs V_g, in which respect the three devices showed some different properties. In fact, it has been proven that SiNW-based FET hysteresis is caused by surface silanol (Si-OH) sites,[33] and chemical passivation (e.g., Si-C, Si−O−Si bonds) on the SiNW surface can lower the number of Si-OH groups and thus the hysteresis effect,[34, 35] which may explain why the surface-modified SiNWs showed less hysteresis compared to the bare device in our study.
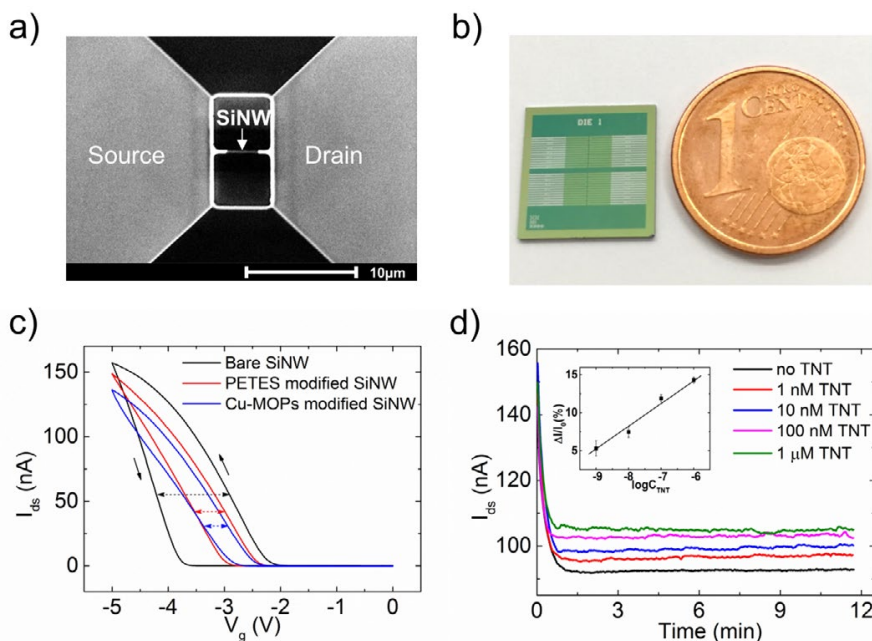
Figure 4.2 (a) SEM image of a SiNW (horizontal line in the center) with contact areas on the left (source) and right (drain); **(b)** Optical image of a SiNW chip before wire-bonding onto a chip holder. The size of the SiNW chip is 1 cm × 1 cm, **(c)** *I-V* curves from a bare SiNW (black curve), a PETES -modified SiNW (red curve), and a Cu-MOPs-modified SiNW (blue curve). **(d)** Current time traces (raw data) from a Cu-MOPs-modified chip while flowing through ethanol solutions with different TNT concentrations; the inset shows the relative steady-state current change ($\Delta I/I_0$) versus TNT concentration.

For determining the sensing capabilities of our SiNW devices, the Cu-MOPs-modified device was exposed to solutions with different concentrations of TNT, and the current I_{ds} was recorded by fixing V_g at -3 V and V_{ds} at 50 mV. According to the transfer characteristics in Fig. 4.2c, such a gate voltage allows the Cu-MOPs-modified SiNW to work in the most sensitive regime, i. e. the depletion/subthreshold regime, where I_{ds} depends exponentially on the V_g, and therefore the most distinct current change can be obtained according to the gate tuning.[36] As shown in Figure 4.2d, the conductive property of the Cu-MOPs modified device is clearly sensitive to the presence of TNT. For every measurement, a rapid decrease of the signal was observed after which the current became stable within approx. 1 min. We speculate that the initial signal drop is related to our chip becoming stable in the depletion regime. As shown in the inset of Figure 4.2d, the relative steady-state current, $\Delta I/I_0$ where I_0 is the steady current in ethanol, shows a linear relationship with the logarithmic TNT concentration over a large concentration range from 1 nM to 1 µM.

Switching from ethanol to 100 nM TNT at a constant back-gate voltage of −3 V led to the exact same signal value, as shown in Figure A-2.2). This result is comparable to the one observed in a study on TNT in DMSO-containing water making use of amine-terminated SiNWs, both in terms of the linearity and the slope of the sensor response plot.[11] Furthermore, when decreasing the TNT concentration down to 100 pM, the nanowire sensor was still able to detect TNT, as shown in Figure A-2.3.

The high sensitivity of the Cu-MOPs-modified device can be rationalized as follows. The detection of molecular recognition on the SiNW surface is within the range of the Debye length (λ_D),[37, 38] which is in our case calculated to be ~ 40 nm. Yet the surface modification elements (PETES and MOPs) are relatively small molecules, resulting in a layer thickness of only about 3 nm in total. Therefore, the molecular binding process takes place very close to the semiconductor surface of the SiNW sensor and thus can effectively result in apparent changes of the current through the SiNW. In addition, TNT binding onto the SiNW surface may also take place via direct physisorption and/or the potential selective binding site (e.g., a pyridyl site, and/or silanol group on the bare area). To distinguish these mechanisms, we also conducted sensing experiments on a "Cu-MOPs-free" device functionalized with PETES only. As shown in Figure A-2.4, the detection sensitivity of this device toward the target TNT was three orders of magnitude lower than the Cu-MOPs-modified sensor, indicating the signal from Cu-MOPs-modified sensor primarily resulted from molecular recognition, instead of physisorption or binding to the pyridyl sites.

Cross-reactivity of the Cu-MOPs modified device to the structurally related nitro-aromatic explosives, 2,4-dinitrotoluene (2,4-DNT) and 4-nitrotoluene (4-NT), was also investigated. As shown in Figure A-2.5, the sensing results clearly show a strong preference for binding explosives with more nitro groups. When sensing at a fixed concentration of 1 nM, the Cu-MOPs had a preferred affinity for TNT and thus led to a marked increase of the electrical signal for TNT over 2,4-DNT by a factor larger than 4, corresponding to an increased sensitivity of 1 to 2 order of magnitude in terms of the concentration. In the case of 4-NT no signal change was observed. This can be understood by its lower electron-withdrawing nature as only one nitro group is present in this case. When the concentration was increased to 1 μM, a change in the conductance was detected, albeit with a very small value compared to TNT. These observations are in line with linear free energy relationships found in e.g. acidity studies of nitro-substituted toluene.[39]
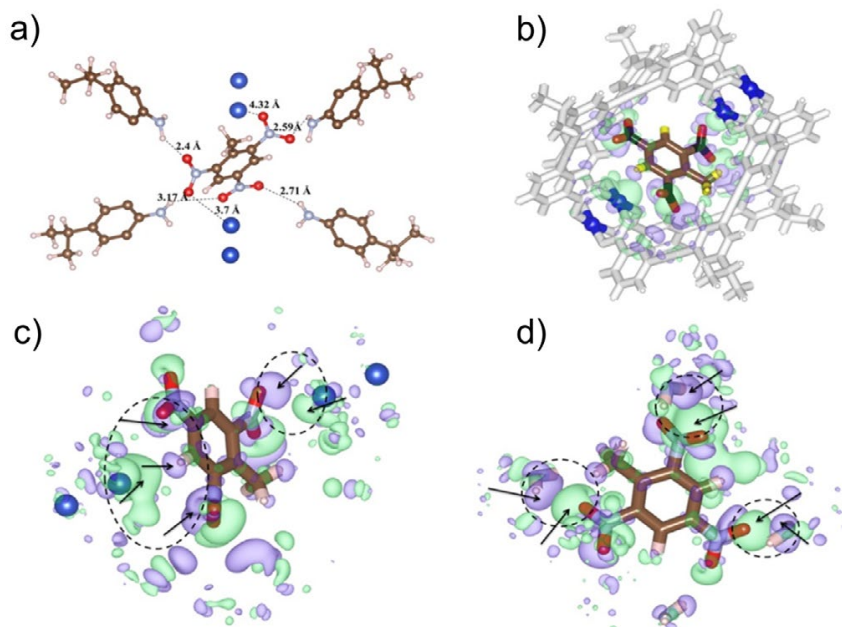
Figure 4.3 (a) Simulated geometries of TNT in Cu-MOPs; **(b)** Difference-electron density of TNT@Cu-MOPs; Difference-electron density of copper cluster-TNT domain **(c)** and –NH₂-TNT domain **(d)**; Cyan constant-density surfaces (iso-surfaces) represent electron accumulation regions, while violet surfaces represent electron depletion regions. An isosurface value of 0.0002 e⁻/bohr³ was adopted.

To elucidate the good selectivity of our sensing system, a DFT computational study was conducted to evaluate the host–guest interactions. The DFT-D2 method was adopted to consider the Van der Waals interactions.[26] As shown in Figure 4.3a, clearly one Cu-MOPs cage can only accommodate one TNT molecule due to the size-fit and thus the complex adopts a 1:1 stoichiometry. For the complex of TNT@Cu-MOPs, two nitro groups of the TNT molecule are directed to two NH_2 groups of Cu-MOPs, while the third nitro group points to two NH_2 groups, with the line formed by the four Cu^{2+} ions of the Cu-MOPs penetrating the aromatic ring of the TNT molecule (Figure 4.3a). The interatomic O–H distances suggest four binding sites between Cu-MOPs and TNT. However, in the cases of DNT and 4-NT, the number of binding sites decreases to 3 and 2, respectively, due to reduced number of NO_2 groups. As shown in Table 4.1, the binding energy of TNT is larger than that of DNT or 4-NT, which is in line with the good sensitivity presented in Figure A-2.5.

Table 4.1 Maximum charge transfer from nitro groups to Cu2+ and amino sites of Cu-MOPs upon adsorption of the explosive molecules TNT, DNT, and NT, using the DDEC method, and the corresponding binding energies; Detailed charge redistribution analysis can be found in Table A-2.1, 2.2, 2.3; All charge transfer values are given in electron charge.

	Cu^{2+}	Amino	Explosive	Binding energy (eV)
TNT@Cu-MOP	-0.0351	-0.0227	0.0471	-0.84
DNT@Cu-MOP	-0.0238	-0.0203	0.0661	-0.75
4-NT@Cu-MOP	-0.0078	-0.0157	0.0371	-0.62

To gain further in-depth understanding of the electron redistribution and/or transfer between Cu-MOPs and the explosive molecules, difference electron-density analysis and density-derived electrostatic chemical net atomic charge (DDEC) calculations were performed.[26] As shown in Figure 4.3b-d, difference-electron density analysis results revealed that significant charge transfer occurs between Cu-MOPs and the trapped TNT. As determined by the DDEC method (Table A-2.1), TNT loses electron density to the adjacent Cu atoms and amino groups of Cu-MOPs, with the maximum charge transfer to a single Cu of −0.0351 and a single amino of -0.0227; such electron withdrawal from TNT mainly occurs to its nitro groups with the maximum charge at a single nitro group of -0.0388. Overall, the net charge transfer from the TNT molecule is −0.0471, reflecting a strong interaction. Similar to TNT, the DNT and 4-NT molecules lose electron density via its nitro groups to the adjacent Cu^{2+} ions and amino groups of Cu-MOPs (Table A-2.2, 2.3). Interestingly, the charge transfer values to both the Cu ions and -NH$_2$ groups are somewhat smaller in DNT and 4-NT than TNT, supporting the observed highest sensitivity for TNT. Although the charge transfer values for the series of explosive molecules does not show an explicit trend, yet, strong charge transfer between Cu-MOPs and explosive molecules is well evidenced. Based on the DFT and DDEC simulations, we conclude that the charge redistribution or transfer inside Cu-MOPs after the trapping of explosive molecule is the prime cause for the modulation of the electrical conductance of SiNW, and that the number of nitro groups plays a prime role in the selectivity of the detection.

Next, to explain the detection scheme of our platform, we propose a model based on band bending of the Cu-MOPs-modified SiNW due to back-gate tuning and surface binding with targets, which links the microscopic events of the surface site

binding with the electrical performance of the SiNWs.[40, 41] As the semiconductor in our case is p-type doped, the Fermi level of the SiNW ($E_{F,NW}$) is close to the valence band (VB). When a back-gate voltage is applied to the device, an electric field is built up between the gate and the SiNW. The electric field can penetrate into the near-surface region of the SiNW channel due to insufficient screening by the charge carriers which are present in the SiNW at a relatively low concentration. Working in the depletion regime, the back-gate potential bends both the valence and conductance bands downward, as the concentration of majority carriers (holes) is less than the background doping concentration. Meanwhile, the number of holes is also affected by changes in the local electrical potential at the front oxide (FOX) side, *i.e.* the side where the chemical recognition process occurs. The observed current increase is attributed to an increased negative front-gate potential as a result of the molecular recognition process. The increased negative front-gate potential originates from a net dipole moment of the TNT-receptor complex pointing towards the SiNW surface. As confirmed by the results of DDEC calculations, this can be interpreted as an increase of the electron density at the copper ion closest to the nanowire surface coming from the aromatic core of the TNT molecule. Noteworthy, upon the formation of a hydrogen bond between the $-NO_2$ group of TNT and the $-NH_2$ group of Cu-MOPs, the dipole moment may change in the direction parallel to the SiNW length, but actually give little value to the conductance/current changes of SiNW (Figure 4.4). In summary, we speculate it is the interaction between trapped molecule TNT and adjacent copper, serving as negative potential on the FOX side of p-doped SiNW, explaining the bending the valence and conduction band upward, and thus leading to higher conductance/current.
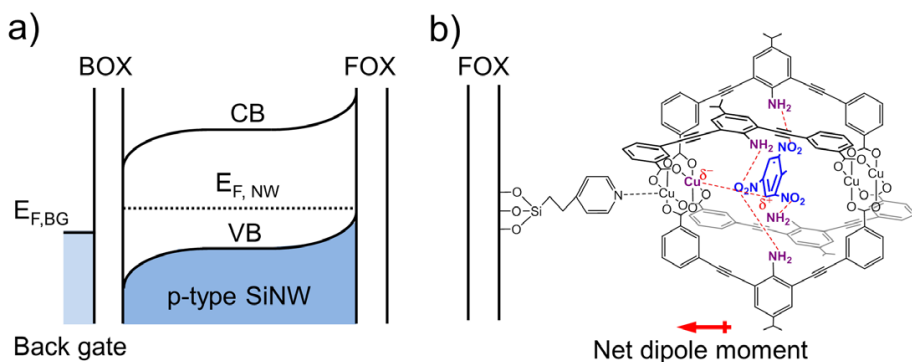
Figure 4.4 (a) Qualitative band diagram of the SiNW responding to the gate tuning and surface binding with TNT, with conduction band minimum (CB), valence band maximum (VB), SiNW Fermi level energy ($E_{F,NW}$) and back-gate Fermi energy ($E_{F,BG}$). BOX, *i.e.* buried oxide, FOX, *i.e.* front oxide; **(b)** Molecular interaction between TNT (in blue) and Cu-MOPs on the FOX of SiNW device.

Finally, the Cu-MOPs-modified SiNW devices have been investigated for their stability in time (Figure A-2.6). During a period of 7 weeks, two devices were characterized by recording the *I-t* curves in pure ethanol and then in 10 nM TNT, in order to obtain $\Delta I/I_0$ data for the target. During the whole period, both of the SiNW chips kept their sensing properties and showed rather consistent results with a little deviation. We believe that the stability benefits from the chemical attachment of the MOPs to the SiNW surface, the non-covalent nature of the resulting heterobinary complex between the explosive molecule and Cu-MOPs, as well as the trapped molecules in the cavity are easily removed by vacuum before further measurements. Figure A-2.7 shows a complete recovery of a Cu-MOPs-modified SiNW device after vacuum, which was subsequently tested in an ethanol solution. All these sensing results strongly prove the good reliability and reproducibility of our developed sensors.

4.4 Conclusions

Based on the unique confinement effect and host-enhanced CT interaction behavior of the Cu-MOPs cage grafted onto the SiNW-FET device, label-free electrical detection and discrimination of explosives with similar structure are realized. These sensing features are on the one hand attributed to the rational integration of multiple weak molecular interactions inside the molecular cage, providing multiple guest-accessible interaction sites and thus bestowing the cavity

with selectivity for a specific target. On the other hand, the formation of host-stabilized CT complexes inside the MOP cavity act as an effective molecular gating element and thus modulate the electrical conductance of the sensing elements. While the sensitive and selective detection is realized, the stability of the MOP-modified sensors reaches a satisfactory level. Importantly, the use of MOP as receptors on a SiNW sensor surface, as performed in this work, promises the design of molecular cages for other analytes and improved selectivities and sensitivities through the careful selection of the bridging ligands and metal ions.[42] When combined with sensing array technology, the systematic variation of the MOP structure over the different array elements may provide a powerful tool marrying the advantages of selective receptor design with arrays. We believe the current work shows the potential of MOPs and other receptor architectures (like MOFs)[43] grafted onto nano- and micrometer-sized electrode structures, and may open a new way to design and develop novel sensing platforms.

References

1.   Cui, Y.; Wei, Q.; Park, H.; Lieber, C. M. *Science* **2001,** 293, 1289-1292.
2.   Cui, Y.; Lieber, C. M. *Science* **2001,** 291, 851-853.
3.   Schmidt, V.; Wittemann, J. V.; Senz, S.; Gosele, U. *Adv. Mater.* **2009,** 21, 2681-2702.
4.   Ramgir, N. S.; Yang, Y.; Zacharias, M. *Small* **2010,** 6, 1705-1722.
5.   Long, Y. Z.; Yu, M.; Sun, B.; Gu, C. Z.; Fan, Z. *Chem. Soc. Rev.* **2012,** 41, 4560-4580.
6.   Cao, A.; Sudhölter, E. J. R.; de Smet, L. C. P. M. *Sensors* **2014,** 14, 245-271.
7.   Dasgupta, N. P., et al. *Adv. Mater.* **2014,** 26, 2137-2184.
8.   Yinon, J. *Anal. Chem.* **2003,** 75, 99A-105A.
9.   Moore, D. S. *Rev. Sci. Instrum.* **2004,** 75, 2499-2512.
10. Hu, Z.; Deibert, B. J.; Li, J. *Chem. Soc. Rev.* **2014,** 43, 5815-5840.
11. Engel, Y.; Elnathan, R.; Pevzner, A.; Davidi, G.; Flaxer, E.; Patolsky, F. *Angew. Chem. Int. Ed.* **2010,** 49, 6830-6835.
12. Wang, D.; Sun, H.; Chen, A.; Jang, S. H.; Jen, A. K. Y.; Szep, A. *Nanoscale* **2012,** 4, 2628-2632.
13. Lichtenstein, A., et al. *Nat. Commun.* **2014,** 5, doi:10.1038/ncomms5195.
14. Yang, Z., et al. *Adv. Funct. Mater.* **2015,** 25, 4039-4048.
15. McAlpine, M. C., et al. *J. Am. Chem. Soc.* **2008,** 130, 9583-9589.
16. He, C., et al. *Angew. Chem. Int. Ed.* **2008,** 47, 877-881.
17. Tranchemontagne, D. J. L.; Ni, Z.; O'Keeffe, M.; Yaghi, O. M. *Angew. Chem. Int. Ed.* **2008,** 47, 5136-5147.
18. Li, J. R.; Zhou, H. C. *Nat. Chem.* **2010,** 2, 893-898.
19. Zhao, D., et al. *Adv. Mater.* **2011,** 23, 90-93.

20. Harris, K.; Fujita, D.; Fujita, M. *Chem. Commun.* **2013,** 49, 6703-6712.
21. Ahmad, N.; Younus, H. A.; Chughtai, A. H.; Verpoort, F. *Chem. Soc. Rev.* **2015,** 44, 9-25.
22. Wang, C., et al. *Adv. Funct. Mater.* **2015,** 25, 6009-6017.
23. Cao, A.; Mescher, M.; Bosma, D.; Klootwijk, J. H.; Sudhölter, E. J. R.; de Smet, L. C. P. M. *Anal. Chem.* **2015,** 87, 1173-1179.
24. Kresse, G.; Furthmüller, J. *Phys. Rev. B* **1996,** 54, 11169-11186.
25. Kresse, G.; Joubert, D. *Phys. Rev. B* **1999,** 59, 1758-1775.
26. Grimme, S. *J. Comput. Chem.* **2006,** 27, 1787-1799.
27. Manz, T. A.; Sholl, D. S. *J. Chem. Theory Comput.* **2010,** 6, 2455-2468.
28. Manz, T. A.; Sholl, D. S. *J. Chem. Theory Comput.* **2011,** 7, 4146-4164.
29. Manz, T. A.; Sholl, D. S. *J. Chem. Theory Comput.* **2012,** 8, 2844-2867.
30. Mescher, M.; de Smet, L. C. P. M.; Sudhölter, E. J. R.; Klootwijk, J. H. *J. Nanosci. Nanotechnol.* **2013,** 13, 5649-5653.
31. Ostaci, R. V., et al. *Langmuir* **2008,** 24, 2732-2739.
32. Mescher, M.; Brinkman, A. G. M.; Bosma, D.; Klootwijk, J. H.; Sudhölter, E. J. R.; de Smet, L. C. P. M. *Sensors* **2014,** 14, 2350-2361.
33. Paska, Y.; Haick, H. *ACS Appl. Mater. Inter.* **2012,** 4, 2604-2617.
34. Wang, B.; Haick, H. *ACS Appl. Mater. Inter.* **2013,** 5, 5748-5756.
35. Wang, B.; Haick, H. *ACS Appl. Mater. Inter.* **2013,** 5, 2289-2299.
36. Gao, X. P. A.; Zheng, G.; Lieber, C. M. *Nano Lett.* **2010,** 10, 547-552.
37. Stern, E.; Wagner, R.; Sigworth, F. J.; Breaker, R.; Fahmy, T. M.; Reed, M. A. *Nano Lett.* **2007,** 7, 3405-3409.
38. Elnathan, R., et al. *Nano Lett.* **2012,** 12, 5245-5254.
39. Lelievre, J.; Farrell, P. G.; Terrier, F. *J. Chem. Soc., Perkin Trans. 2* **1986**, 333-336.
40. Zhang, Z.; Yates, J. T. *Chem. Rev.* **2012,** 112, 5520-5551.
41. Chen, C. Y., et al. *ACS Nano* **2012,** 6, 9366-9372.
42. Custelcean, R. *Chem. Soc. Rev.* **2014,** 43, 1813-1824.
43. Sachdeva, S., et al. *Small* **2017,** 13, 1604150.

Chapter 5

Enhanced Vapor Sensing using Silicon Nanowire Devices Coated with Pt Nanoparticle Functionalized Porous Organic Frameworks

Abstract: Recently various porous organic frameworks (POFs, crystalline or amorphous materials) have been discovered, and were used for a wide range of applications, including molecular separations and catalysis. Silicon nanowires (SiNWs) have been extensively studied for diverse applications, including transistors, solar cells, lithium ion batteries and sensors. Here we demonstrate the covalent attachment of POFs onto SiNW surfaces and explored the effect on the electrical sensing properties of SiNW-based devices. The surface modification by POFs was easily performed by polycondensation on amine-modified SiNWs. Platinum nanoparticles were formed in these POFs by impregnation with chloroplatinic acid followed by chemical reduction. The final hybrid system showed highly enhanced sensitivity for methanol vapor detection. We envisage that the integration of SiNWs with POF selector layers, loaded with different metal nanoparticles will open up new avenues, not only in chemical and biosensing, but also in separations and catalysis.

5.1 Introduction

Improved sensitivity and selectivity in the detection of gas-phase molecules for environmental monitoring, process control and safety, and medical diagnosis is of utmost importance.[1] One promising approach for the direct electrical detection of analytes is by using nanowires configured as field-effect transistors (FETs), which exhibit superior sensitivity as given by their high surface-to-volume ratio and the direct signal amplification by the transistor function.[2, 3] Particularly silicon nanowire-based FETs (SiNW-FETs), pioneered by Lieber's group,[4] have been studied for more than 15 years now and have attracted a great deal of interest, mainly for their controllable properties and compatibility with very-large-scale integration (VLSI) processes and complementary metal–oxide–semiconductor (CMOS) technologies.[5, 6] While most SiNW-FET studies focus on detection of analytes in aqueous solutions,[7, 8] different gas-phase applications of electrical SiNW-based devices are attracting increasing interest.[9] For instance, the research group of Haick published a number of systematic studies on the fundamentals and applications of functionalized SiNW-based FETs for the detection of volatile organic compounds (VOCs).[10, 11] In addition, surface functionalization of SiNWs with Pd nanoparticles,[12] oligopeptides,[13] diphenylchlorophosphate (DPCP) receptors,[14] or 3-aminopropyltrimethoxysilane (APTES)[15] allowed for the rapid detection of H_2, acetic acid vapors, DPCP and explosives, respectively. All these studies have shown the advantages of the controlled surface modification of the SiNWs in tuning the sensor selectivity.

A variety of porous materials, such as metal organic polyhedra (MOP),[16] metal organic frameworks (MOFs)[17] and covalent organic frameworks (COFs),[18] have gained a lot of interest due to their exceptionally high specific surface areas, high specific gas storage and separation capabilities and their potential in catalysis and sensing application.[19-21] The chemical diversity of these porous materials allows for a fine-tuning of the chemical and physical properties by tailored synthesis.[22] In addition, the exposure of properly designed affinity sites on the porous materials enable further coupling of functional substrates, for instance to Au plasmonic substrates and to SiNWs platforms, expanding their application window significantly.[19, 23] Along these lines, we developed and explored a unique hybrid construct: porous organic framework (POF)-decorated SiNWs for the investigation of chemical vapor sensing. POFs are extremely attractive as affinity layers as they are not only highly porous, but also highly stable due to the formation of covalent bonds rather than metal coordination bonds; some of the early reported MOF

structures decompose gradually if environmental moisture is present.[24] In addition, post-synthesis strategies can be applied to POFs to further tune their physico-chemical properties. We report here on a surface modification strategy to covalently bind POFs to SiNW-based devices, after which the electrical properties of the resulting hybrid construct were investigated upon changes in the environmental humidity and methanol vapors. Moreover, the post-synthesis functionalization of the POF-SiNW hybrid by the *in-situ* formation of Pt nanoparticles (PtNPs) results in advanced sensing properties of methanol vapors.

5.2 Experimental

5.2.1 Surface functionalization

The silicon wafers and SiNW chips were cleaned by sonication in acetone for 2 min, followed by a rinsing step with ethanol and Milli-Q water, and then dried by a N_2 gas flow. Next, the devices were cleaned/oxidized with air plasma for 2 min (Harrick PDC-002 at a pressure of ∼0.2 mbar and an RF coil power of 29.6 W). To obtain an amino-terminated surface, the cleaned devices subsequently submerged in a 1 vol % solution of 3-amino propyl triethoxysilane (APTES) in ethanol (95%) at room temperature for half an hour. Afterwards, the devices were removed from the silane solution and were rinsed under flows of ethanol and then baked at 150 °C for 5 mins.[15] The POF-modified surface was prepared in the optimized condition, the APTES-modified SiNW chip and Si wafer were immersed a DMSO solution (30 ml) containing melamine (0.313 g / 2.5 mmol) and terephthaldehyde (0.5 g / 3.75 mmol), the solution was then heated at 180 °C for 14 hours. Afterwards, the devices were rinsed with acetone, THF and CH_2Cl_2 for several times and dried using a N_2 gas flow. The POF-SiNW devices and pieces of Si wafer were stored under an atmosphere of N_2 until further analysis or post-treatment. To get PtNP@POF-SiNW, the POF-SiNWs device was treated with H_2PtCl_6 followed by a reduction step using $NaBH_4$, the ratio of H_2PtCl_6 to N atoms in POF was 1: 37.

5.2.2 Gas sorption analysis

The POF surface area and pore size distributions were measured by N_2 adsorption and desorption at 77 K in a Quantachrome Autosorb-6B setup. The surface areas were calculated in the relative pressure (P/P_0) range from 0.01 to 0.10, where P_0 was 765 mmHg. Pore size distributions and pore volumes were derived from the adsorption branches of the isotherms using the non-local density functional theory (NL-DFT) pore model for carbon slit, as these were found to give the best fit. Samples were degassed at 393 K for 16 h under N_2 flow before analysis. CO_2

isotherms at 273 K were measured using a Tristar II 3020 (Micromeritics), and P_0 was 26039 mmHg. Prior to the measurements, the samples were degassed at 393 K under N_2 flow for at least 16 h.

5.2.3 X-ray photoelectron spectroscopy

XPS measurements were performed on a K-alpha Thermo Fisher Scientific spectrometer using a monochromatic Al Kα X-ray source. The measurements were performed at ambient temperature and chamber pressure of about 10^{-8} mbar. The spot size was 400 μm. A flood gun was used for charge compensation. All the spectra measured were corrected by setting the reference binding energy of carbon (C1s) at 284.8 eV. The spectra were analyzed using the Thermo Avantage software package.

5.2.4 Ellipsometry

The ellipsomerty measurements were carried out on a commercial imaging nulling-ellipsometer (EP3 Nanoscope, Accurion). The light source was a He-Ne laser with a wavelength of 658 nm. Measurements were performed for three different spots on each specimen. The following refractive indices were used in a three-layer model of substrate-organic-layer air: $n_{SiO2} = 1.46$, $n_{air}=1$, $n_{APTES} =1.6$.[24]

5.2.5 Sensor fabrication and characterization

The surface-modified SiNW chips were wire-bonded using conductive glue and Al wires (25 μm in diameter) to the chip holder, and then placed in a home-built gas cell for vapor sensing.[25, 26] For SiNW FET measurements, a standard Keithley 4200 semiconductor characterization system equipped with three source–measurement units was used for the electrical characterization of the SiNW device during the exposure to different vapors and vapor conditions.

5.2.6 Other measurements

Fourier transform infrared (FTIR) spectra were collected with a Nicolet 8700 spectrometer, using the KBr pellet method. Surfaces of the Si wafer and SiNW were analyzed with FEI Nova NanoSEM™ scanning electron microscopes (SEM). UV-vis measurements were performed on a Shimadzu spectrophotometer at room temperature. Transmission electron microscopy (TEM) images and tomography were obtained with a JEOL JEM1400 plus & JEM3200 FSC. Tomographic construction was performed using IMOD.[27]

5.3 Results and discussion

POFs were covalently grafted onto the SiNW surface via the polycondensation of melamine and terephthaldehyde on the amine-modified SiNWs,[28] as illustrated in Fig. 5.1a, b. The POF-modified SiNWs together with the precipitated materials were harvested and cleaned for different characterizations.
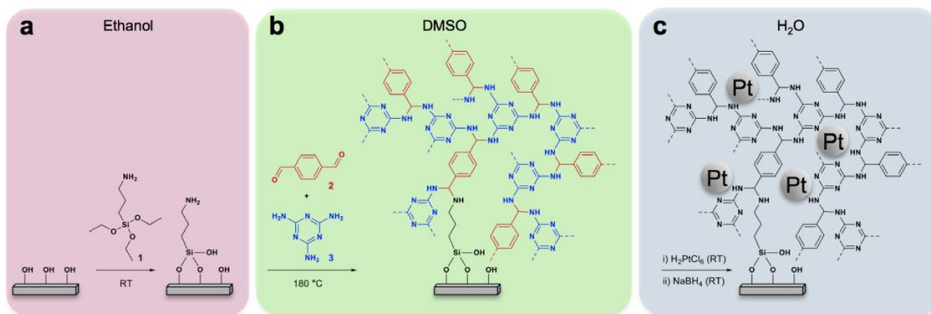
Figure 5.1 Schematic representation of **(a)** APTES grafting to the silanol terminated surface of SiNW, **(b)** the covalent modification process of the SiNW surface with melamine-terephthaldehyde based POFs, **(c)** the metalation of a POF-SiNW via an *in-situ* chemical reduction. Molecule 1-3: APTES, melamine, terephthaldehyde, respectively.

The molecular details of the reactants and the effect of different solvents, temperature, reaction time and the use of catalyst on the products were examined by Fourier Transform Infrared spectroscopy (FTIR), as shown in Figure A-3.1. Only in the case of DMSO as the solvent, the precipitate in the reaction solution was found to be flocculent. Reactions at the other conditions gave granular products. For the products obtained in all solvents the FTIR spectra show vibrations around 1550 cm^{-1} and 1480 cm^{-1}, which are attributed to the stretching vibration of the triazine ring,[29] indicating the successful incorporating of the melamine into the molecular network. However, the vibrations around 1690 cm^{-1} (C=O stretching), 3420 cm^{-1} and 3470 cm^{-1} (NH$_2$ stretching) are absent or strongly attenuated only for the product synthesized in DMSO, which proves the highest conversion of the functional groups initially present in the monomers was achieved in DMSO. Therefore, the reaction was optimized in this solvent. Moreover, the bands corresponding to imine bond vibration (*e. g.* 1600 cm^{-1}) was absent in the FTIR spectra, which indicates the aldehyde function has reacted twice with an amino group from the melamine building block forming aminal moieties. The high boiling point combined with the high polarity of DMSO contributes to the increased solubility of the initially formed polycondensated product via imine bonds, making subsequent condensations to aminal bonds possible as indicated by the structure in Figure 5.1b.[30] In addition,

92

considering the (in)stability of the Al electrodes on the SiNW chip during this reaction, we optimized the reaction time to 14 hours. Longer reaction times showed similar FTIR spectra of the product, as shown in Figure A-3.1b.
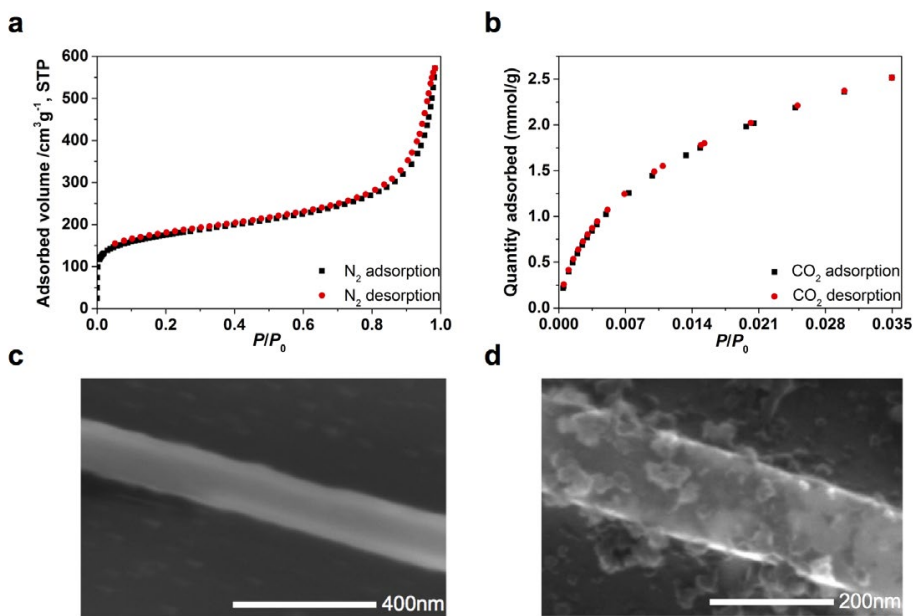
Figure 5.2 (a) N_2 sorption isotherm acquired at 77 K, **(b)** CO_2 sorption isotherm acquired at 273 K of the POF powder synthesized in optimized condition, **(c)** SEM image of the bare SiNW, **(d)** SEM image of the SiNW decorated by POFs.

The porous structure of the obtained flaky POF material synthesized in optimized condition was investigated by N_2 gas sorption at 77 K (Figure 5.2a). At low relative pressures a rapid uptake of N_2 is observed, indicating the presence of micropores. At high relative pressures (*i.e. $P/P_0 > 0.8$*) some hysteresis is observed, which is attributed to the presence of mesopores where some capillary condensation can take place. At high relative pressures (*i.e. $P/P_0 > 0.9$*) a steep rise in adsorption was observed, which indicates the presence of even larger pores, likely due to inter-particle porosity.[30] The calculated Brunauer-Emmett-Teller (BET) specific surface area were found to be 620 m²/g and 640 m²/g for POFs synthesized for 14 hours and 72 hours, respectively, which are lower than the value of 1377 m²/g as reported the first time for this material,[28] but very similar to more recently reported values for microporous organic polymer materials prepared via polycondensation (values ranging from 70 to 614 m²/g).[30-32] From the N_2 adsorption isotherms recorded at 77 K, the pore size distribution (PSD) was calculated with the use of Density Functional

Theory (DFT), resulting in a pore diameter ranging from 1 to 55 nm (*i.e.*, micro- to mesopores; Figure A-3.2). Considering the presence of N atoms in the POF network and the likely favorable interaction with CO_2, CO_2 sorption isotherms were measured up to 1.2 bar at 273 K (Figure 5.2b). At 1 bar ($P/P_0 = 0.029$), the observed CO_2 uptake is 2.3 mmol/g, which is very similar to the high values of ~2.0 mmol/g and ~1.5 mmol/g as reported for the similar polymer networks (PI-1and PI-2) rich in N atoms.[31] The high value of CO_2 uptake here can be attributed to the high density of nitrogen in the POF structure originated from the melamine building blocks.
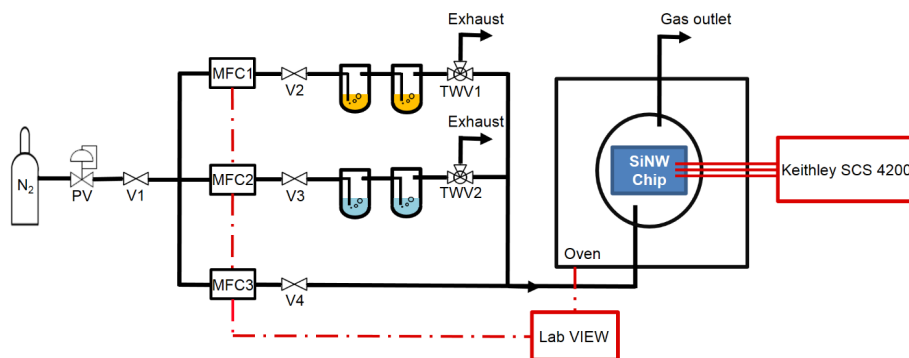
Figure 5.3 Vapor sensing set-up, PV: pressure valve, V: manual valve, MFC: mass flow controller, TWV: three-way valve.

Similar surface modifications on silicon wafers were performed as model system for the SiNWs. These modified wafers were investigated by X-ray photoelectron spectroscopy (XPS) and compared with the unmodified wafers. The relative atomic surface composition of Si, O, C and N is shown in Table A-3.1. Upon modification with APTES the N percentage increases from 0 to 2.5%, indicating the successful silanization. Meanwhile, the ellipsometry measurements showed 0.7 nm as the optical thickness, which indicates a monolayer of APTES formed on the Si wafer.[24] After the POF polycondensation and being coupled to the APTES layer, the N percentage increases to a value of 31%. The observed N/C ratio is found to be very similar to the ratio observed in the pure POF powder (31%). Inspection of the SiNW before and after surface modification by using scanning electron microscopy (SEM) showed the presence of flaky POF material on the nanowire (Figure 5.2d). Similar flaky POF structures were observed on the modified silicon wafers (Figure A-3.3).
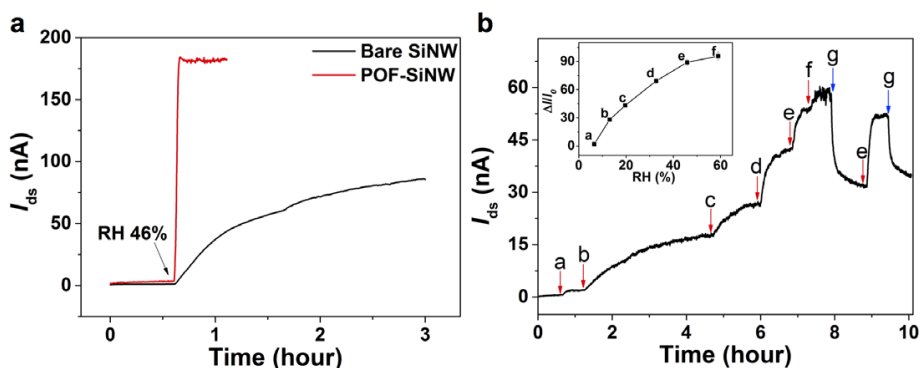
Figure 5.4 Variation of drain-source current (I_{ds}) of bare SiNW and POF-modified SiNW with humidity at V_g = -3 V and V_{ds} = 0.05 V, **(a)** Real-time variation of I_{ds} after a step-wise increase of the relative humidity from 0 to 46%, **(b)** Increase of I_{ds} in time after the successive increase of RH from 0 to 60% (labels a-f refer to the injection of RH in 6.5, 13, 20, 33, 46 and 60%, respectively, while label g indicated the start of a pure N_2 flow). The inset shows the relative increase of I_{ds} as function of RH.

Next, we have compared the electrical device response towards changes in humidity for POF-modified SiNWs and bare SiNWs using our home-built vapor sensing apparatus (Figure 5.3).[25, 26] Both types of p-doped SiNWs were set in the depletion mode by the application of a back-gate potential of V_g = -3 V, and the varying drain-source current (I_{ds}) was registered under the conditions of a constant source-drain voltage (V_{ds}) set to 0.05 V. Step-wise increase of the relative humidity to RH = 46% shows for the bare SiNW a very slow increase of I_{ds} reaching more or less equilibrium after 2 h. The POF-modified SiNW showed a fast increase of I_{ds} and equilibration after *ca*. 3 min, which is around 40 times faster as compared to unmodified sensor. The I_{ds} at equilibrium for the POF-modified SiNWs is about two times higher than for the bare SiNWs. In both situations the I_{ds} increases, indicating an increase of the concentration of the majority charge carriers (here holes). This is understood as that the injection of water vapor results in partial deprotonation of surface silanol groups on the SiNW, due to the pK_a value of Si-OH being ~4.[33] The resulting negatively charged Si-O⁻ on the surface will bend the SiNW valence band up, leading to more holes flowing through the p-doped SiNW channel, thus explaining the observed increase of I_{ds}. For the POF-modified SiNWs this effect is enhanced both in time and in overall drain-source current effect. This is attributed to the presence of the flaky POF structure with its high specific surface area and its richness in N atoms. The high specific surface area will contribute to a fast and increased uptake of water into the porous structure. The water taken up and the

present nitrogen containing groups in the POF will facilitate the partial deprotonation of the silanol groups on the surface. The POF-modified SiNWs were also investigated with varying RH between 6 and 60% and the I_{ds} was found to increase with RH (Figure 5.4b). The sensitivity response for humidity variation of the POF-modified SiNW sensor are found to be very high; within the concentration range studied, the signal increased by ~2 orders of magnitude, which is comparable to the values reported for humidity sensors using nanoporous polymer membranes[34] and graphene oxide.[35] In addition, the POF-modified sensor showed a satisfactory level of repeatability towards water vapor sensing, as it is demonstrated in Figure A-3.4.
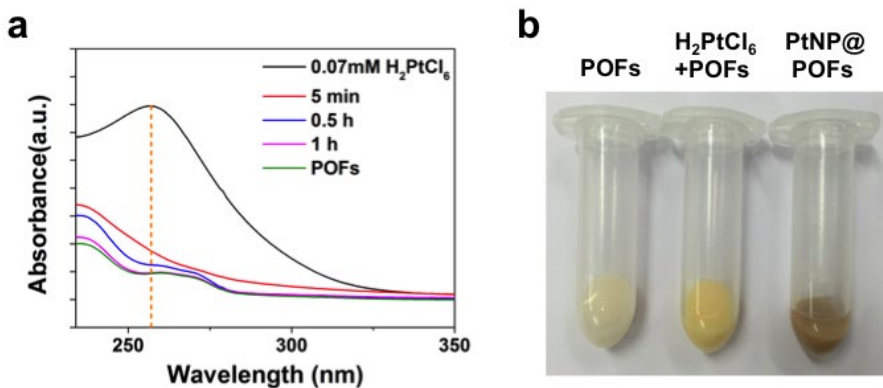
Figure 5.5 (a) UV-vis measurements of 0.07 mM H_2PtCl_6 in water and the aqueous supernatant in the presence of POFs at different time intervals of contacting, showing the decrease of H_2PtCl_6 concentration and indicating the POF affinity for H_2PtCl_6, **(b)** Sediments of three aqueous suspensions: POFs, metalation products and metalation products after *in-situ* reduction of the Pt^{4+}.

Given the high CO_2 uptake of the POF powder, we tested the CO_2 sensing using POF-modified SiNWs. However, varying amounts of CO_2 in N_2 in the range of 0.5-5% at room temperature and 1 bar in the presence of water (and without water) did not show any sensor response. We speculate that in a dry state at room temperature, CO_2 may interact with POFs through physisorption. In such a case no ions are formed and therefore it hardly will affect the electrical properties of SiNWs. While primary/secondary amines, as well as triazine, can form carbamates with CO_2,[36-37] we consider chemisorption to be unlikely, as the CO_2 isotherm in Figure 5.2b shows hardly any adsorption-desorption hysteresis, suggesting a completely reversible physical adsorption in our system. For a wet state, CO_2 reacted with water and carbonic acid was formed, however, an obvious change of pH was absent, therefore the water sensing dominates the outcome.
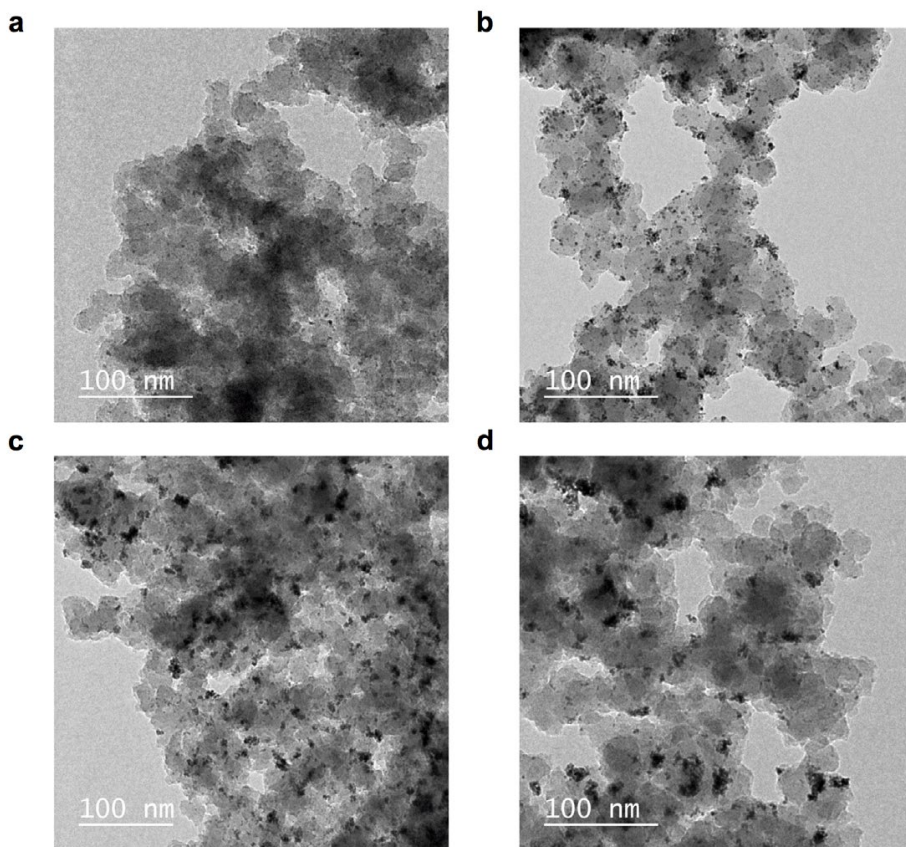
Figure 5.6 TEM images after NaBH$_4$ reduction of POFs containing different amounts of H$_2$PtCl$_6$, showing the formed Pt nanoparticles with different particle sizes. The molar ratio between H$_2$PtCl$_6$ and N atoms in POFs is **(a)** 1 : 100, **(b)** 1 : 37, **(c)** 1 : 20, and **(d)** 1 : 4.

To further explore the application of POF-modified SiNW, we studied the post-synthesis functionalization of the porous layer through Pt metalation. This functionalization strategy started with impregnating the POF material with an aqueous chloroplatinic acid solution (H$_2$PtCl$_6$), followed by a reduction step using sodium borohydride (NaBH$_4$), as illustrated in Figure 5.1c. The chloroplatinic acid protonates the nitrogen sites in the POF to ammonium groups having the negatively charged [HPtCl$_6$]$^-$ as the counter ion. A suspension of POF in H$_2$PtCl$_6$ aqueous solution was shaken for different time intervals and the UV-vis absorption spectrum of the supernatant was recorded (Figure 5.5a). A clear decrease of the H$_2$PtCl$_6$ absorption at 259 nm in time is observed, indicating the adsorption of the metal precursor in the POF precipitate. After the metalation, the POF changed color from

off-white to yellow (Figure 5.5b). Subsequently, this material was treated with $NaBH_4$, and a clear color change from yellow to dark brown was observed for the POF material, indicating that the *in-situ* reduction to metallic Pt has taken place.

Next, the sample was inspected by transmission electron microscopy (TEM). Clear Pt nanoparticles of ca. 2 nm in diameter were observed, well dispersed over the flaky polymeric organic framework (Figure 5.6b). In the TEM image recorded before the reduction step, no nanoparticles were observed and the images are similar to the untreated POFs (Figure A-3.5). Varying molar ratios of H_2PtCl_6 : N in POF have been investigated further: 1 : 100, 1 : 20, and finally 1 : 4 (Figure 5.6a, c, and d, respectively). Upon increasing Pt : N ratio the single particle diameter was found to increase to 3-4 nm (Figure 5.6c) and for the highest ratios also the presence of agglomerates is observed (Figure 5.6d). To get a better insight in the tomography of the hybrid materials, TEM images were taken from different tilted angles, from which a 3D representation was reconstructed (Electrical Supporting Information). From these results it can be seen that the formed Pt nanoparticles and agglomerates are found predominantly at the outer surface of the POF material and hardly inside the porous structure. This can be rationalized by a $NaBH_4$ reduction process that starts at the outside, resulting in the formation of Pt nanoparticles that block further entrance of the reducing agent into the porous structure. Table A-3.2 summarizes the textural properties and CO_2 uptake of the metalized POFs with different molar ratios of H_2PtCl_6 : N in POF, nicely showing that the BET surface, micropore volume and CO_2 uptake reduction for increasing amounts of PtNPs.

To verify the metalation of POF and further *in-situ* reduction taken place on POF-modified Si substrate, XPS analysis was conducted. Figure 5.7a (powder sample) and 5.7c (modified Si wafer) show high-resolution region spectra of Pt 4f of the metalation of the products before the reduction. Both spectra show two main peaks at 73.2 eV and 76.8 eV, corresponding to Pt $4f_{7/2}$ and $4f_{5/2}$ of $PtCl_4^{2-}$ species , respectively.[37] After the $NaBH_4$ reduction, two peaks at 71.5 eV and 74.7 eV, corresponding to Pt^0 $4f_{7/2}$ and $4f_{5/2}$, respectively, are much more prominent in the spectra, which indicates the anchored Pt species are predominantly in the metallic state.
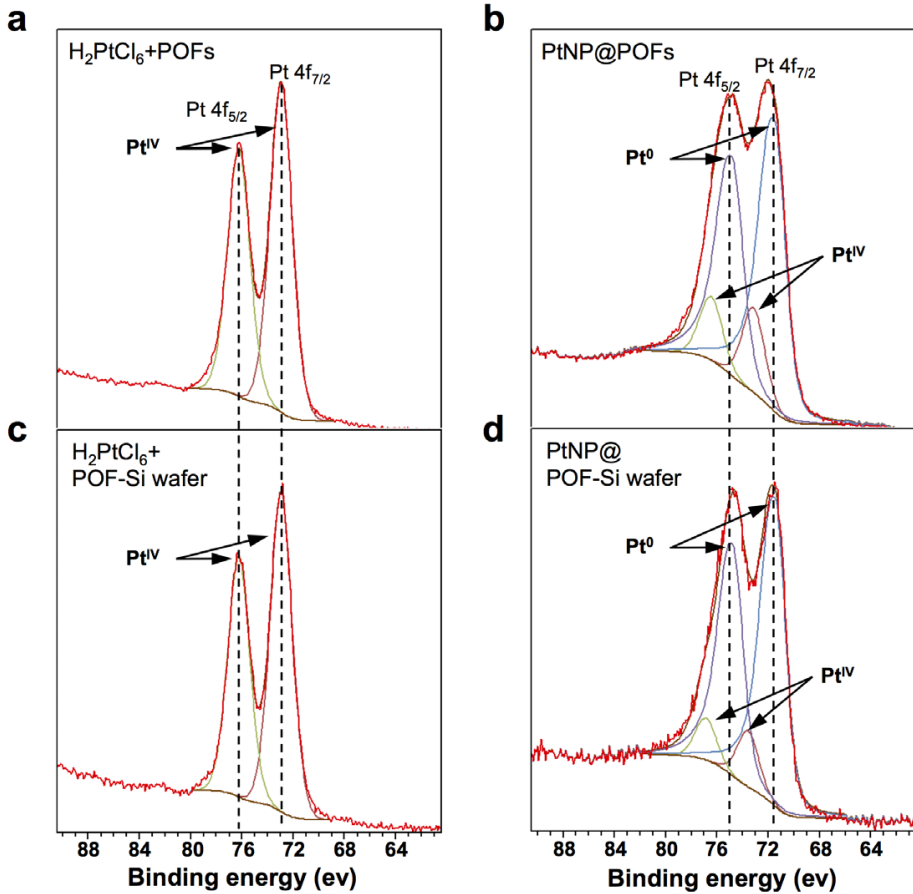
Figure 5.7 Pt4f XPS region spectra of **(a)** metalation of POF powder, **(b)** metalation of POF powder after reduction, **(c)** metalation of POF-Si wafer, **(d)** metalation of POF-Si wafer after reduction.

The method for the successful POFs impregnation with H_2PtCl_6 and the subsequent chemical reduction to metallic Pt nanoparticles has also been applied to POF-decorated SiNWs, to see whether this would have an effect on the affinity properties of the sensor coating. We first investigated the electrical behavior of PtNP@POF-functionalized SiNWs to varying methanol vapor concentrations in the range of 1200 to 6400 ppm. Under the same depletion-mode conditions as described before the change of I_{ds} was monitored. Increasing the methanol vapor concentration results in an increase of I_{ds} (Figure 5.8a). From the comparison with the response observed for the bare SiNW (which showed hardly any response) and the POF-SiNW (response increase of ca. 150 %; Figure 5.8b), the enhanced effect of the Pt

99

nanoparticles on the methanol response becomes very clear (increase of response of ca. 1350%). The gradually enhanced sensing resulting from these devices can be interpreted as follows. For the bare SiNW the injection of methanol vapor with the indicated concentration was not sufficient to affect the silanol dissociation; a similar performance has been reported by others.[38] For the POF-SiNW the injection of methanol showed a small increase of response. As explained earlier, we attribute this effect to a pre-concentration of methanol in the porous POF, and it contributes to the dissociation of the silanol groups, inducing a (more) negative surface charge, increasing the current of the p-type SiNW. For the PtNP@POF-SiNWs, the observed enhanced response toward methanol vapor, indicates an even higher methanol preconcentration due to the presence of PtNPs, and concomitant more negatively surface charge. Also, the enhancement could be resulted from the improved sensitivity of the device due to the capacitive coupling of the gate potential via these PtNPs to the SiNW.[39]
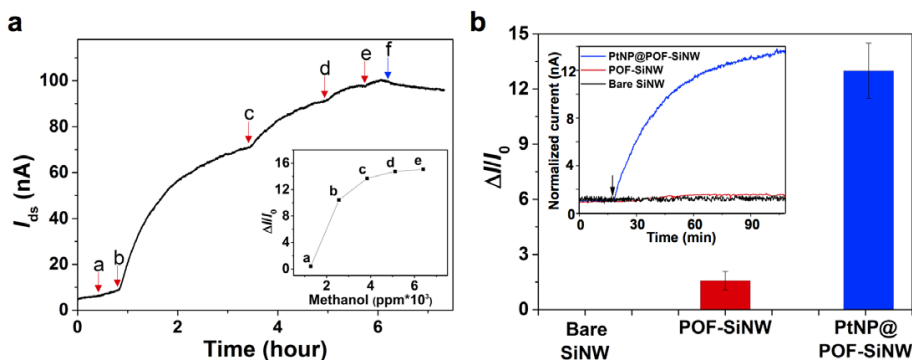
Figure 5.8 (a) Increase of Ids in time after the successive increase of the methanol vapor concentration from 1200 to 6400 ppm of PtNP@POF-SiNW devices (labels a-e represent the moment of the injection of methanol vapor concentration at 1200, 2500, 3800, 5100, and 6400 ppm, and f is the pure N_2 flow) at V_g = -3 V and V_{ds} = 0.05 V. The inset shows the relative increase of I_{ds} ($\Delta I/I_0$) as function of the methanol vapor concentration. **(b)** Normalized response upon exposure to 3000 ppm of methanol vapor for bare SiNW, POF-SiNW and PtNP@POF-SiNW sensors.

5.4 Conclusions

Polymeric organic frameworks (POFs) formed by the polycondensation of melamine and terephthaldehyde in DMSO as the solvent have been successfully covalently coupled to APTES-modified silicon nanowires. The observed increased sensitivity for water vapor detection, compared to the unmodified silicon nanowires, is attributed to the enhanced water affinity by the high surface area POF, resulting

100

in an increased surface silanol dissociation and concomitant increase of majority charge carriers (holes) and therefore an increase of the drain-source current (I_{ds}). Post-synthesis modification of the porous POF by chloroplatinic acid treatment and subsequent sodium borohydride reduction results in the formation of Pt^0 nanoparticles. The diameter of these nanoparticles was found to be 2-4 nm and depended on the loading density of chloroplatinic acid. The Pt^0 nanoparticles are found at the outer surface of the POF as deduced from 3D-TEM imaging. The presence of the Pt^0 nanoparticles in the POF contributes to the observed enhanced sensitivity for the detection of methanol vapor, likely as a consequence of the pre-concentration of methanol vapor and the capacitive coupling of the gate potential via the PtNPs to the SiNW.

With this study we have shown for the first time that POFs can be utilized successfully for the formation and dispersion of Pt^0 nanoparticles and that such an affinity layer can be bound covalently to the surface of SiNWs. These modified nanowires showed highly enhanced response towards methanol vapors. Here the introduced POF-SiNW platform is expected to become a challenging system for other post synthesis modification with a range of different metal nanoparticles. Such systems might find utilization not only in chemical and bio sensing, but also in gas separations and catalysis.

References

1.   Tricoli, A.; Righettoni, M.; Teleki, A. *Angew. Chem. Int. Ed.* **2010,** 49, 7632-7659.
2.   Allen, B. L.; Kichambare, P. D.; Star, A. *Adv. Mater.* **2007,** 19, 1439-1451.
3.   Chandran, G. T.; Li, X.; Ogata, A.; Penner, R. M. *Anal. Chem.* **2017,** 89, 249-275.
4.   Cui, Y.; Lieber, C. M. *Science* **2001,** 291, 851-853.
5.   Stern, E., et al. *Nature* **2007,** 445, 519-522.
6.   Mescher, M.; de Smet, L. C. P. M.; Sudhölter, E. J. R.; Klootwijk, J. H. *J. Nanosci. Nanotechnol.* **2013,** 13, 5649-5653.
7.   Duan, X.; Li, Y.; Rajan, N. K.; Routenberg, D. A.; Modis, Y.; Reed, M. A. *Nat. Nanotechnol.* **2012,** 7, 401-407.
8.   Bae, T. E.; Jang, H. J.; Yang, J. H.; Cho, W. J. *ACS Appl. Mater. Interfaces* **2013,** 5, 5214-5218.
9.   Cao, A.; Sudhölter, E. J. R.; de Smet, L. C. P. M. *Sensors* **2014,** 14, 245-271.
10.   Paska, Y.; Stelzner, T.; Christiansen, S.; Haick, H. *ACS Nano* **2011,** 5, 5620-5626.
11.   Paska, Y.; Stelzner, T.; Assad, O.; Tisch, U.; Christiansen, S.; Haick, H. *ACS Nano* **2012,** 6, 335-345.
12.   Chen, Z. H.; Jie, J. S.; Luo, L. B.; Wang, H.; Lee, C. S.; Lee, S. T. *Nanotechnology* **2007,** 18, 345502.
13.   McAlpine, M. C., et al. *J. Am. Chem. Soc.* **2008,** 130, 9583-9589.

14. Clavaguera, S., et al. *Angew. Chem. Int. Ed* **2010,** 49, 4063-4066.
15. Engel, Y.; Elnathan, R.; Pevzner, A.; Davidi, G.; Flaxer, E.; Patolsky, F. *Angew. Chem. Int. Ed* **2010,** 49, 6830-6835.
16. Vardhan, H.; Yusubov, M.; Verpoort, F. *Coord. Chem. Rev.* **2016,** 306, 171-194.
17. Furukawa, H.; Cordova, K. E.; O'Keeffe, M.; Yaghi, O. M. *Science* **2013,** 341, 1230444.
18. Feng, X.; Ding, X.; Jiang, D. *Chem. Soc. Rev.* **2012,** 41, 6010-6022.
19. Wang, C., et al. *Adv. Funct. Mater.* **2015,** 25, 6009-6017.
20. Stassen, I.; Burtch, N.; Talin, A.; Falcaro, P.; Allendorf, M.; Ameloot, R. *Chem. Soc. Rev.* **2017,** 46, 3185-3241.
21. Ma, H., et al. *J. Am. Chem. Soc.* **2016,** 138, 5897-5903.
22. Das, S.; Heasman, P.; Ben, T.; Qiu, S. *Chem. Rev.* **2017,** 117, 1515-1563.
23. Cao, A., et al. *Nano Lett.* **2017,** 17, 1-7.
24. Wang, C.; Liu, X.; Keser Demir, N.; Chen, J. P.; Li, K. *Chem. Soc. Rev.* **2016,** 45, 5107-5134.
25. Zhu, M. J.; Lerum, M. Z.; Chen, W. *Langmuir* **2012,** 28, 416-423.
26. Sachdeva, S., et al. *ACS Appl. Mater. Interfaces* **2017**, *9*, 24926-24935.
27. Sachdeva, S., et al. *Small* **2017**, *13*, 1604150.
28. Kremer, J. R.; Mastronarde, D. N.; McIntosh, J. R. *J. Struct. Biol.* **1996,** 116, 71-76.
29. Schwab, M. G.; Fassbender, B.; Spiess, H. W.; Thomas, A.; Feng, X. L.; Mullen, K. *J. Am. Chem. Soc.* **2009,** 131, 7216-7217.
30. Mircescu, N. E.; Oltean, M.; Chis, V.; Leopold, N. *Vib. Spectrosc.* **2012,** 62, 165-171.
31. Xu, C.; Hedin, N. *J. Mater. Chem. A* **2013,** 1, 3406-3414.
32. Laybourn, A., et al. *Polym. Chem.* **2012,** 3, 533-537.
33. Biswal, B. P.; Chandra, S.; Kandambeth, S.; Lukose, B.; Heine, T.; Banerjeet, R. *J. Am. Chem. Soc.* **2013,** 135, 5328-5331.
34. Leung, K.; Nielsen, I. M. B.; Criscenti, L. J. *J. Am. Chem. Soc.* **2009,** 131, 18358-18365.
35. Yang, B.; Aksak, B.; Lin, Q.; Sitti, M. *Sensor Actuat B-Chem* **2006,** 114, 254-262.
36. Borini, S., et al. *ACS Nano* **2013,** 7, 11166-11173.
37. Prasetyanto, E. A.; Ansari, M. B.; Min, B.-H.; Park, S.-E. *Catal. Today* **2010,** 158, 252-257.
38. Goeppert, A.; Czaun, M.; May, R. B.; Prakash, G. K. S.; Olah, G. A.; Narayanan, S. R. *J. Am. Chem. Soc.* **2011,** 133, 20164-20167.
39. Fu, R.; Zeng, H.; Lu, Y.; Lai, S. Y.; Chan, W. H.; Ng, C. F. *Carbon* **1995,** 33, 657-661.
40. Niskanen, A. O.; Colli, A.; White, R.; Li, H. W.; Spigone, E.; Kivioja, J. M. *Nanotechnology* **2011,** 22, 295502.
41. Choi, B., et al. *Solid-State Electron.* **2015,** 114, 76-79.

Chapter 6

General Discussion and Outlook

6.1 General discussion

This thesis describes the research that has been done on the project of 'surface-modified silicon nanowires (SiNWs) for chemical sensing', covering the functionalization of SiNWs with ionophores, molecular cages, porous polymers containing nanoparticles for the detection of various analytes present in both the liquid and gas phase.

In Chapter 2, we have reviewed a series of reported SiNW-based gas sensors in terms of their measurement principles, chosen affinity materials and surface modification strategies, used NW dimensions, target molecules, and reported detection limits. About one third of the studies on gas-phase sensors make use of bare SiNW surfaces, *i.e.*, oxide surfaces. The other studies show that additional surface modification with affinity elements/layers can tune the chemical selectivity and sensor sensitivity. One of the examples is that Pt NP-modified SiNWs showed improved sensitivity and selectivity for the detection of H_2, compared to the bare SiNW device.

In Chapter 3, we reported SiNW-FETs modified with two different ionophores that are incorporated into a siloprene polymer matrix for the simultaneous sensing of different alkali metal ions in aqueous solution. The following features contribute to the excellent selectivity, sensitivity and high stability of this multichannel ion sensor: (1) the high affinity of the investigated ionophores valinomycin and Na-ionophore IV for potassium and sodium, respectively, (2) the good adhesion between siloprene-based ion-selective membranes (ISMs) and the surface of SiNW-FETs, (3) the individually addressable SiNWs on a single chip as made by a top-down approach. The ISMs, prepared via a drop-casting methods, were also inspected in a conventional ion-selective electrode (ISE) configuration, allowing a direct comparison. While the responses for K^+ were similar for both sensor configurations, remarkably, the Na^+ response of the ISM-covered SiNW device was found to be higher than the expected Nernstian behavior as found in the ISE configuration. The addition of a Na^+ buffering hydrogel layer between the SiO_2 of the SiNW and the ISM reduced the response to the expected value, showing the importance of keeping the boundary potential at the SiO_2/ISM interface constant.

Chapter 4 represents the use of metal−organic polyhedra (MOPs) covalently coupled to the surface of SiNW-based FETs for the label-free electrical detection and discrimination of explosives having similar molecular structures. The MOP cages were grafted onto a pyridyl-terminated SiNW-FET device. The sensor showed

a good electrical sensing capability to various explosives, especially towards the sensing of 2,4,6-trinitrotoluene (TNT), with a detection limit below the nanomolar level in an ethanol solution. These sensing features are on the one hand attributed to the rational design and integration of multiple weak molecular interactions inside the molecular cage towards the specific binding of the desired molecule, here TNT. On the other hand, the formation of host-stabilized charge-transfer complexes inside the MOP cavity acts as an effective molecular gating element, able to modulate the electrical conductance of the SiNW. Band-bending theory was used to rationalize the functioning of the sensor.

In Chapter 5, we have demonstrated the successful covalent attachment of porous organic frameworks (POFs) onto SiNW surfaces and explored the effect on the electrical sensing properties of SiNW-based devices. In this research, POFs were formed by the polycondensation of melamine and terephthaldehyde in dimethyl sulfoxide (DMSO), and covalently coupled to amine-modified SiNWs. The observed increased sensitivity for water vapor detection, compared to the unmodified SiNWs, was attributed to the enhanced water affinity by the high surface area of POF. This contributes to an increased degree of surface silanol dissociation, which does affect the gate potential. The more negative charge at the nanowire interface increases the amount of majority charge carriers (holes) of the p-doped SiNW, and thus leads to an increase of the drain-source current. Post-synthesis modification of the porous POF by using chloroplatinic acid and subsequent sodium borohydride reduction resulted in the formation of Pt^0 nanoparticles inside the POF structure. Different amounts of chloroplatinic acid were applied to the same amount of POF material to investigate any effect on the size of formed Pt NPs. The presence of Pt NPs in the POF structure resulted in the enhanced sensitivity for the detection of methanol vapor. This is interpreted by a preconcentration of methanol in the Pt NP@POF structure and the concomitant capacitive coupling to the gate potential.

In this thesis different types of chemical gating-principles have been investigated.

In Chapter 3, alkali metal ions in aqueous solutions were detected by applying a fixed back gate and variable front gate while changing the aqueous electrolyte composition. The aqueous electrolyte was connected to the electrical circuit via the Ag/AgCl reference electrode.

In Chapter 4, detection was performed in ethanol solutions. Since the conductance in pure ethanol is very low, the front-gate potential was fixed, and we have studied the variation of the back gate to monitor the presence of TNT. The use

of both front and back gating for sensing in liquid phases is important to contribute to fast, stable and reproducible measurements.

For the sensing in the vapor phase, as described in Chapter 5, front gating is not possible. In such situations only back-gate control can be applied. Therefore, the potential at the front side is not defined and is freely floating, making the measurements less stable. To increase the stability, we have applied a pulsed back-gate potential, which can effectively reduce/eliminate charge trapping, reducing hysteresis.

6.2 Outlook

In this thesis it is shown that SiNW-based chemical sensors are approaching viability for a range of applications, although most of these applications are still away from commercialization. In nearly all cases, SiNW-based devices are made in academic or industrial research labs, allowing to perform fundamental studies and proof-of-concepts under controlled conditions and for different applications. There is only a few (semi) academic suppliers/companies of SiNW-based sensor platforms. For instance, Nanosens B.V. operating in close contact with the MESA+ Research Institute for Nanotechnology and Philips High Tech Campus. With partners they produce bio/chemical sensors based on SiNWs as well as other metal NWs (Au, Pt, Ag, *etc*.) for use in life sciences, health care, security, and water control. Another start-up company is Vista therapeutics (Santa Fe, New Mexico), collaborating with the Lieber research group. They work on the development of SiNW-based biosensors.

In the final Sections of this thesis a number of perspectives on the fabrication process (Section 6.2.1), the surface chemistry (Section 6.2.2), and the integration of different sensors (Section 6.2.3) are provided.

6.2.1 The fabrication of SiNWs

Competition between bottom-up and top-down fabrication processes of nanowires has emerged, but still both methods can be further improved. The top-down fabrication process, using photo-lithography, starts from semiconductor-on-insulator (SOI) wafers and provides high-quality SiNWs, but often requires an extremely careful lithographic process. The fabrication steps that have been used to date are expensive and tedious; therefore, mass production is not realistic at the moment. The bottom-up fabrication, in which the nanowires are grown or deposited starting from molecular or atomic precursors, still suffers from inherent drawbacks,

such as random positioning of the formed wires, chemical contamination, and in general incompatible with standard silicon processing technology. Therefore, there is an ongoing need for better, improved or even completely new methods.

Furthermore, one should also keep in mind that some potential environmental and health hazards might arise when more and more nanostructure materials are being produced and sold. Their long-term impact on environment and health is still unclear. It is very important to be responsible and take precautions while handling these nanostructures.[1]

6.2.2 Surface modification

In general, the quality of the thin native SiO_2 layer covering the SiNW is very important. The electrical insulating properties should be perfect to prevent any leakage currents. Only for such conditions, the quality of the capacitive coupling between the outside (where the dissociable silanol groups are located), and the inside (where the semiconductor charge carriers remain) is guaranteed. Research is done on other insulating materials to replace or modify the native oxide, for instance Al_2O_3,[2] and covalently attached alkyl monolayers[3], prepared from 1-alkenes and 1-alkynes showed promising results and could be further explored.

Besides the covalent functionalization of the SiO_2-covered SiNW via silanization, the layer-by-layer deposition of polyelectrolytes could be further explored. Polycations readily adsorb on the negatively charged SiO_2 surface at pH > 4.0. This allows to simply and conveniently modify these surfaces. A variety of deposition methods can be used, including dip-coating, spin-coating, spray-coating and flow-based techniques. However, there have been only a few studies on the non-covalent modification of SiNWs. It would be interesting to incorporate ion-channel peptides in the deposited lipid bilayer on SiNW, as the peptides would act as affinity elements for ion detection and bestow selectivity, and the physisorption on SiNWs with lipid bilayer could bring stability and sensitivity. In both the gas- and liquid-phase sensing cases, the influence of various parameters such as the concentration of the target, diffusion through the solution or gas phase to reach the sensor surface, and kinetics of the surface binding reaction, all play an important role. Therefore, extended analytical experiments on Cu-MOP-modified SiNW sensors as presented in Chapter 4 could be interesting, to demonstrate the respective performance of sensing explosives under ambient conditions. Moreover, given the low stability of the Cu-MOP cage in water, the design of other molecular cages through a careful

design and selection of the bridging ligands and metal ions is needed for the ultimate detection of explosive vapor, *e.g.*, in airports and train stations.[4]

In this thesis, ionophores (crown ethers in Chapter 3), a molecular cage (Cu-MOP in Chapter 4) and amorphous porous materials as POFs in Chapter 5, were proved to be working as affinity layers when applied to the surface of the SiNWs. It would be also interesting to functionalize the SiNWs with other crystalline porous materials, *e.g.* covalent-organic frameworks (COFs) and metal-organic frameworks (MOFs). These types of materials are interesting as the crystalline structure of such affinity layers may result in higher efficiency of molecule-specific preconcentration, compared to the amorphous structure presented in Chapter 5.

6.2.3 Integration

The modification of individual NWs that are part of a larger array is needed to perform multi-analysis using a single device. So far two approaches have been reported to modify individual nanowires for gas sensing, one based on the tuning of the etching conditions and the other one on nanoscale-localized Joule heating. There are other possible techniques that can be used to functionalize SiNWs individually, for instance, via a commercially available hollow cantilever of the atomic force microscope and molecular printing machine.[5] Both methods are able to dispense very small volumes of liquid at a well-defined position.

In addition, incorporation of a reference SiNW sensor on each device is highly recommended to eliminate the influence of unspecific binding and local environmental changes. Also, a micro-sized reference electrode on the same chip device is desired to allow the application of the dual-gating principle to reduce the hysteresis and current drift. Finally, apart from the development of highly selective affinity elements, promising concepts for improving selective detection could be: using an array of broadly cross-reactive SiNW-based sensors in conjunction with pattern recognition methods,[6] and/or combining SiNW-based FET devices with other powerful analytical tools on the same platform, such as silicon optical microrings.[7]

Looking on longer terms, we believe that continued advances in the preparation of SiNWs with well-defined structures and defect-free interfaces, the modification of selective and stable affinity or receptor layers on SiNW surface, and assembling larger sensor arrays and integrating them with electronics[8] will lead to exquisite sensor system performances that might be just close to an ideal sensor device.

References

1. Yokel, R. A.; MacPhail, R. C. *J. Occup. Med. Toxicol.* **2011,** 6, 7.
2. Chen, S.; Bomer, J. G.; Carlen, E. T.; van den Berg, A. *Nano Lett.* **2011,** 11, 2334-2341.
3. Scheres, L.; Giesbers, M.; Zuilhof, H. *Langmuir* **2010,** 26, 4790-4795.
4. Wales, D. J., et al. *Chem. Soc. Rev.* **2015,** 44, 4290-4321.
5. Ghatkesar, M. K.; Garza, H. H. P.; Staufer, U. *Microelectron. Eng.* **2014,** 124, 22-25.
6. Vishinkin, R.; Haick, H. *Small* **2015,** 11, 6142-6164.
7. Ullien, D., et al. *Opt. Express* **2014,** 22, 16585-16594.
8. Ramgir, N. S.; Yang, Y.; Zacharias, M. *Small* **2010,** 6, 1705-1722.

Appendix-1

Supporting information to Chapter 3:

Ionophore-Containing Siloprene Membranes: Direct Comparison between Conventional Ion-Selective Electrodes and Silicon Nanowire-based Field-Effect Transistors
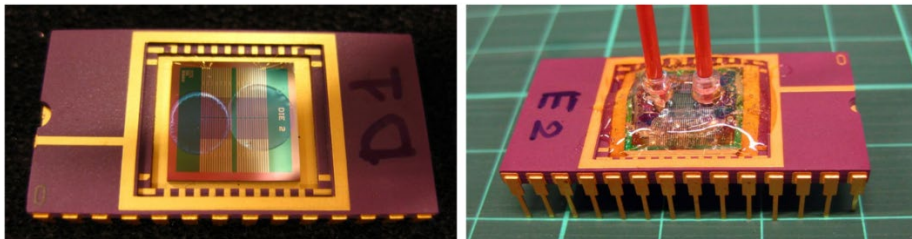
Figure A-1.1 (left) Wire-bonded chip modified with two ISMs next to each other. (right) Wire-bonded chip after the fluidics have been placed and the system has been glued to prevent leakage.
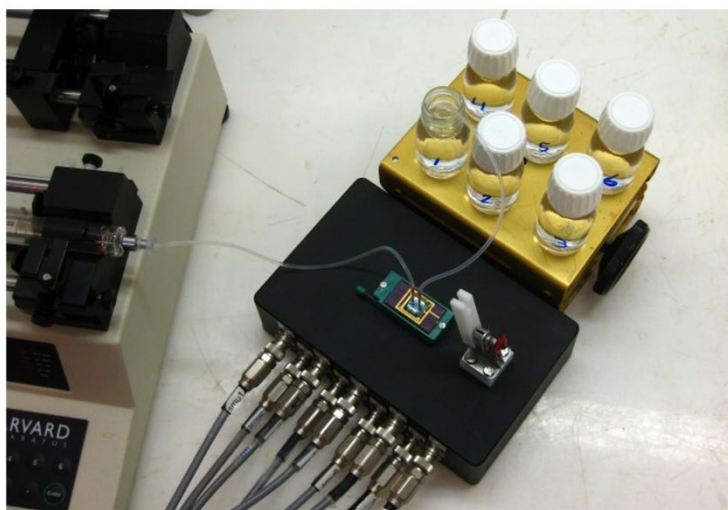
Figure A-1.2 A photograph of the setup by which the NW-FETs have been tested. The sample is placed on top of the black box, after which the tubing is connected. The solutions are sucked into the system from the bottles in the top-right corner using the pump on the left. The Ag/AgCl electrode is placed in the bottle from which the solution is sucked.
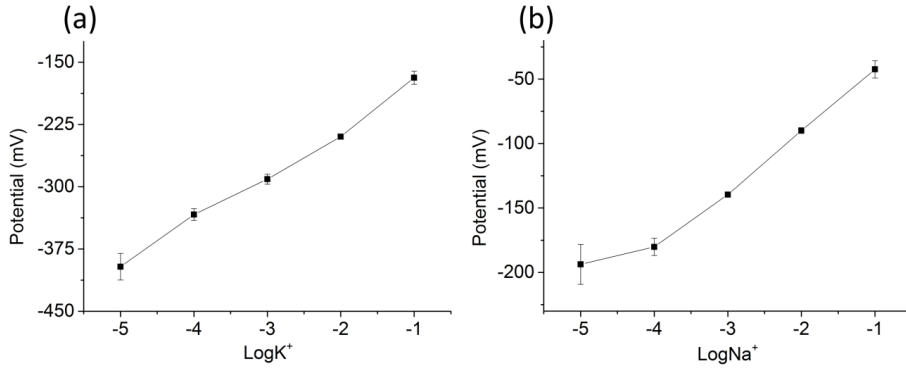
Figure A-1.3 (a) K^+ response of a valinomycin/siloprene modified ISE, (b) Na^+ response of a Na ionophore IV/siloprene modified ISE.

Table A-1.1 pH values of different concentrations of NaCl solution with a constant Cl^- strength of 0.1 M.

C_{Na+} (M)	10^{-5}	10^{-4}	10^{-3}	10^{-2}	10^{-1}
pH (24.2 °C)	6.82	6.87	6.71	6.71	6.73

Table A-1.2 V_t values of bare SiNW-FETs in the presence of different Na^+ concentrations.

V_t (V) from 0.1 M Na^+	-3.02	-3.02	-3.03	-3.02	-3.03	-3.024 (mean)
V_t (V) from 0.01 M Na^+	-3.01	-3.00	-3.00	-3.00	-3.00	-3.002 (mean)
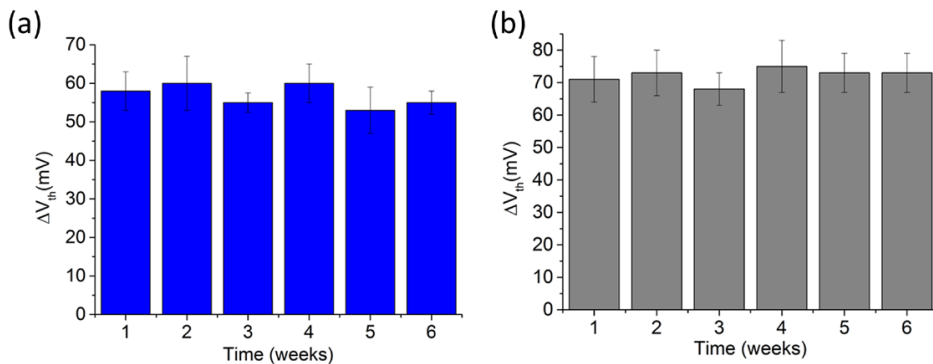
Figure A-1.4 Long-term stability analysis of SiNW-FETs modified by K-ISMs (a), and Na-ISMs (b). ΔV_t refers to the shift of V_t measured from 0.01 M to 0.1 M KCl solution (a) and the corresponding NaCl solution (b).

Appendix-2

Supporting information to Chapter 4:

Metal Organic Polyhedra Coated Si Nanowires for the Sensitive Detection of Trace Explosives
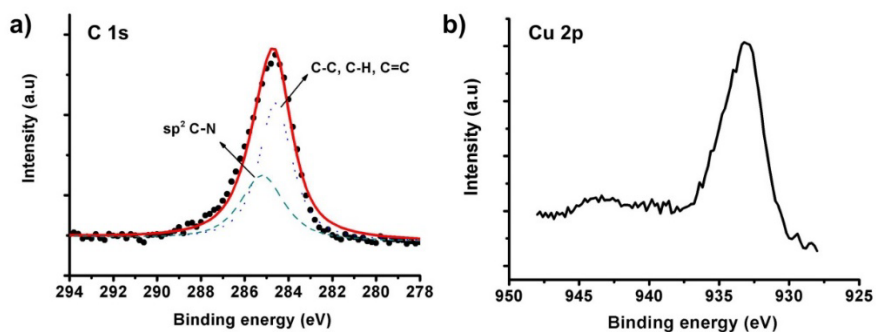
Figure A-2.1 High-resolution C1s spectra (a) and Cu2p spectra (b) of the PETES-(Cu-MOPs)-decorated Si surface.
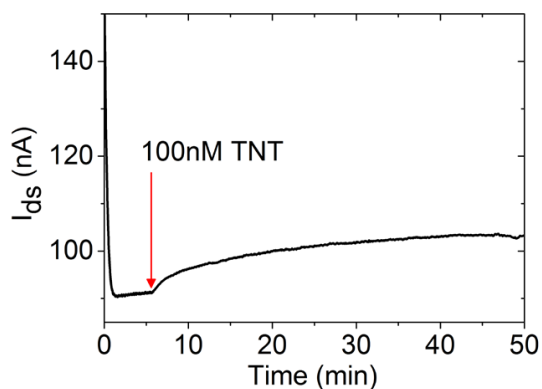
Figure A-2.2 Time trace showing the response of the Cu-MOP-modified SiNW device after incubation with ethanol, setting the back gate at -3 V at t = 0, and switching the solution to 100 nM TNT in ethanol at t = 6 min.
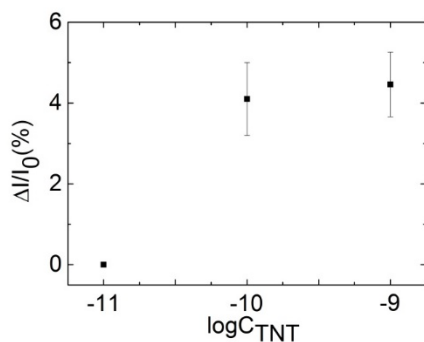
Figure A-2.3 Relative conductance change versus TNT concentration below nanomolar level.
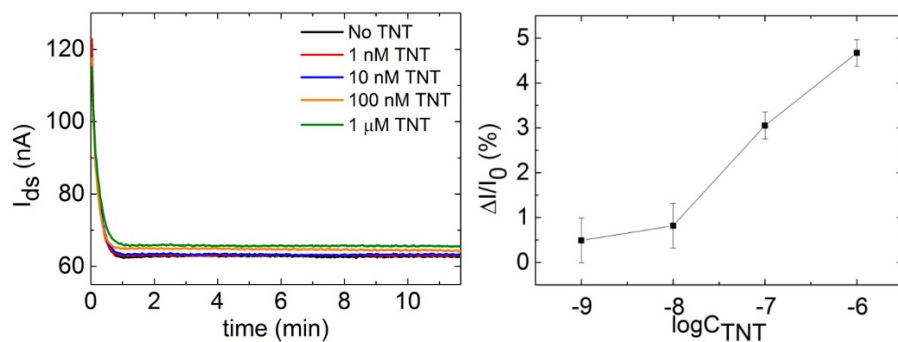
Figure A-2.4 The raw data of current-time curve from a PETES-modified chip exposed to different TNT concentrations.
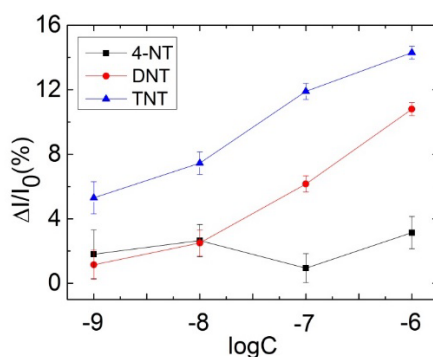
Figure A-2.5 Relative current change ($\Delta I/I_0$) versus explosive (TNT, DNT, and NT) concentrations.
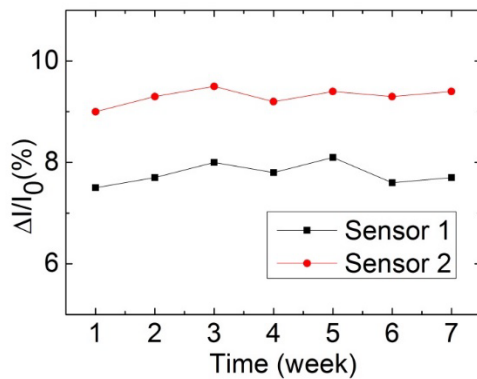
Figure A-2.6 Stability data for two different sensors taken over a period of 7 weeks.
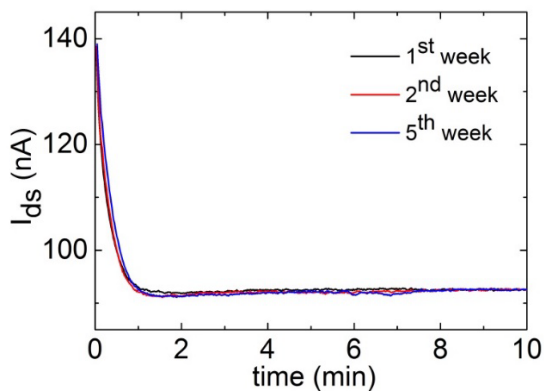
Figure A-2.7 Recovery test of one Cu-MOPs modified SiNW sensor in ethanol solution after each time vacuum.

Table A-2.1 Charge redistribution upon adsorption of TNT in MOPs using the DDEC charge Analysis method. All charge redistribution values are given in electron charge.[a]

	Cu^{2+}	$-NH_2$	$-NO_2$	TNT
TNT@MOP	0.0031	-0.0037	0.0122	0.0471
	-0.0206	-0.0098	0.0026	
	0.0050	-0.0227	0.0388	
	-0.0351	-0.0019		

[a]"-" denotes electron accumulation; "+" denotes electron depletion

Table A-2.2 Charge redistribution upon adsorption of DNT in MOPs using the DDEC charge Analysis method. All charge redistribution values are given in electron charge.[a]

	Cu^{2+}	$-NH_2$	$-NO_2$	DNT
DNT@MOP	0.0022	-0.0143	0.0227	0.0661
	-0.0185	0.0045	0.0374	
	0.0006	-0.0053		
	-0.0238	-0.0203		

Table A-2.3 Charge redistribution upon adsorption of 4-NT in MOPs using the DDEC charge Analysis method. All charge redistribution values are given in electron charge.[a]

	Cu^{2+}	$-NH_2$	$-NO_2$	4-NT
4-NT@MOP	0.0019	-0.0047	0.0229	0.0371
	-0.0078	0.0169		
	-0.0032	-0.0139		
	-0.0068	-0.0157		

Appendix-3

Supporting information to Chapter 5:

Enhanced Vapor Sensing using Silicon Nanowire Devices Coated with Pt Nanoparticle Functionalized Porous Organic Frameworks
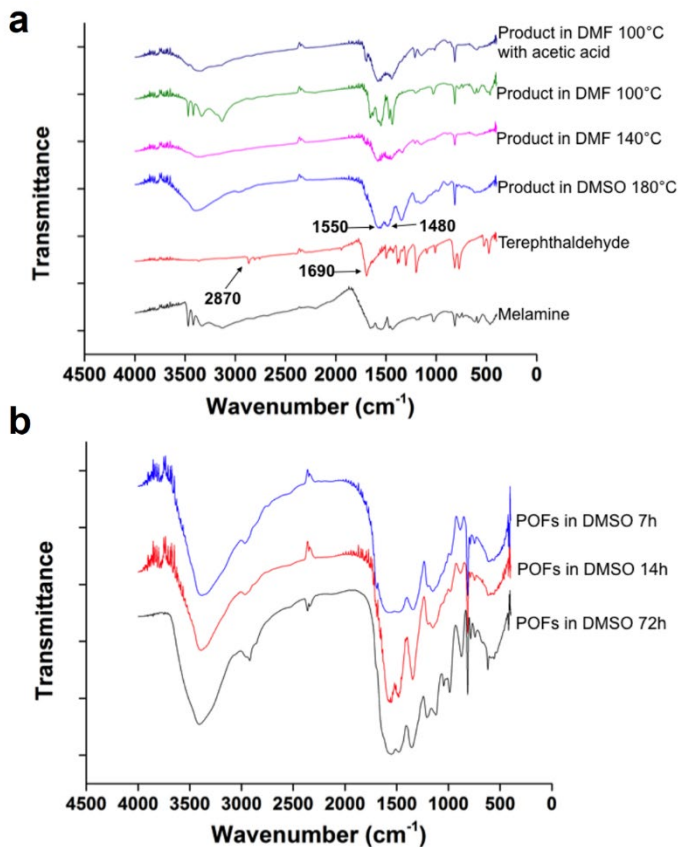
Figure A-3.1 FTIR spectra of the product prepared **(a)** in different solvents and with/without catalyst, **(b)** in a DMSO solution with different reaction time.
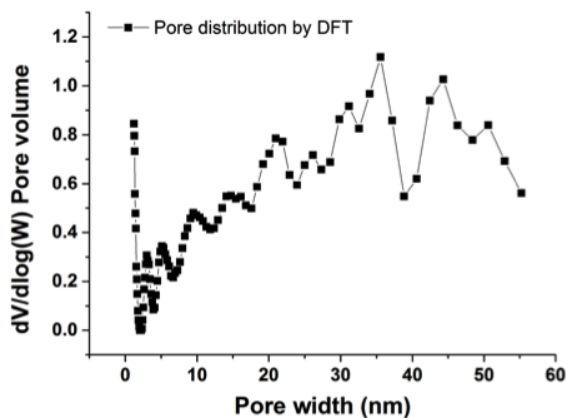
Figure A-3.2 Pore size distribution of the POF product, predicted from the data of N_2 sorption using a DFT method.

122
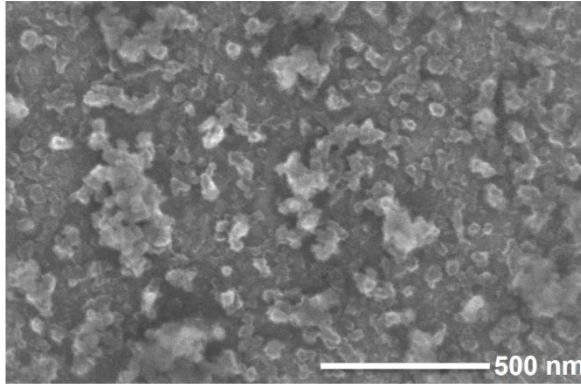
Figure A-3.3 SEM image of the POF-modified Si wafer.
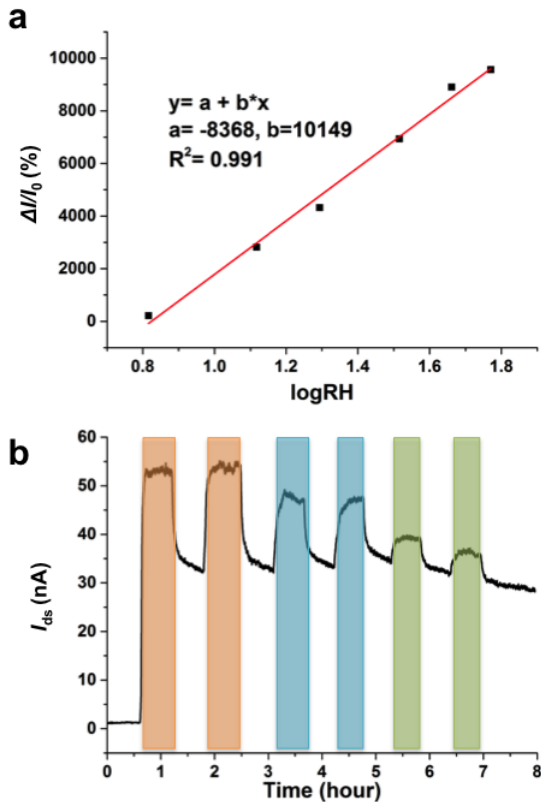
Figure A-3.4 (a) Semi-log relation between the normalized signal increase and the different RH, **(b)** Repeatability of POF-modified SiNW device (yellow 46% RH, blue 38% RH, green 30% RH).
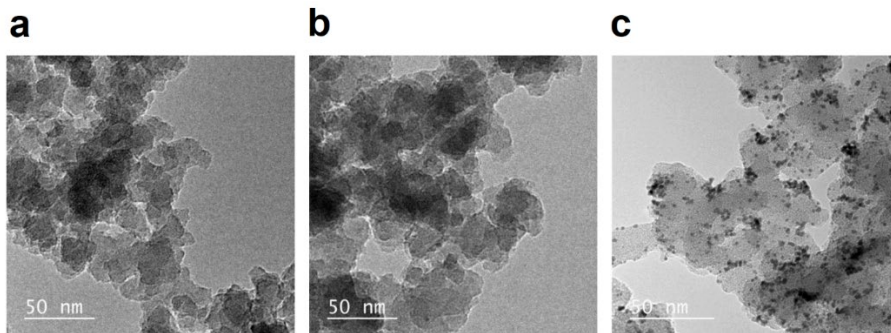
Figure A-3.5 TEM images of **(a)** pure POF powder, **(b)** impregnated POF with Pt^{4+}, **(c)** impregnated products after *in-situ* reduction using $NaBH_4$ as reductant.

Table A-3.1 Surface elemental information of different samples as obtained by XPS (values are rounded to integers).

Sample	Si (at.%)	O (at.%)	C (at.%)	N (at.%)
Bare Si wafer	54	36	10	0
APTES-modified Si wafer	45	32	19	4
POF-modified Si wafer	2	9	58	31
POF powder	0	9	59	31

Table A-3.2 Comparison of the BET surface, micropore volume and CO_2 uptake between pure POFs and the metalation product (PtNP@POF) (- not measured).

	Pure POF	100:1	20:1	4:1
BET surface (m^2/g)	609.9	271.9	207.6	54.5
Micropore volume (cm^3/g)	0.102	0.047	0.0412	0.009
CO_2 uptake (cm^3/g) at 1 bar	55	46	39	-

Samenvatting

Chemische sensoren spelen een belangrijke rol in milieumonitoring, procescontrole en veiligheid, en in medische diagnostiek. Silicium nanodraden ('silicon nanowires', SiNWs) zijn zeer geschikt voor dergelijke toepassingen vanwege hun unieke eigenschappen. Ook kunnen chemische modificaties van deze nanodraden bijdragen aan een hoge sensitiviteit en selectiviteit met betrekking tot het detecteren van chemische componenten in verscheidene fasen. Dit proefschrift handelt over het onderzoek dat is uitgevoerd in het kader van het project 'chemische sensoren gebaseerd op SiNWs' ('chemical sensors based on SiNWs'). In dit onderzoek is gekeken naar de invloed van verschillende chemische modificaties van SiNWs met ionoforen, moleculaire kooien ('molecular cages') en poreuze polymeren die nanodeeltjes bevatten, op de detectie van verschillende componenten in zowel vloeistoffen als gassen.

Hoofdstuk 2 geeft een overzicht van de tot nu toe in de literatuur beschreven chemische sensoren, waarbij gebruik wordt gemaakt van SiNWs. Hier wordt ingegaan op de detectie- principes, chemische modificaties en toegepaste strategieën, nanodraadafmetingen, analyten en detectielimieten. Ongeveer een derde van de onderzochte studies naar gas- sensoren beschrijft het gebruik van het onbehandelde oxide-oppervlak (SiO_2) van SiNWs. De overige studies, welke worden behandeld in dit hoofdstuk, laten zien dat modificaties van SiNWs kunnen bijdragen aan een hogere chemische selectiviteit en sensor sensitiviteit. Een goed voorbeeld hiervan is de verbeterde H_2 detectie door gebruik te maken van SiNWs welke zijn gemodificeerd met Pt nanodeeltjes.

In Hoofdstuk 3 wordt ingegaan op de gelijktijdige detectie van alkali-metaalionen (Na^+ en K^+) in de waterfase middels gemodificeerde SiNW veld-effect transistoren (SiNW-FET). Voor de modificatie van de SiNW is in dit onderzoek gebruik gemaakt van twee verschillende ionoforen (valinomycine en Na-ionofoor IV), welke zijn verwerkt in een silopreen polymeer matrix. De gevonden excellente selectiviteit, sensitiviteit en stabiliteit van deze sensoren kunnen worden toegeschreven aan: (1) de grote affiniteit van deze twee ionoforen voor respectievelijk K^+ en Na^+, (2) de goede hechting tussen de ion-selectieve silopreen membranen en het oxide oppervlak van de SiNWs en (3) de top-down configuratie van individueel aanstuurbare SiNWs op een enkele chip. De ion-selectieve membranen, geprepareerd via 'drop-casting', zijn ook toegepast in een conventionele ion-selectieve electrode configuratie om zo te kunnen vergelijken met de SiNW-FET configuratie. Hieruit bleek dat, terwijl de respons voor K^+ vergelijkbaar was voor

beide typen sensoren, de respons voor Na$^+$ veel hoger was voor de SiNW-FET sensor. De vervolgens gevonden lagere respons bij het toepassen van een hydrogel tussenlaag, ten behoeve van Na$^+$ buffering tussen het oxide oppervlak van de SiNW en het ion selectieve membraan, demonstreert het belang van een constante grenspotentiaal aan de oxide / membraan grensvlak.

Hoofstuk 4 beschrijft de eerste toepassing van metaal-organische polyhedra (MOPs), welke covalent gebonden zijn aan het SiNW-FET oppervlak, ten behoeve van de labelvrije electrische detectie en onderscheiding van explosieven met een overeenkomstige moleculaire structuur. Deze MOP kooien zijn gebonden aan een pyridyl-gefunctionaliseerde SiNW-FET en tonen goede eigenschappen voor de electrische detectie van verschillende explosieven, en in het bijzonder 2,4,6-trinitrotolueen (TNT). Dit kon worden gedetecteerd op nano-molair concentratieniveau in ethanol oplossing. Deze sensoreigenschappen kunnen worden toegeschreven aan zowel het rationele ontwerp en de integratie van meerdere zwakke moleculaire interacties in de MOPs ten opzichte van de specifieke binding met het analyt (in dit geval TNT), als wel door het vormen van een ladingsoverdracht complex dat door de MOP wordt gestabiliseerd. Dit gevormde complex moduleert vervolgens de electrische geleiding door de silicium nanodraad. De bandbuiging theorie is hier toegepast om het functioneren van deze sensor te onderbouwen.

Hoofstuk 5 handelt over de toepassing van de covalente binding tussen poreuze organische netwerken ('porous organic frameworks', POFs) en SiNW, en de effecten van deze modificatie op de eigenschappen van de SiNW sensoren. De POF structuren zijn gevormd door polycondensatie van melamine en terephthaldehyde in DMSO als oplosmiddel in aanwezigheid van SiNWs, die al in een eerder stadium gefunctionaliseerd waren met aminopropylgroepen. De hierbij waargenomen verhoogde sensitiviteit ten opzichte van waterdamp in vergelijking met niet-gemodificeerde SiNWs kon worden toegeschreven aan een verhoogde affiniteit voor water door het aanwezige POF netwerk. Deze verhoogde locale waterconcentratie draagt bij aan een toename van de dissociatie van de oppervlakte silanolgroepen van de SiNW. De hiermee gepaard gaande toegenomen negatieve oppervlaktepotentiaal verhoogt het aantal meerderheidsladingsdragers ('majority charge carriers'. Dat zijn hier de 'gaten'), en daarmee de 'source-drain' stroom. Post-synthese modificatie van deze poreuze POFs werd uitgevoerd door eerst chloorplatinazuur (H$_2$PtCl$_6$) op te nemen en vervolgens met natrium boorhydride te reduceren tot platina nanodeeltjes. Verschillende hoeveelheden van chloorplatinazuur zijn toegepast om de effecten op de grootte van de gevormde nanodeeltjes te bestuderen. De aanwezigheid van deze platina nanodeeltjes zorgde voor een toegenomen gevoeligheid voor de detectie van

126

methanoldamp. Deze waarneming kan worden geïnterpreteerd als een effect van preconcentratie van methanol in de Pt^0-POF structuur en de daarvan als gevolg zijnde capacitatieve koppeling met de 'gate' potentiaal.

Kort samengevat bevestigen de resultaten zoals beschreven in dit proefschrift de toepasbaarheid van SiNW sensoren voor een breed gebied van sensortoepassingen. Het is niet ondenkbaar dat door voortdurende verbetering van de fabricatie van SiNWs met nauwkeurig gedefinieerde structuren en defectvrije grensvlakken, in combinatie met selectieve en stabiele oppervlaktemodificaties, integratie in arraystructuren en electronica, zullen gaan zorgen voor tot nu toe onovertroffen sensor prestaties.

List of publications

- **Cao, A.**; Shan, M.; Paltrinieri, L.; Evers, W.; Chu, L.; Poltorak, L.; Klootwijk, J. H.; Seoane, B.; Gascon, J.; Sudhölter, E. J. R.; de Smet, L. C. P. M. "Enhanced vapor sensing using silicon nanowire devices coated with Pt nanoparticle functionalized porous organic frameworks", under revision.

- **Cao, A.**; Zhu, W.; Shang, J.; Klootwijk, J. H.; Sudhölter, E. J. R.; Huskens, J.; de Smet, L. C. P. M. "Electrical sensing capability of metal-organic polyhedra-coated Si nanowires to various explosives", *Nano Lett.* **2017**, *17*, 1−7.

- **Cao, A.**; Mescher, M.; Bosma, D.; Klootwijk, J. H.; Sudhölter, E. J. R.; de Smet, L. C. P. M. "Ionophore-containing siloprene membranes: direct comparison between conventional ion-selective electrodes and silicon nanowire-based field-effect transistors", *Anal. Chem.* **2015**, *87*, 1173−1179.

- **Cao, A.**; Sudhölter, E. J. R.; de Smet, L. C. P. M. "Silicon nanowire-based devices for gas-phase sensing", *Sensors* **2014**, *14*, 245-271.

- Chu, L.; Korobko, A.V.; **Cao, A.**; Sachdeva, A.; Liu, Z.; de smet, L. C. P. M.; Sudhölter, E. J. R.; Picken, S. J.; Besseling, N. A. M. "Mimicking an atomically-thin 'vacuum spacer' to measure the Hamaker Constant between Graphene Oxide and silica", *Adv. Mater. Interfaces* **2017**, 4, 1600495.

- Ma, M.; Hansen, H. A.; Valenti, M.; Wang, Z.; **Cao, A.**; Dong, M.; Smith, W. A.; "Correlation of CO_2 reduction activity and selectivity with compositionally variant bimetallic electrocatalysts", *Nano Energy* **2017**, 42, 51-57.

Prior to this thesis

- **Cao, A.**; Zhang C. "Real-time detection of transcription factors using target-converted helicase-dependent amplification assay with zero-background signal", *Anal. Chem.* **2013**, *85*, 2543−2547.

- **Cao, A.**; Zhang C. "Sensitive and label-free DNA methylation detection by ligation-mediated hyperbranched rolling circle amplification", *Anal. Chem.* **2012**, *84*, 6199−6205.

- Xu, Q.; **Cao, A.**; Zhang C. "Rapid and label-free monitoring of exonuclease III-assisted target recycling amplification", *Anal. Chem.* **2012**, *84*, 10845−10851.

- **Cao, A.**; Ai, H.; Ding, Y.; Dai, C.; Fei, J. "Biocompatible hybrid film of β-cyclodextrin and ionic liquids: A novel platform for electrochemical biosensing", *Sensors and Actuators B* **2011**, 155, 632–638.

Acknowledgements/致谢

thankful to the support staff who help me through my PhD, Astrid, Marian, Karin, Els and Caroline, thank you very much. OMI is a small and great group, all the former and current members made it wonderful. Marleen, Daniela, Venkatesh, Zhen, Aldo and Sumit, thank you veterans for the great time at work and outside of it. Your presence made my early OMI life colorful. Sumit, thank you for all the discussions/chats in the past years. Rajeev, Naveen, Lukasz, Stijn, Jorrit, Mohammad, Liangyong, Hamid and Laura, thank you for the group lunch together, we shared our experiences in and outside of the work. Rajeev, I wish you all the best in your coming life in Spain. Lukasz and Laura, thanks for all the help in work and countless coffee break, Laura, good luck for your graduation soon.

I have been lucky enough to be a SFD member in TU/e nearly one year before my PhD graduation. Dick, once again, thanks a lot for giving me this great opportunity. Albert, thank you for allowing me to work in your group. Also, I am very grateful for the guidance and discussions especially when Dick was absent. Danqing, thank you for the link to Eindhoven. Wish you lots of success in your career. Of course, other SFD members are appreciated, Hao, Lihua, Mathew, Rob, Sarah, Marina, Tom, Ellen, Simon, Anne Helene, Dirk Jan, Hitesh, Koen, Sander, Jeroen, Monali, Wei, Marjolijn, Shaji, Xiaohong, Gilles, Fabian, Davey, Stijn, Marc, Yuanyuan, Xinglong and Ting, thanks a lot for your help and discussions and providing a positive working environment.

The special thanks to my other friends in Netherlands. Bobo and Clement, Kai and Julie, Zhen, Wuyuan, Ruby, Liangyong, Ming, Jicheng, Xiaohui, Yiming, Kai-Liu, Yunlong, Meixia, Min, Shouen, Yan-Ni and Wei-Song, I enjoyed every small gathering with all of you, and thank you for your presence, my life in Netherlands is more enjoyable. Ruby, best wishes for your future life.

最后，谢谢我亲爱的家人: 弟弟和弟妹，特别感谢你们每一次我回国的豪吃豪喝的款待；姑姑，姑父和叔叔们，谢谢你们多年的支持和关心；奶奶，爸爸和生母，感谢你们对我的疼爱，没有你们就不会有我。另外，感谢潘全这些年的照顾，你的陪伴和支持让我度过所有的难关，期待我们美好的将来。

<div align="right">Anping Cao
December, 2017</div>

Curriculum Vitae

Anping Cao was born in Hunan (China) on September 3. She completed her Bachelor's study in Pharmacy from Xiangtan University in 2008. Three years later, she received her Master degree in Analytical Chemistry at Xiangtan University. In 2011, she joined Shenzhen Institutes of Advanced Technology, Chinese Academy of Sciences, and worked on biosensors for the detection of DNA and proteins. In 2013, she started her PhD project in the Department of Chemical Engineering, Delft University of Technology, under the supervison of Dr. ir. Louis C. P. M. de Smet and Prof. dr. Ernst J. R. Sudhölter. She investigated silicon nanowires as chemical sensors for the detecion of ions, explosives and chemical vapors. In 2017, she continued her research career as a postdoctoral researcher at Eindhoven University of Technology, under the supervision of Prof. dr. Dick J. Broer, working in the field of dynamic liquid crystal networks for gas separation.